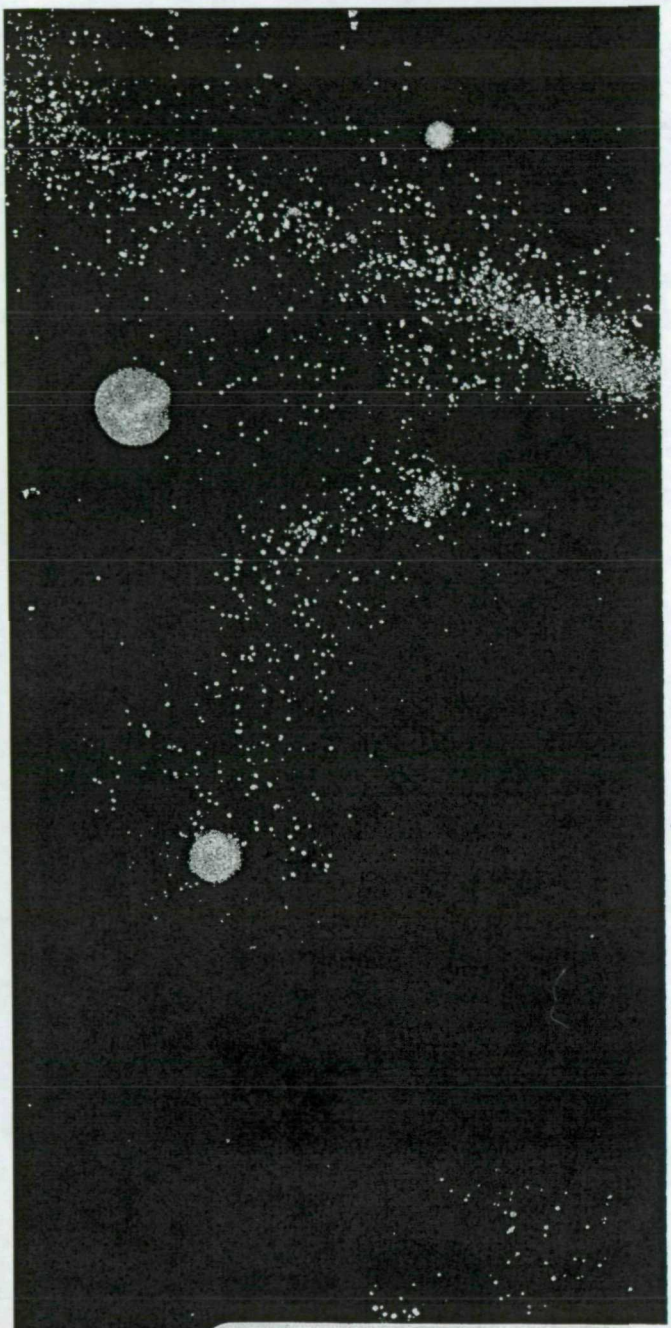

D5-15814-4

APOLLO/SATURN V POSTFLIGHT LUNAR IMPACT TRAJECTORY - AS-512 S-IVB/IU

(NASA-CR-133285) APOLLO/SATURN 5 POSTFLIGHT LUNAR IMPACT TRAJECTORY - AS -512 S-4B/IU (Boeing Co., Huntsville, Ala.) 123 p

N73-73308

Unclas
00/99 17845

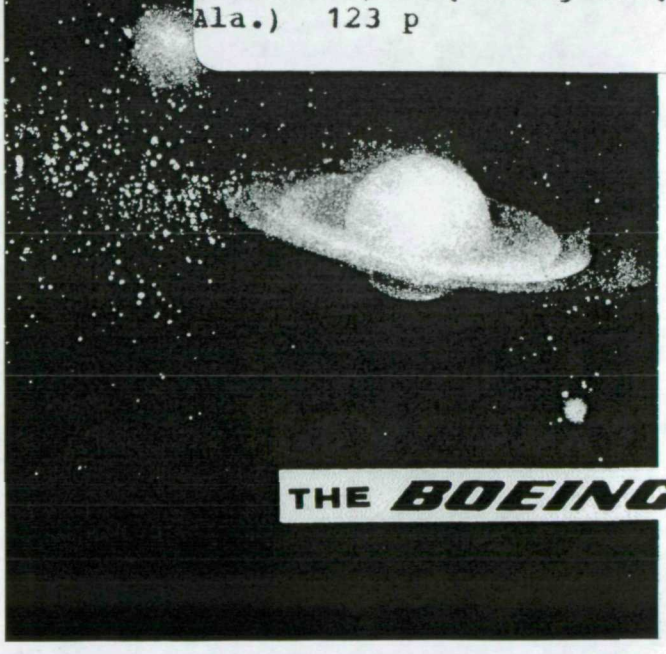

APRIL 11, 1973

THE BOEING COMPANY - SPACE DIVISION

DOCUMENT NO. D5-15814-4

TITLE APOLLO/SATURN V POSTFLIGHT LUNAR IMPACT TRAJECTORY - AS-512 S-IVB/IU

MODEL NO. SATURN V CONTRACT NO. NAS8-5608, SCHEDULE II, PART IX, TASK DIRECTIVE 290 (PART B)

TRACKING AND FLIGHT RECONSTRUCTION
G. T. PINSON

APRIL 11, 1973

D. E. CHICHESTER, MANAGER
FLIGHT TECHNOLOGY

ISSUE NO. ISSUED TO

THE BOEING COMPANY SPACE DIVISION LAUNCH SYSTEMS BRANCH

ABSTRACT AND LIST OF KEY WORDS

This document presents the postflight trajectory for the Apollo/Saturn V AS-512 spent S-IVB/IU stage from CSM separation to lunar impact. The lunar impact coordinates and conditions are included. Some combinations of small S-IVB/IU stage related forces are hypothesized to account for small translational perturbations. Trajectory dependent parameters in geocentric and selenocentric inertial coordinates (PACSS4, reference epoch at mean of 1972) are listed at selected time points from Command Service Module separation to lunar impact.

Data relating to the tracking residuals (observed minus model calculated (O-C)) are also given for the best-estimate trajectory.

Apollo/Saturn V
S-IVB/IU Spent Stage
AS-512
Postflight Trajectory
Lunar Impact Conditions
Apollo 17
BET

CONTENTS

PARAGRAPH		PAGE
	ABSTRACT AND LIST OF KEY WORDS	ii
	CONTENTS	iii
	ILLUSTRATIONS	v
	TABLES	vii
	REFERENCES	viii
	ACKNOWLEDGEMENT	ix
	GLOSSARY OF TERMS	x
	LIST OF ABBREVIATIONS	xi
	SOURCE DATA PAGE	xiii
	SECTION 1 - INTRODUCTION AND SUMMARY	1-1
	SECTION 2 - BEST-ESTIMATE TRAJECTORY AND LUNAR IMPACT MANEUVERS DISCUSSION	2-1
2.1	CSM/LM DOCKING, EJECTION, AND EVASIVE MANEUVERS	2-2
2.2	SAFING AND LUNAR IMPACT TARGETING MANEUVERS	2-3
2.3	PASSIVE THERMAL CONTROL AND PERTURBATION	2-4
2.4	LUNAR IMPACT CONDITIONS	2-5
	SECTION 3 - BEST-ESTIMATE TRAJECTORY DETERMINATION	3-1
3.1	DATA UTILIZATION	3-1
3.1.1	Pre-PTC Time Arc Data Utilization	3-1
3.1.2	Early PTC Time Arc Data Utilization	3-1
3.1.3	Late PTC Time Arc Data Utilization	3-2
3.2	TRAJECTORY ANALYSIS AND ACCURACY	3-2
3.2.1	Pre-PTC Trajectory Segment Analysis and Accuracy	3-2
3.2.2	Early PTC Trajectory Segment Analysis and Accuracy	3-2
3.2.3	Late PTC Trajectory Segment Analysis and Accuracy	3-4
3.3	LUNAR IMPACT POINT ACCURACY	3-5
	APPENDIX A - ANALYSIS METHODS	A-1
A.1	INITIAL STATE PROPAGATION	A-1
A.2	CALCULATION OF OBSERVABLES	A-2
A.3	CORRECTION OF INITIAL STATE	A-6

CONTENTS (Continued)

PARAGRAPH		PAGE
	APPENDIX B - MATHEMATICAL MODEL OF TUMBLING S-IVB/IU	B-1
	APPENDIX C - BEST-ESTIMATE TRAJECTORY HISTORY	C-1

ILLUSTRATIONS

FIGURE		PAGE
2-1	Translunar Coast Maneuvers Overview	2-6
2-2	AS-512 Instrument Unit Platform Velocity Accumulation During Lunar Impact Targeting	2-7
2-3	AS-512 Instrument Unit Platform Gimbal Angles During Lunar Impact Targeting	2-8
2-4	Early PTC Tumble Residuals	2-9
2-5	Late PTC Tumble Residuals	2-10
2-6	Comparison of Gravity-Only and Perturbed Trajectory Residuals	2-11
2-7	Apollo 17 Lunar Landmarks	2-12
2-8	AS-512 S-IVB/IU Lunar Impact Heading and Impact Angles	2-13
3-1	AS-512 S-IVB/IU Tracking Data Availability	3-7
3-2	Ascension and Madrid Range-Rate Residuals for Pre-PTC Data Fit	3-8
3-3	Carnarvon, Bermuda and Merritt Island Range-Rate Residuals for Pre-PTC Data Fit	3-9
3-4	Carnarvon C-Band and Madrid Range Residuals for Pre-PTC Data Fit	3-10
3-5	Madrid Range-Rate Residuals for PTC Data Fit - Best-Estimate Trajectory	3-11
3-6	Tidbinbilla Range-Rate Residuals for PTC Data Fit - Best-Estimate Trajectory	3-12
3-7	Goldstone Range-Rate Residuals for PTC Data Fit - Best-Estimate Trajectory	3-13
3-8	Madrid and Goldstone Range-Rate Residuals for PTC Data Fit - Best-Estimate Trajectory	3-14
3-9	Canberra and Bermuda Range-Rate Residuals for PTC Data Fit - Best-Estimate Trajectory	3-15
3-10	Greenbelt Range-Rate Residuals for PTC Data Fit - Best-Estimate Trajectory	3-16
3-11	Ascension Range-Rate Residuals for PTC Data Fit - Best-Estimate Trajectory	3-17
3-12	Merritt Island Range-Rate Residuals for PTC Data Fit - Best-Estimate Trajectory	3-18
3-13	Hawaii Range-Rate Residuals for PTC Data Fit - Best-Estimate Trajectory	3-19
3-14	Guam Range-Rate Residuals for PTC Data Fit - Best-Estimate Trajectory	3-20
3-15	Carnarvon Range-Rate Residuals for PTC Data Fit - Best-Estimate Trajectory	3-21
3-16	Comparison of Gravity-Only Trajectory and Best-Estimate Trajectory Range Residuals	3-22
3-17	Madrid, Goldstone and Tidbinbilla Range Residuals for Late Data PTC Fit - Best-Estimate Trajectory	3-23

ILLUSTRATIONS (Continued)

FIGURE		PAGE
3-18	Range-Rate and Range Residual at Lunar Impact	3-24
3-19	Range-Rate Residuals at Lunar Impact	3-25
3-20	Distribution of Lunar Impact Solutions	3-26
A-1	Diagram for USB Range Calculation	A-8
B-1	Vehicle Rotations and Rotation Rates	B-10
B-2	Vehicle Attitude and Attitude Rates	B-11
B-3	Relationship Between the Angular Momentum Coordinate System and PACSS4	B-12
B-4	Simulated Range-Rate Modulations	B-13
B-5	Simulated S-IVB/IU Velocity Change During PTC	B-14

TABLES

TABLE		PAGE
2-I	Significant Event Times	2-14
2-II	Reconstructed Lunar Impact Maneuvers	2-15
2-III	Perturbing Acceleration During PTC	2-16
2-IV	Stage and Trajectory Impact Parameters	2-17
3-I	Tracking Station Locations	3-27
3-II	Pre-PTC Trajectory Segment - Residual Statistics and Data Utilization	3-28
3-III	Early PTC Trajectory Segment - Residual Statistics and Data Utilization	3-29
3-IV	Late PTC Segment Residual Statistics and Data Utilization for Best-Estimate Trajectory	3-30
3-V	Late PTC Segment Residual Statistics and Data Utilization for Best Gravity-Only Trajectory	3-31
3-VI	Trajectory Solutions and Lunar Impact Points	3-32
3-VII	Apollo 17 Lunar Impact Times	3-33

REFERENCES

1. NASA Document MPR-SAT-FE-73-1, "Saturn V Launch Vehicle Flight Evaluation Report - AS-512 Apollo 17 Mission," February 28, 1973.

2. GSFC Memorandum, X-832-72-203, "Apollo 16 STDN Metric Tracking Performance (Final Report)," August 1972.

3. Boeing Document D5-15560-12, "Apollo/Saturn V Postflight Trajectory - AS-512," April 11, 1973.

4. Unpublished paper, "Interpretation and Utilization of the Derived Covariance Matrix," T. J. Galbraith, The Boeing Company.

5. "Introduction to Sequential Smoothing and Prediction,' Norman Morrison, McGraw-Hill Book Company, copyright 1969.

6. Lockheed Missiles and Space Company Document (LMSC/HREC D162559) TM54/30-235, "LID User's Manual," September 1970.

7. NASA Document SE-008-001-1, "Project Apollo Coordinate System Standards," June 1965.

8. "An Introduction to Optimal Estimation," Paul B. Liebelt, Addison-Wesley Publishing Company, copyright 1967.

9. "Introduction to Space Dynamics," William T. Thomson, John Wiley & Sons, Inc., copyright 1961.

ACKNOWLEDGEMENT

The analyses presented in this document were conducted under the technical direction of R. McCurdy by the following Saturn Engineering personnel:

TRACKING AND FLIGHT RECONSTRUCTION

J. Burgen
G. Engels
T. Galbraith
J. Jaap
P. Johnson
E. Timmons

BOEING COMPUTER SERVICES

C. Dorries
R. Simmons

Questions concerning the information presented should be directed to the technical supervisor of this analysis:

G. T. Pinson, JC-40
The Boeing Company
Huntsville, Alabama

GLOSSARY OF TERMS

TERM	DEFINITION
Impact Maneuvers	The S-IVB/IU APS burn maneuvers to accomplish lunar targeting of the spent S-IVB/IU stage.
Initial State	A twelve element vector containing, in order, the initial position, initial velocity, non-gravitational acceleration biases, and non-gravitational acceleration scale factors.
Passive Thermal Control Maneuver	The maneuver which starts and maintains rotation of the spent S-IVB/IU stage about the center of mass to prevent differential solar heating.
Range	The average of the uplink and down-link signal travel distances.
Range Rate	The change in range per unit time computed over a finite interval.
Safing Maneuvers	The APS Evasive Burn, CVS Vent, and LOX Dump maneuvers of the spent S-IVB/IU stage to separate it from the CSM/LM and to prepare it for lunar targeting.
Tracking Data Residual	Difference between observed and calculated values of a tracking parameter, e.g., range rate.
Trajectory Segment	A portion of a composite trajectory determined from tracking data over a particular time arc which may be propagated by the model equations prior to or following the data arc.
Timebase 8	A time reference established by the LVDC following an inhibit removal by ground command. This time reference follows the docking maneuvers and precedes the safing maneuvers.

LIST OF ABBREVIATIONS

ABBREVIATIONS	DEFINITION
ACN3	Ascension 30' STDN USB
APS	Auxiliary Propulsion System
APS-1	First Lunar Impact Targeting Burn
APS-2	Second Lunar Impact Targeting Burn
BDA3	Bermuda 30' STDN USB
BDAQ	Bermuda C-Band Radar
BET	Best-Estimate Trajectory and Impact Point
CPH	Cycles Per Hour
CSM	Command and Service Module
CRO3	Carnarvon 30' STDN USB
CROQ	Carnarvon C-Band Radar
CVS	Continuous Vent System
DSN	Deep Space Network
ETC3	Greenbelt Experimental Test Center 30' STDN USB
GDS8	Goldstone 85' STDN USB
GDSW	Goldstone 85' DSN USB
GMT	Greenwich Mean Time
GWM3	Guam 30' STDN USB
HAW3	Hawaii 30' STDN USB
HSK8	Canberra 85' STDN USB
HSKW	Tidbinbilla 85' DSN USB
IU	Instrument Unit
JPL	Jet Propulsion Laboratory
JSC	Johnson Space Center

LIST OF ABBREVIATIONS (Continued)

ABBREVIATION	DEFINITION
LID	Lunar Impact Determination
LIT	Lunar Impact Team
LM	Lunar Module
LOX	Liquid Oxygen
LV	Launch Vehicle
LVDC	Launch Vehicle Digital Computer
MAD8	Madrid 85' STDN USB
MADW	Madrid 85' DSN USB
MIL3	Merritt Island 30' STDN USB
MNBY	Mean Nearest Besselian Year
MSFC	Marshall Space Flight Center
PACSS	Project Apollo Coordinate System Standard
PTC	Passive Thermal Control
STDN	Spaceflight Tracking and Data Network
TCS	Thermal Control System
USB	Unified S-Band

SOURCE DATA PAGE

The following listed government-furnished documentation was used in the preparation of this document:

Exhibit FF Line Item Number	GFD Title	Date Received
S&E-AERO-17	Tracking and Communications Network Specification	10/1/72
S&E-AERO-73	Operational Trajectory for Saturn V Vehicles	12/8/72
S&E-AERO-104	S-IVB Stage Predicted Nominal Tracking Coverages	10/1/72
S&E-AERO-105	Real-Time Predicted Propulsion and Attitude Data and Associated Timelines	12/14/72
S&E-AERO-106	Pertinent State Vectors Determined in Real-Time by GSFC and MSC and Associated Terminal Conditions	12/7/72
S&E-AERO-107	Postflight Tracking Data, C-Band and USB Measured Parameters	12/13/72
S&E-AERO-109	Postflight S-IVB Telemetered Guidance Velocity and Vehicle Attitude Data and Associated Timelines from Translunar Injection to Loss of Telemetry	1/31/73
S&E-AERO-110	S-IVB Spent Stage Predicted Disposal Trajectory	12/22/72
S&E-AERO-111	S-IVB Spent Stage Preflight Targeting Objectives	10/1/72

SECTION 1

INTRODUCTION AND SUMMARY

The AS-512 flight (Apollo 17 mission) was launched at 05:33:00 GMT on December 7, 1972. S-IVB stage reignition occurred during the first TLI opportunity and the second burn of the S-IVB stage injected the spacecraft onto a translunar trajectory. Following translunar injection, the Command and Service Module (CSM) was separated and docked with the Lunar Module (LM) and the combination was ejected from the S-IVB/IU stage. A series of maneuvers of the S-IVB/IU spent stage followed resulting in a lunar impact trajectory. This report discusses the reconstruction of the different maneuvers experienced by the spent stage, the analysis of tracking data from the Spaceflight Tracking and Data Network (STDN), the resulting best-estimate trajectory, and the associated lunar impact point.

The AS-512 S-IVB/IU lunar impact mission objectives are:

a. The lunar impact point should be within 350 km of the preselected target at 7.0 degrees south latitude and 8.0 degrees west longitude.

b. The actual impact point should be determined within 5 km (0.165 degree).

c. The time of impact should be determined within 1 second.

All three mission objectives have been met. The S-IVB/IU impacted the lunar surface at

4.23 ± 0.09 degrees south latitude and
12.36 ± 0.05 degrees west longitude at
20:32:41 ± 0.05 seconds on December 10, 1972.

This location, determined by trajectory reconstruction, is 156 km northwest of the target and is within the 350-km mission objective. The lunar impact point is considered accurate in position to within 3 km. The time quoted above is taken from the loss of signal time at five tracking sites of the STDN network.

During the Apollo 17 mission, the Lunar Impact Team (LIT) elected to conserve APS propellant by selecting a more efficient attitude and a shorter burn time for the first APS lunar targeting burn. Also during the mission, Johnson Space Center (JSC) reported perturbing accelerations acting on the vehicle.

SECTION 1 (Continued)

Real-time orbit determination using data immediately after APS-1 indicated the S-IVB/IU would impact outside the target region. Based on this data, the LIT specified a second APS targeting burn to place the S-IVB/IU onto a trajectory to the desired impact point.

After the second APS targeting burn, the S-IVB/IU was placed in a three-axis tumble mode to distribute both solar heating and onboard forces. During this passive thermal control (PTC) mode tracking data indicates that the vehicle experienced rotational and translational accelerations.

The lunar impact conditions, together with several items of significance derived from the analysis and the best-estimate trajectory, are described in Section 2. The data used in the analysis and the accuracy of the best-estimate trajectory are discussed in Section 3. All times quoted in this report are Greenwich Mean Time (GMT). The ephemeris used for the analysis is JPL DE19 with a time correction of 43.18 seconds. Latitude and longitude in this report are quoted as positive north and east, respectively, unless otherwise noted.

Appendix A describes the methods used to analyze the tracking data and the Instrument Unit's velocity measurements. Appendix B contains the equations which model the tumbling S-IVB/IU, range-rate modulation and integration of body-fixed forces. Appendix C presents a time history of trajectory parameters from CSM/LV separation to lunar impact. The lunar impact point and associated data presented in this report supersedes the data presented in Reference 1.

SECTION 2

BEST-ESTIMATE TRAJECTORY AND LUNAR IMPACT MANEUVERS DISCUSSION

The AS-512 S-IVB/IU trajectory presented in this report represents the best estimate of the actual trajectory. A list of significant events associated with this trajectory is presented in Table 2-I. Appendix C contains a listing of significant parameters of the trajectory at selected time points from CSM/LV separation to lunar impact.

The following three periods of flight were established for the purpose of reconstructing the best-estimate trajectory listed in Appendix C.

a. Pre-PTC Time Arc - from CSM/LV separation (9:15:28, December 7, 1972) to PTC initiation (17:04:50, December 7, 1972)

b. Early PTC Time Arc - from PTC Initiation until 22:00:00, December 8, 1972.

c. Late PTC Time Arc - from 22:00:00, December 8, 1972, until lunar impact (20:32:41, December 10, 1972).

Tracking data during these three time arcs were used with the Lunar Impact Determination (LID) program to determine associated best-estimate trajectory segments. Appendix A contains a brief description of the LID program.

This section discusses the following four areas of significant interest with the trajectory information derived from the three trajectory segments associated with the time arcs listed above:

a. CSM/LM Docking, Ejection, and S-IVB/IU Evasive Maneuvers.

b. Safing (CVS Venting and LOX Dump) and Lunar Impact Targeting Maneuvers.

c. Passive Thermal Control and Perturbations.

d. Lunar Impact Conditions.

Although the prime objective of this report is to present the findings associated with item (d) above, this analysis is extended to provide a reconstruction of the various maneuvers noted in items (a) through (c) above.

SECTION 2 (Continued)

Figure 2-1 presents line-of-sight range-rate residuals from the Ascension (ACN3) USB tracking station. Residuals are obtained by differencing observed range and range-rate data from a tracking station with calculated range and range-rate data from a sophisticated orbital model fitting portions of the data (observed minus calculated).

The residuals at the top of Figure 2-1 graphically depict the major S-IVB/IU velocity changes arising from the different maneuvers, while the residuals at the bottom of Figure 2-1 show the results of including a model of velocity changes during the pre-PTC time arc. Telemetered IU accelerometer data after CSM/LV separation were used to assist in reconstructing the various maneuvers depicted in Figure 2-1. Also, a small constant non-gravitational acceleration was required between the APS burns in order to properly fit the model to the data. The resulting residuals with the maneuvers and the perturbing acceleration have a magnitude of 100 mm/s or less during the entire pre-PTC tracking arc and indicate the validity of the reconstruction.

Table 2-II summarizes the significant reconstructed maneuvers experienced by the S-IVB/IU following CSM/LV separation. The calculated directions of the accelerations caused by the maneuvers are also presented in Table 2-II for comparison with the platform gimbal angles.

Figure 2-2 shows the accumulated AS-512 Instrument Unit platform velocity data during the time period from CSM/LV separation through the APS lunar impact burns. Figure 2-3 provides two platform gimbal angles during the same time period.

2.1 CSM/LM DOCKING, EJECTION, AND EVASIVE MANEUVERS

CSM/LV separation occurred at 09:15:28, December 7, 1972, and docking occurred 883 seconds later at 09:30:11. CSM/LM ejection occurred at 10:18:02 with the APS evasive burn attitude maneuver initiated 422 seconds later at 10:25:04. The 80-second APS evasive burn was initiated at 10:36:01, one second later than Timebase 8 initiation.

The reconstructions of the ejection and evasive burn maneuvers are depicted in Table 2-II. The reconstructed ejection pitch and yaw angles differ by 11 and 3 degrees, respectively, from the platform gimbal angles. Since the velocity change is not too large, these differences are not significant. The reconstructed evasive burn attitude compares well with the platform gimbal angles.

2.2 SAFING AND LUNAR IMPACT TARGETING MANEUVERS

Following the APS evasive burn, a LOX dump attitude maneuver was initiated at 10:45:40 (see Figure 2-3). A 300-second CVS vent was initiated at 10:52:40, December 7, 1972, and 280 seconds later the 48-second LOX dump was initiated at 10:57:20.

The Lunar Targeting Team decided (in real time) to place the S-IVB/IU in a more effective attitude for the first APS lunar targeting burn (APS-1) in order to conserve APS propellant. The maneuver to this new attitude was initiated at 11:35:26 and the 98-second APS-1 burn was initiated 454 seconds later at 11:43:00, December 7, 1972.

Following the APS-1 burn, the S-IVB/IU was maneuvered to a communications attitude at 11:50:45, December 7, 1972.

Although onboard trajectory perturbing mechanisms such as the thermal control system sublimator were inhibited where possible, JSC reported difficulty in the real-time post APS-1 orbit determination due to onboard perturbations. These perturbations were solved for using the LID program by modeling a constant acceleration between the APS burns. The solved for acceleration needed to fit the model to the tracking data was on the order of 0.1 mm/s^2. These effects may in part be due to the IU gas bearing system venting and associated APS attitude control firings. Calculations yield approximately 0.02 mm/s^2 theoretical acceleration from this combination. Because JSC experienced real-time orbit determination difficulties due to these perturbations, the planned contingency delay of 1 hour for targeting the second APS impact burn (APS-2) was incorporated.

Upon completion of the post APS-1 orbit determination, JSC reported the S-IVB/IU would impact the moon at 9.64 degrees south latitude and 15.29 degrees east longitude, 678 ± 300 km from the target.

The LIT at MSFC generated the specification for an APS-2 burn. At 16:35:40, December 7, 1972, the S-IVB/IU was maneuvered to the APS-2 attitude and 740 seconds later at 16:48:00 the 102-second APS-2 burn was initiated.

The reconstruction of the CVS Vent, LOX Dump, APS-1, and APS-2 maneuvers is depicted in Table 2-II. The reconstructed pitch and yaw angles for the CVS vent differ from the platform gimbal angles by 4 and 17 degrees, respectively. This may indicate the CVS velocity change is not along the longitudinal axis of the vehicle but, since the accelerometer changes are quite small, these differences may not be significant. The reconstructed LOX dump and APS burns pitch and yaw angles compare favorably with the platform gimbal angles.

2.3 PASSIVE THERMAL CONTROL AND PERTURBATIONS

Following the APS-2 lunar impact burn, S-IVB/IU stage roll, pitch, and yaw body rates of +0.5 degree/second, -0.3 degree/second, and -0.3 degree/second, respectively, were commanded at 17:04:50, December 7, 1972, to initiate a three-axis tumbling motion. Approximately 22 seconds later, at 17:05:12 the flight control computer was commanded off leaving the S-IVB/IU stage with a rotational motion about the C-G. This rotational motion provided passive thermal control (PTC). Also, the three-axis tumbling motion was planned to minimize the translational effect of any S-IVB/IU stage related perturbing forces by distributing their effects in all directions about the coasting stage's C.G. motion.

Appendix B presents a mathematical model of the tumbling S-IVB/IU. Equations for the range-rate modulations and for the inertial integration of body-fixed translational accelerations are included in Appendix B. These equations were incorporated in a computer program and several cases studying the three-axis tumbling motion were done. Two important conclusions were reached.

a. In order to accomplish the significant changes in the range-rate modulation as seen on Apollo 17 and previous vehicles either in amplitude or period, onboard torques are required.

b. The tumble motion as commanded on Apollo 17 and previous vehicles does not completely distribute body-fixed forces in all directions. Therefore, there are net accumulated translational effects.

One study case of particular interest showed that an acceleration of 1 mm/s^2 along the longitudinal axis of the vehicle resulted in an accumulated inertial velocity change of 1.5 m/s in a 10-hour period. This velocity change contrasts with a 36 m/s change for the same acceleration without the PTC maneuver.

Both rotational torques and translational accelerations are observed in the Apollo 17 tracking data following PTC initiation.

Figure 2-4 presents range-rate residuals showing the first 24 hours of PTC tumble. This plot was made continuous by combining residual plots from four range-rate trackers (Madrid USB, Goldstone DSN, Tidbinbilla DSN, and Bermuda USB). The initial tumble rate of 5.2 cph (0.52 degree per second) is close to the commanded pitch, yaw, and roll rates. Following PTC, a 14- to 16-hour period occurs during which the tumble changes from a "three-axis" rotation to a "spin/precession" rotation. Figure 2-5 shows Madrid USB, Canberra

2.3 (Continued)

USB, and Greenbelt USB range-rate residuals 20 hours, 41 hours, and 74 hours after PTC initiation, respectively. At 20 hours after PTC initiation, the S-IVB/IU had a spin rate around the longitudinal axis of 14.5 cph (1.45 degrees per second) and a precession rate of 5 cph (0.5 degree per second). During the next 55.5 hours to impact, the nature of the tumble changed little. The spin rate increased to 21 cph (2.1 degrees per second) and the precession rate increased to 6.5 cph (0.65 degree per second). The amplitude and period changes depicted in Figures 2-4 and 2-5 are significant. These changes indicate the presence of perturbing moments.

The residuals at the top of Figure 2-6 show the presence of non-gravitational accelerations after PTC initiation. Figure 2-6 compares Greenbelt USB, Ascension USB and Guam USB range-rate residuals for a gravity-only trajectory with range-rate residuals for a trajectory modeling perturbing forces. The trajectory associated with the residuals at the top of Figure 2-6 was produced by fitting data after 22:00:00, December 8, with a gravity-only model. The deviations in the residuals before 22:00:00 indicate that non-gravitational forces acted on the S-IVB/IU. The trajectory associated with the residuals at the bottom of Figure 2-6 was produced by letting the LID program solve for non-gravitational accelerations from 16:49:42, December 7, to lunar impact. The improvement in the residuals confirms the presence of perturbing influences acting on the vehicle. The resulting non-gravitational accelerations are presented in Table 2-III. The associated analysis is discussed in Paragraph 3.2.2.

2.4 LUNAR IMPACT CONDITIONS

The AS-512 S-IVB/IU impacted the lunar surface on December 10, 1972, at 20:32:41 ± 0.05 second. The impact coordinates derived from the best-estimate trajectory are:

4.23 ± 0.09 degrees south latitude and
12.36 ± 0.05 degrees west longitude.

The impact point is 156 km northwest of the targeted point, 337 km east of the Apollo 12 seismometer, 156 km east of the Apollo 14 seismometer, 1,032 km southwest of the Apollo 15 seismometer and 851 km west of the Apollo 16 seismometer. The final impact point is plotted in Figure 2-7 along with other points of interest. Table 2-IV presents a description of the stage and trajectory parameters at impact. Figure 2-8 defines the incoming heading angle and the impact angle.

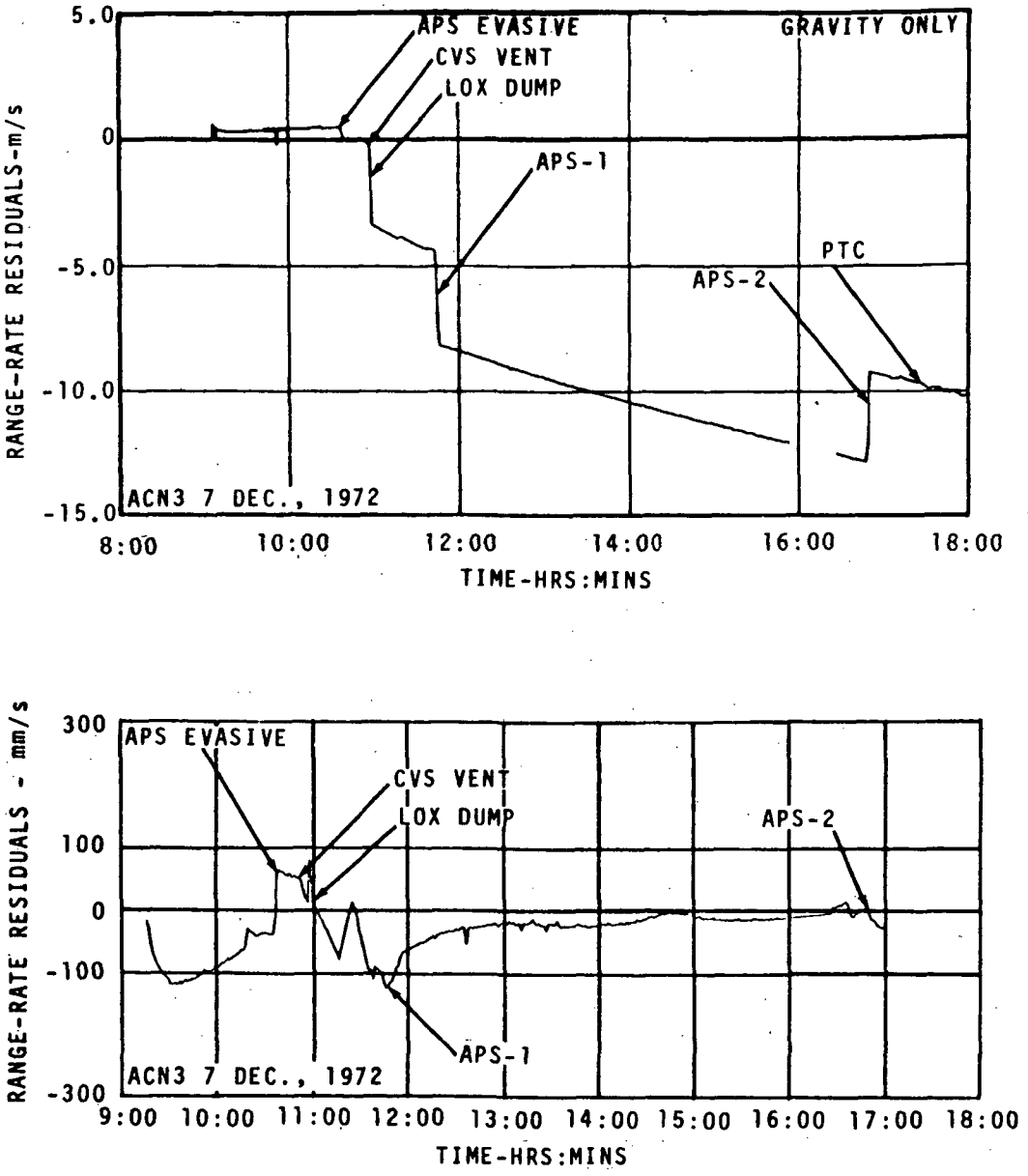

FIGURE 2-1. TRANSLUNAR COAST MANEUVERS OVERVIEW

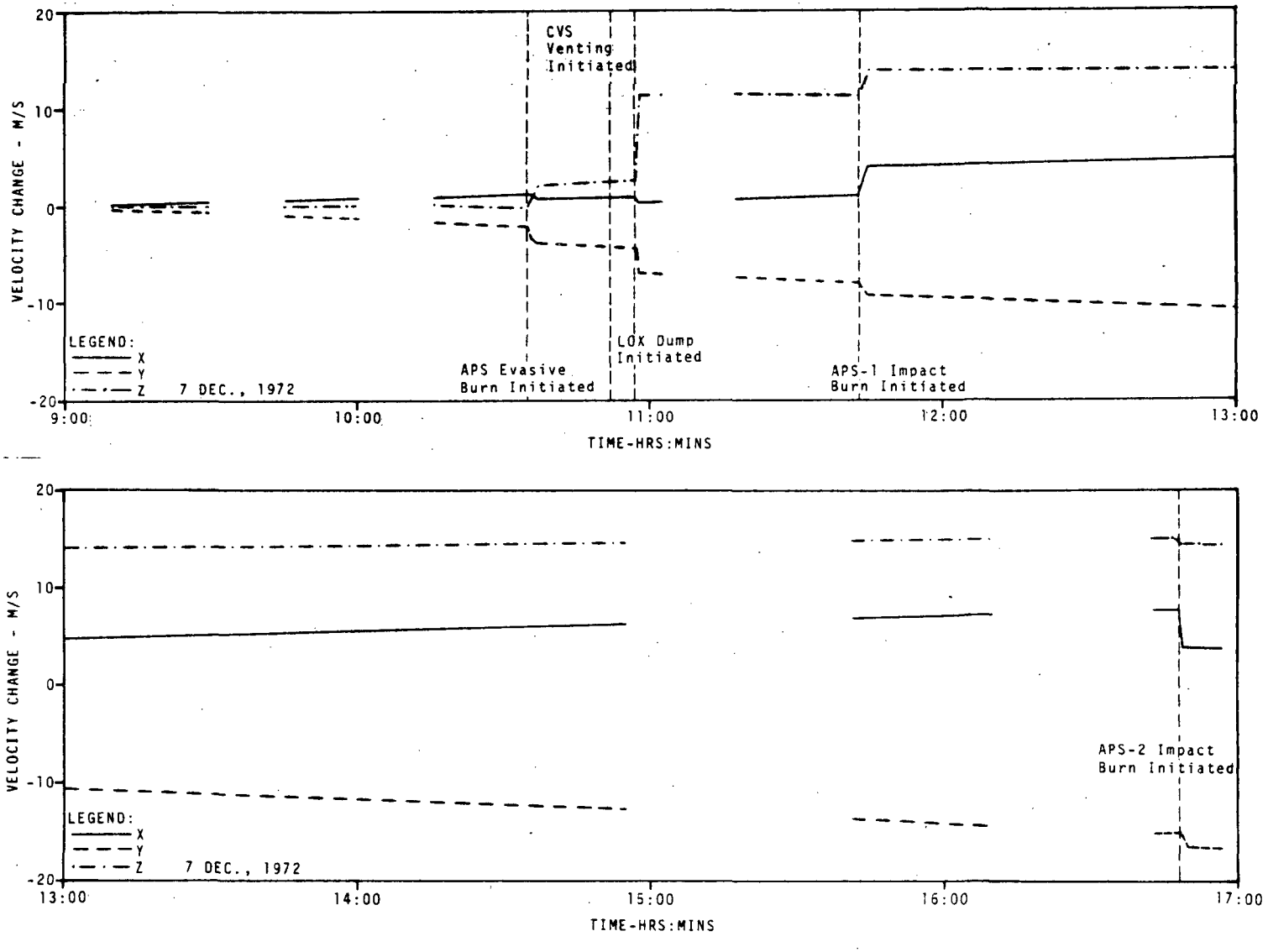

FIGURE 2-2. AS-512 INSTRUMENT UNIT PLATFORM VELOCITY ACCUMULATION DURING LUNAR IMPACT TARGETING

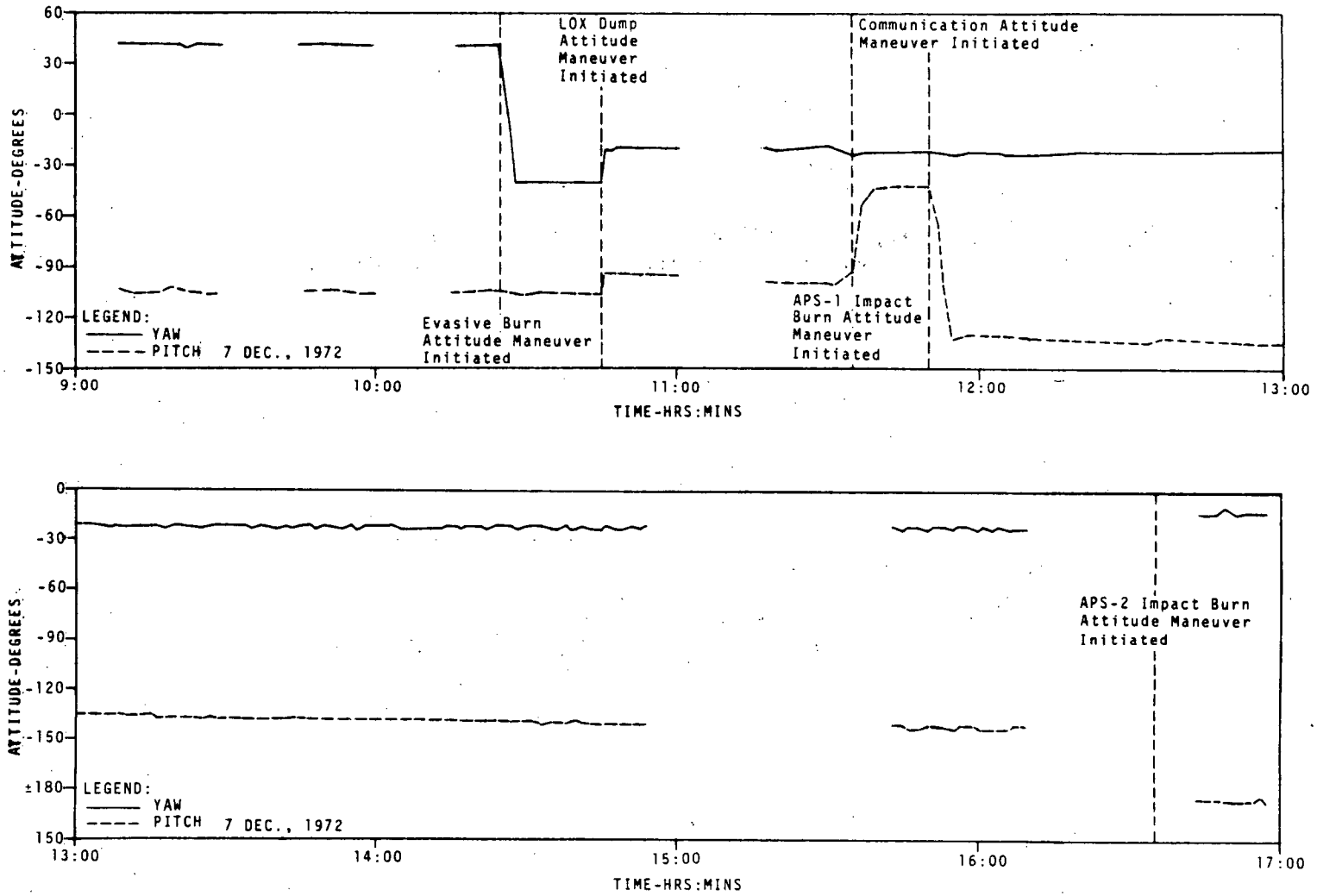

FIGURE 2-3. AS-512 INSTRUMENT UNIT PLATFORM GIMBAL ANGLES DURING LUNAR IMPACT TARGETING

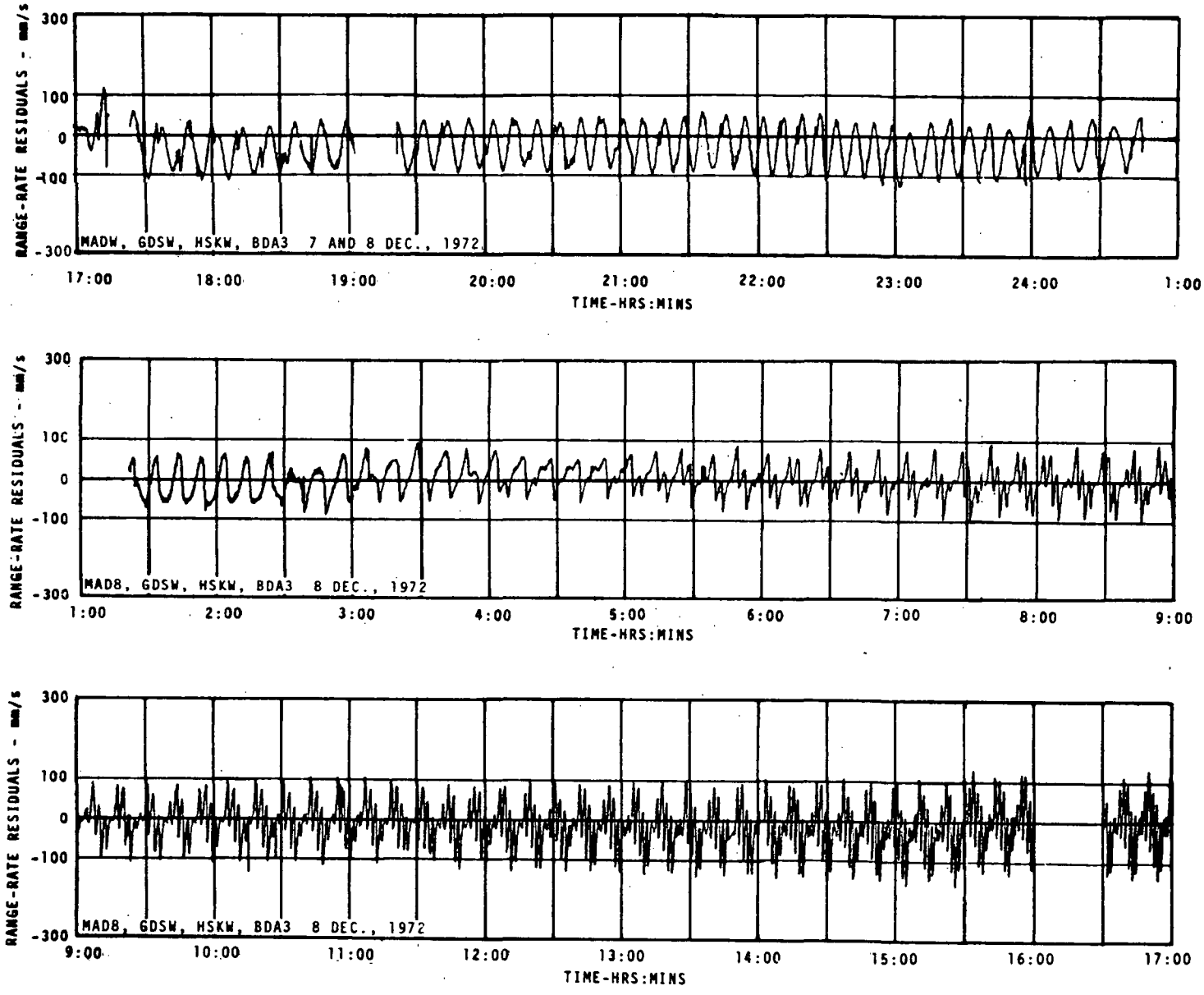

FIGURE 2-4. EARLY PTC TUMBLE RESIDUALS

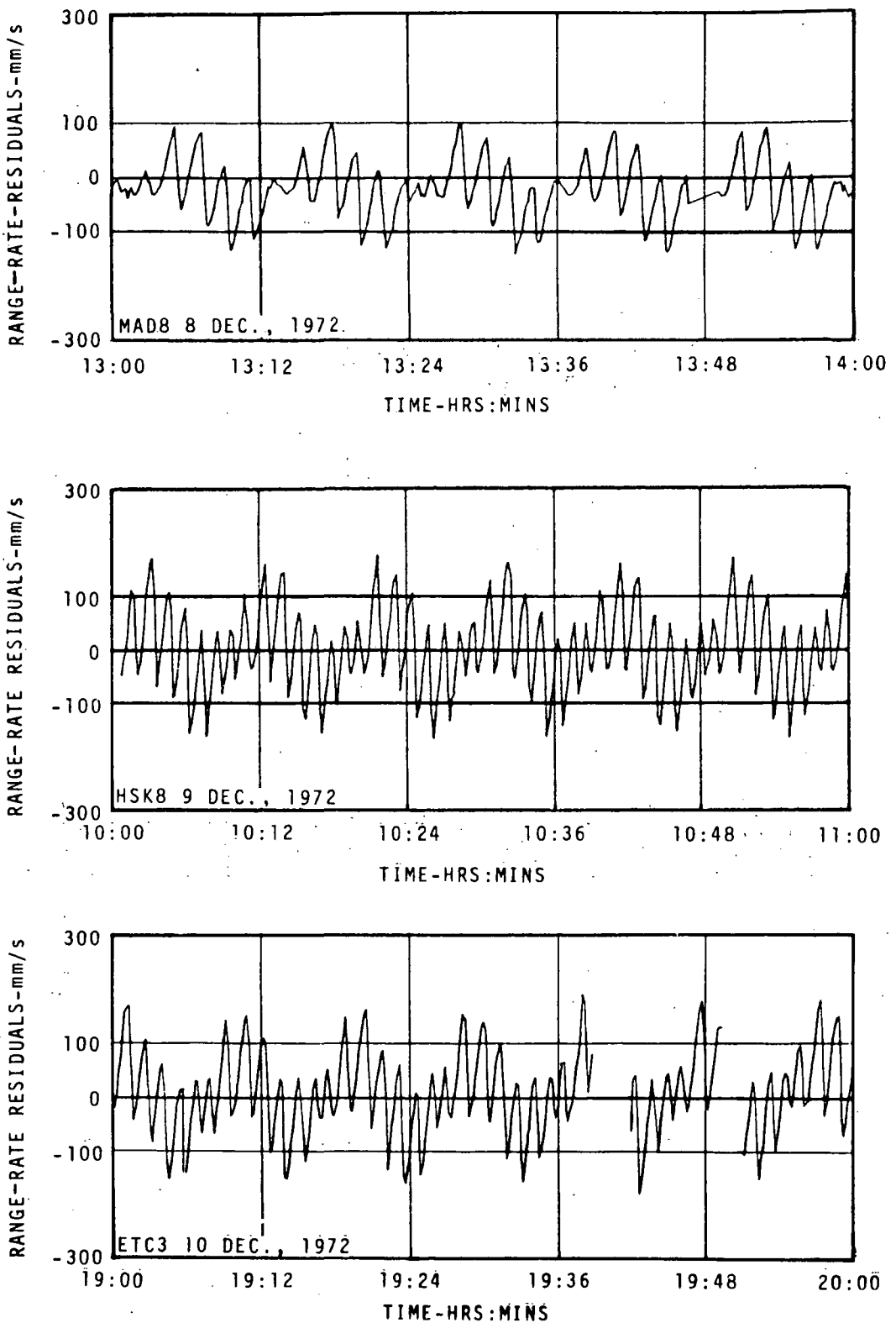

FIGURE 2-5. LATE PTC TUMBLE RESIDUALS

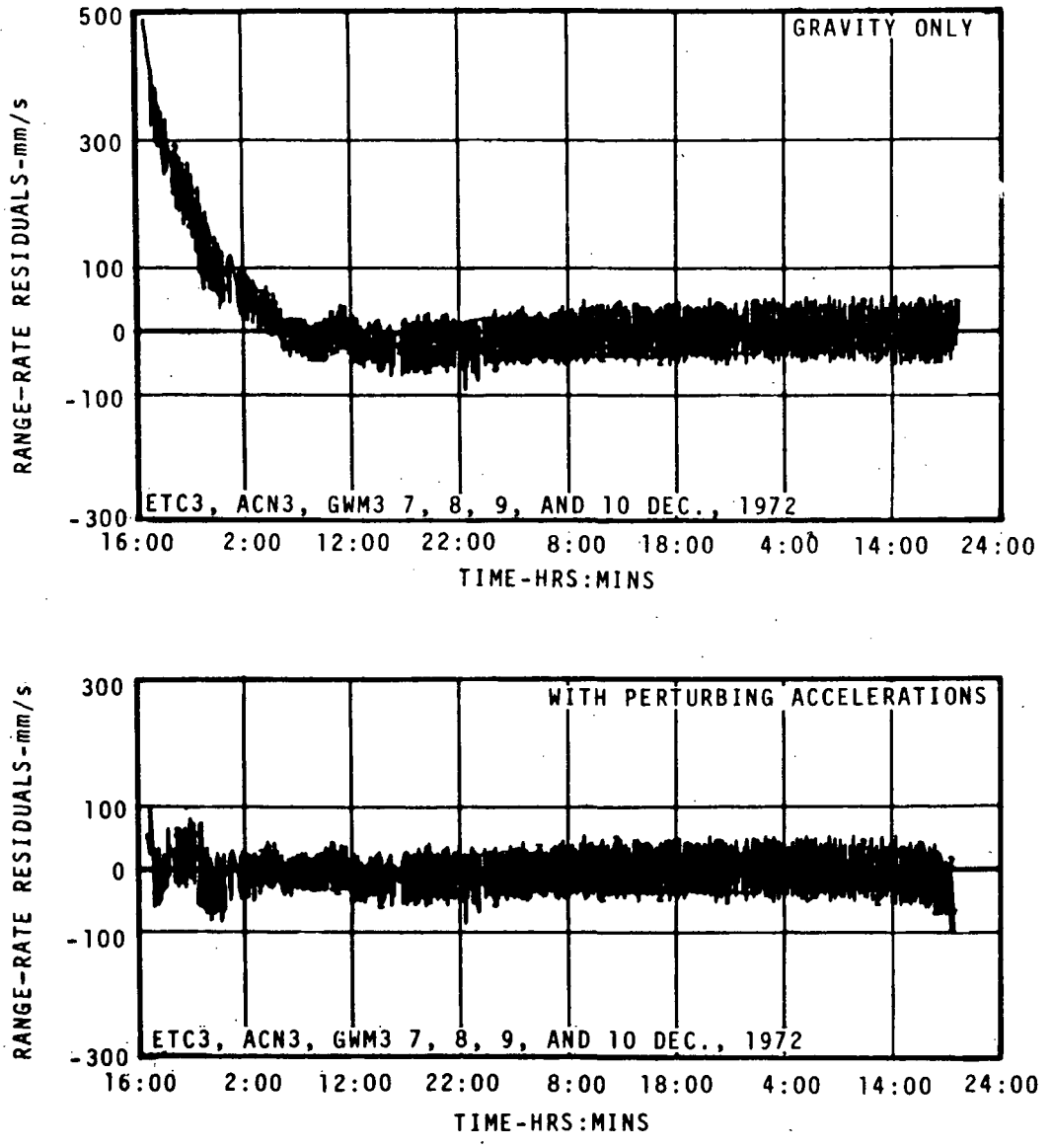

FIGURE 2-6. COMPARISON OF GRAVITY-ONLY AND PERTURBED TRAJECTORY RESIDUALS

POINT	DESCRIPTION	LAT-DEG	LONG-DEG
I	IMPACT	-4.23	-12.36
T	TARGET	-7.00	-8.00
12	APOLLO 12 SEISMOMETER	-3.04	-23.42
14	APOLLO 14 SEISMOMETER	-3.67	-17.47
15	APOLLO 15 SEISMOMETER	26.07	3.65
16	APOLLO 16 SEISMOMETER	-8.97	15.51

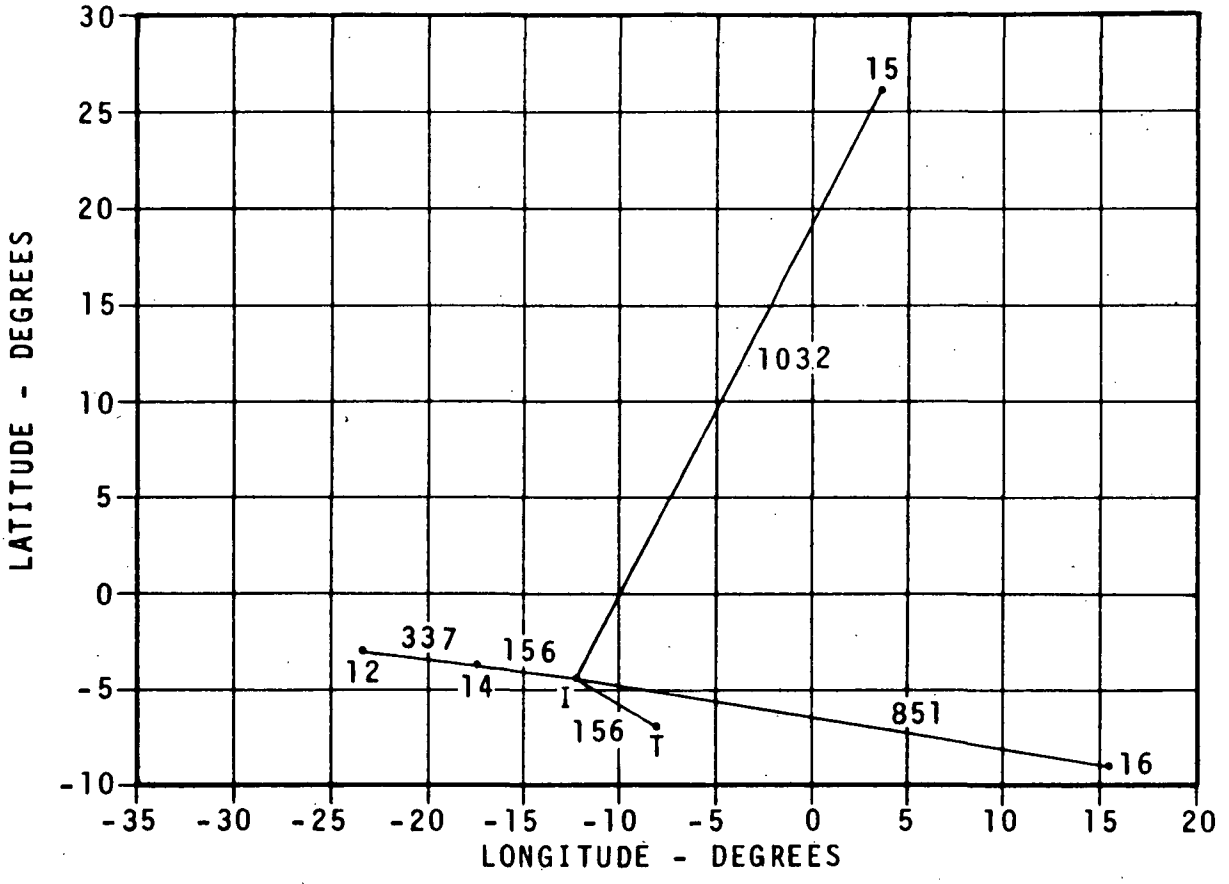

NOTE: DISTANCES FROM IMPACT POINT IN KILOMETERS

FIGURE 2-7. APOLLO 17 LUNAR LANDMARKS

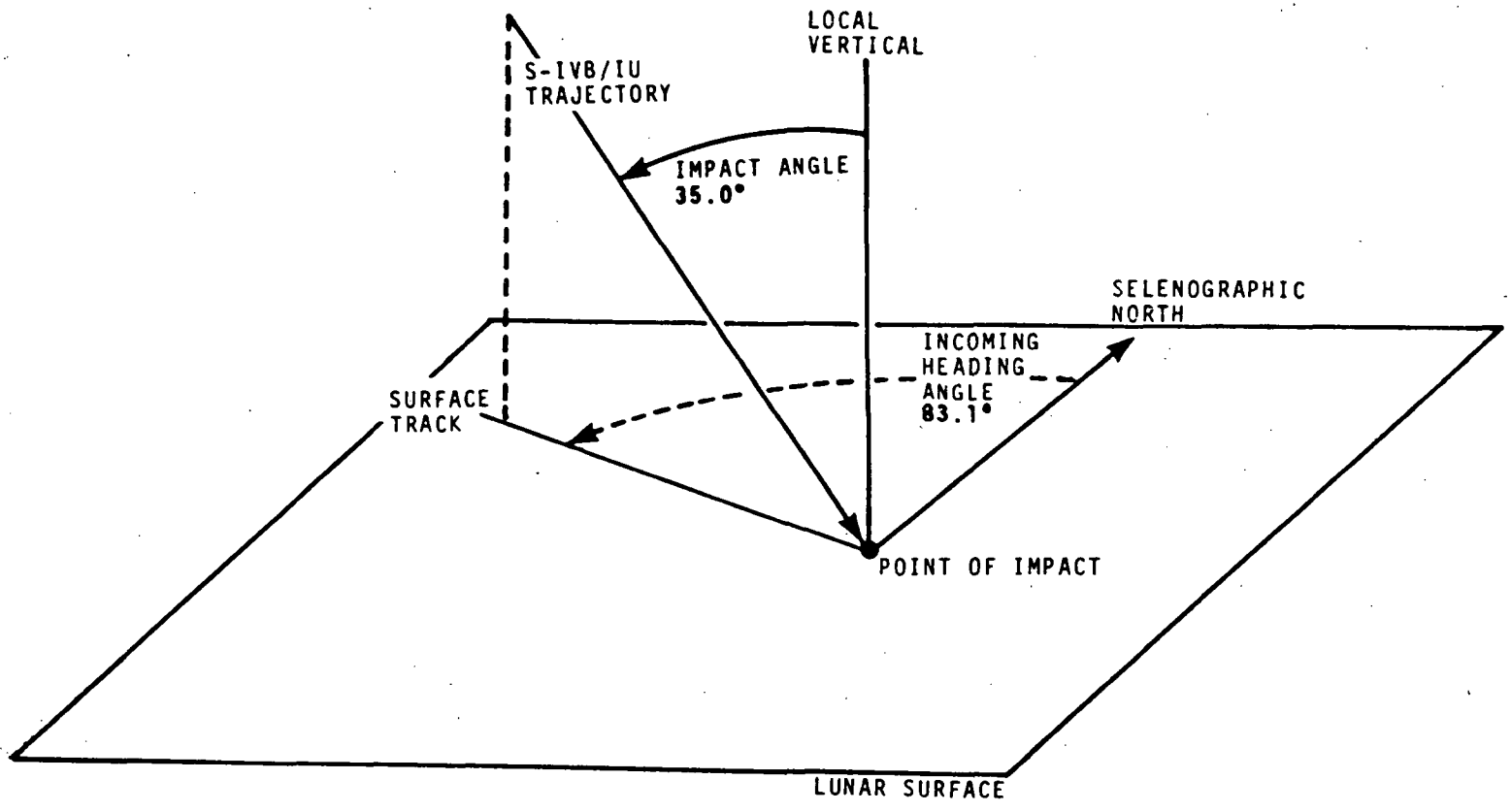

FIGURE 2-8. AS-512 S-IVB/IU LUNAR IMPACT HEADING AND IMPACT ANGLES

TABLE 2-I. SIGNIFICANT EVENT TIMES

EVENT	GREENWICH MEAN TIME HR:MIN:SEC	RANGE TIME HR:MIN:SEC
Range Zero	7 December 1972 05:33:00	00:00:00
CSM/LV Separated	09:15:28	03:42:28
CSM/LM Docked	09:30:11	03:57:11
CSM/LM Ejected	10:18:02	04:45:02
Evasive Burn Attitude Maneuver Initiated	10:25:04	04:52:04
Timebase 8 Initiated	10:36:00	05:03:00
APS Evasive Burn Initiated	10:36:01	05:03:01
LOX Dump Attitude Maneuver Initiated	10:45:40	05:12:40
CVS Venting Initiated	10:52:40	05:29:40
LOX Dump Initiated	10:57:20	05:24:01
APS-1 Impact Burn Attitude Maneuver Initiated	11:35:26	06:02:26
APS-1 Impact Burn Initiated	11:43:00	06:10:00
Communication Attitude Maneuver Initiated	11:50:45	06:17:45
APS-2 Impact Burn Attitude Maneuver Initiated	16:35:40	11:02:40
APS-2 Impact Burn Initiated	16:48:00	11:15:00
PTC Commanded	17:04:50	11:31:50
Lunar Surface Impacted	10 December 1972 20:32:41	86:59:41

TABLE 2-II. RECONSTRUCTED LUNAR IMPACT MANEUVERS

PARAMETER	CSM/LM EJECTION	APS EVASIVE BURN	CVS VENT	LOX DUMP	APS-1 IMPACT BURN	APS-2 IMPACT BURN
Initiation 7 December Hr:Min:Sec	10:18:02	10:36:01	10:52:40	10:57:20	11:43:00	16:48:00
Duration, sec	20*	80	280	48	98	102
PACSS13 Acceleration						
$\ddot{X}$, mm/s^2	5.000	-5.875	-0.250	-12.710	29.080	-41.470
$\ddot{Y}$, mm/s^2	-8.500	-22.500	-0.054	-54.170	-14.280	-6.667
$\ddot{Z}$, mm/s^2	-10.000	27.750	1.642	181.200	25.920	-2.745
Velocity Change, M/S	0.281	2.896	0.465	9.098	4.066	4.293
effective pitch, deg	-117	-102	-99	-94	-42	176
effective yaw, deg	37	-38	-2	-17	-20	-9
Vehicle Gimbal Angles						
pitch, deg	-106	-104	-95	-95	-43	176
yaw, deg	40	-40	-19	-19	-22	-11

*Arbitrary duration

NOTE: The IU platform (and PACSS13) were aligned as follows:
X-axis vertical up from Pad 39A (28.608422° latitude and -80.604133° longitude) at 5:32:53:04 on 7 December 1972; Z-axis downrange along a 91.503° launch azimuth; Y-axis completes the right hand system.

TABLE 2-III. PERTURBING ACCELERATION DURING PTC

START	STOP	$\ddot{X}_{13}$ mm/s^2	$\ddot{Y}_{13}$ mm/s^2	$\ddot{Z}_{13}$ mm/s^2	$\|A\|$ mm/s^2
7 December 1972 16:49:42 (PTC Start)	7 December 1972 23:30:00	0.0047	-0.0218	-0.0067	0.0233
7 December 1972 23:30:00	8 December 1972 07:00:00	0.0095	-0.0218	-0.0077	0.0250
8 December 1972 07:00:00	8 December 1972 22:00:00	0.0079	0.0032	-0.0074	0.0113
8 December 1972 22:00:00	10 December 1972 20:32:41	-0.0008	-0.0007	0.0005	0.0012

TABLE 2-IV. STAGE AND TRAJECTORY IMPACT PARAMETERS

PARAMETER	VALUE
Dry Stage Mass, kg	∿13,973
Velocity Relative to Surface, km/s	2.544
Kinetic Energy, joules	$\sim 46 \times 10^9$
Impact Angle Measured from Vertical, deg	35.0
Incoming Heading Angle Measured from North to West, deg	83.1
Lunar Radius at Impact Point, km	1,738.44
Selenographic Longitude, deg	-12.36
Selenographic Latitude, deg	-4.23
Impact Time, Hr:Min:Sec, on 10 December 1972	20:32:41
Distance to Target, km	156
Distance to Apollo 12 Seismometer, km	337
Distance to Apollo 14 Seismometer, km	156
Distance to Apollo 15 Seismometer, km	1,032
Distance to Apollo 16 Seismometer, km	851

THIS PAGE LEFT BLANK INTENTIONALLY

SECTION 3

BEST-ESTIMATE TRAJECTORY DETERMINATION

The best-estimate trajectory determined in this analysis consists of three separate trajectory segments corresponding to the three time arcs outlined in Section 2. The available tracking data were used appropriately to determine initial state vectors with components consisting of selected combinations of initial positions, velocities, and where needed, acceleration biases over chosen time periods. The initial position and velocity values were then propagated forward by integrating the LID program model equations with the solved-for acceleration biases. The trajectory listing presented in Appendix C was derived from these three separate trajectory segments.

This section discusses the data used in the analysis, the reconstruction of the three trajectory segments, the associated data residuals, and the estimated accuracy of the different segments. This section also establishes the basis for the quoted uncertainty in the impact point.

3.1 DATA UTILIZATION

The tracking data used for this analysis was selected from two C-band and thirteen USB tracking stations listed in Table 3-I. The station locations listed in this table are taken from Reference 2. The time arcs of the data available for this analysis are shown in bar chart form in Figure 3-1 for both range-rate and range data. Different portions of the data were used to establish the separate trajectory segments as discussed below.

3.1.1 Pre-PTC Time Arc Data Utilization

The best estimate of the pre-PTC segment was established from 1,125 range-rate measurements from five USB tracking stations plus 95 range measurements from one C-band tracking station and one USB tracking station. The breakdown by station and the time arcs of data used are presented in Table 3-II.

3.1.2 Early PTC Time Arc Data Utilization

The best estimate of the early PTC segment was established from 1,479 range-rate measurements from thirteen USB stations and 360 range measurements from three USB stations. The breakdown by station and time arcs of the data used are shown in Table 3-III.

3.1.3 Late PTC Time Arc Data Utilization

The best estimate of the late PTC segment was established from 1,368 selected range-rate measurements from eleven USB tracking stations and 360 range measurements from three USB tracking stations. The breakdown by station and the time arcs of data used are presented in Table 3-IV.

3.2 TRAJECTORY ANALYSIS AND ACCURACY

Each of the trajectory segments composing the best-estimate trajectory was established separately by using the data discussed above.

The quality of a particular trajectory solution can be judged by examining the tracking data residuals. Large residual means or skewness indicates failure to fit the data. These tracking data residuals are obtained by differencing the observed data from a tracking site with calculated data from a tracking model based upon a particular trajectory segment. All tracking data residuals presented in this report consist of differences between observed and calculated quantities (O-C).

3.2.1 Pre-PTC Trajectory Segment Analysis and Accuracy

The tracking data outlined in Paragragh 3.1.1, over a time period of 7 hours and 45 minutes which included the modeled maneuvers, were used in the LID program to obtain the pre-PTC trajectory segment. The vehicle state at CSM/LV separation was obtained from the AS-512 launch vehicle postflight trajectory (Reference 3). The LID program generated the pre-PTC trajectory arc included in Appendix C by using the data shown in Table 3-II plus the maneuver models shown in Table 2-II and solving for an acceleration of 0.1 mm/s^2 from the termination of APS-1 to the initiation of APS-2.

Figures 3-2 and 3-3 depict the range-rate residuals from the Ascension (ACN3), Madrid (MADW), Carnarvon (CRO3), Bermuda (BDA3), and Merritt Island (MIL3) tracking stations during the pre-PTC arc. Figure 3-4 depicts the range residuals for Carnarvon (CROQ) and Madrid (MADW) tracking stations. The residual statistics for the pre-PTC data are given in Table 3-II. The accuracies of the pre-PTC trajectory segment are estimated to be within ±1.5 kilometers in radius magnitude and ±1.5 m/s in velocity magnitude.

3.2.2 Early PTC Trajectory Segment Analysis and Accuracy

The tracking data outlined in Paragraph 3.1.2, over a period of 76 hours were used to establish the early PTC trajectory

3.2.2 (Continued)

segment and provide the trajectory data in Appendix C from PTC initiation to 18:00:00, December 8, 1972. Preliminary investigations of this trajectory arc indicated non-gravitational forces were acting on the vehicle. Inspections of the time history of the correction to the initial state resulted in selecting three time periods over which different non-gravitational accelerations were permitted to act. The LID program was then used to solve for initial position and velocity vectors and an acceleration vector for each of the three time periods. The three time periods and their accelerations are given in Table 2-III; the fourth entry in this table is discussed in Paragraph 3.2.3. It is to be noted that non-gravitational acceleration continued at a significant level (0.02 mm/s^2) for approximately 15 hours after PTC initiation. After the 15-hour period, the acceleration level reduced 50% for the next 15 hours.

Onboard systems which could contribute to the perturbation are the IU thermal control system (TCS) sublimator, the IU gas bearing system, and the S-IVB LOX chilldown pump purge. The TCS sublimator was inhibited from before APS-1 to after APS-2. However, following APS-2 this system was reactivated and considerable subliming would take place to dissipate the increased system heat. Eventually, the battery voltage should decrease, the water valve stay open and continuous subliming take place until the coolant pump ceases to circulate fluid. Therefore, the sublimator should have a limited lifetime and, coupled with the other subsystem venting, may cause the significant perturbations for the 30-hour time period following PTC initiation shown in Table 2-III.

The range-rate residuals from twelve USB trackers during this arc are shown in Figures 3-5 through 3-15. Note: Only the residual plots prior to 22:00:00, December 8, apply to this trajectory arc. The residuals statistics for the data used while solving for this trajectory segment are shown in Table 3-III.

The accuracies of the trajectory data for the early PTC arc are estimated to be within ±2 kilometers in radius magnitude and ±2 m/s in velocity magnitude near PTC initiation and ±200 meters and ±200 mm/s, respectively, near the end of the segment. The non-gravitational accelerations and time periods given in Table 2-III are to be considered only representative of the actual non-gravitational accelerations.

3.2.3 Late PTC Trajectory Segment Analysis and Accuracy

The tracking data outlined in Paragraph 3.1.3, over a time period of 47 hours before lunar impact, were used in the LID program to obtain the late PTC trajectory segment and provide the trajectory data in Appendix C from 00:00:00, December 9, 1972, to lunar impact. Initial attempts to properly fit the 76 hours of data available after PTC initiation with a gravitational model were not acceptable. Range and range-rate residual statistics and trends plus time histories of changes in the initial state for various gravitational model fits were much greater than desired except for solutions using data only after 22:00:00, December 8, 1972.

The gravitational solutions using data after 22:00:00, December 8, 1972, were marginally acceptable. Table 3-V shows the residual statistics for the best gravitational model fit (see Run 8 in Table 3-VI) of the data over a time arc from 22:00:00, December 8, 1972, to lunar impact. The top of Figure 3-16 shows the range residuals from the three USB tracking stations providing range measurements (Goldstone-GDSW, Tidbinbilla-HSKW, and Madrid-MADW) for the best gravitational fit. Though the range residuals and trends are small, they evidence small non-gravitational forces acting to lunar impact.

In order to improve the data fitting during this trajectory segment, small non-gravitational accelerations were added to the gravitational acceleration model. The LID program was used to solve for a number of initial position and velocity components plus small non-gravitational acceleration biases over various time periods by using different combinations of range and range-rate data over different time arcs and different stations. Table 3-VI gives the impact conditions derived from a set of solutions which have acceptable residual statistics and trends. Run 24 of Table 3-VI represents the best-estimate trajectory for this analysis with the acceleration vector for the trajectory segment shown as the last entry in Table 2-III. This acceleration to impact is equivalent to a force of 0.014 N which is compatible with a tumbling vehicle source (S-IVB LOX chilldown pump purge) estimated to have a force of 0.09 N acting continuously to impact.

Table 3-IV gives a statistical summary of the run selected as the best-estimate trajectory. These residual statistics should be contrasted with the best gravitational fit statistics listed in Table 3-V. Also, the range residuals for the best-estimate trajectory shown at the bottom of Figure 3-16 should be contrasted to those for the best gravity-only fit shown at the top of Figure 3-16. Range residuals for the best-estimate trajectory are shown in Figures 3-16 (at the bottom), 3-17 and

3.2.3 (Continued)

3-18. The range-rate residuals of the best-estimate trajectory for eleven USB trackers are shown in Figures 3-5 through 3-15, 3-18, and 3-19.

The accuracies of this trajectory segment are estimated to be within ±100 meters in radius magnitude and ±50 mm/s in velocity magnitude.

3.3 LUNAR IMPACT POINT ACCURACY

The most accurate quantity associated with the lunar impact parameters is the lunar impact time since direct loss-of-signal times from five USB trackers were recorded. The loss-of-signal times, the transmission delay times, and the calculated impact times are shown in Table 3-VII. Based on these data, the impact time is taken at 20:32:41, December 10, 1972, with an accuracy of ±0.05 seconds. The average of the impact times resulting from the selected trajectory solutions reported in Table 3-VI is somewhat earlier than the actual observed impact time. This discrepancy (equivalent to about 1.5 km) is attributed to errors in the ephemeris and in the quoted local lunar surface elevation. The local lunar radius is reported at 1738.44 km. This radius was input to the LID program and is reflected in the data shown in Appendix C for the impact point.

The final lunar impact point is 4.23 degrees south latitude and 12.36 degrees west longitude. The accuracy of the impact coordinates is conservatively estimated at ±0.09 degree latitude and ±0.05 degree longitude. These accuracies are based upon the variations in latitude and longitude resulting from a large number of lunar impact solutions and on the quality of the late PTC trajectory solution. In particular, the range-rate and range residuals from five tracking stations observing the vehicle just prior to lunar impact are excellent (see Figures 3-18 and 3-19).

Figure 3-20 depicts the best-estimate lunar impact point plus nine other solutions used to verify the best-estimate solution plotted within a rectangular box representing the quoted accuracy of the impact point. It is to be noted that the standard deviations of the impact points for the above 10 runs, listed in Table 3-VI, are well within the quoted accuracy estimates. The combination of the latitude and longitude accuracy estimates gives the 3 km position accuracy quoted for the lunar impact point in Sections 1 and 2.

A check on the 3 km accuracy was made by propagating a scaled covariance matrix of the best-estimate initial state to the

3.3 (Continued)

moon, diagonalizing it, and noting that the largest position related eigenvalue is compatible with the quoted accuracy. The covariance matrix associated with the best-estimate initial state was scaled by multiplying it by the number of observations in order to remove conditional effects due to the observations (see Reference 4). As an additional check, a chi-squared test of a neighboring impact point (Run 46) verifies within a high confidence the hypothesis that the neighboring impact point is a likely member of the ensemble of vectors represented by the scaled position-partitioned covariance matrix of the best-estimate state propagated to the moon (see Reference 5). Since the neighboring run starts at APS-2 and solves for an initial state plus an acceleration history from APS-2 to 22:00:00, December 8, satisfying the hypothesis above lends additional confidence to the overall trajectory reconstruction to impact.

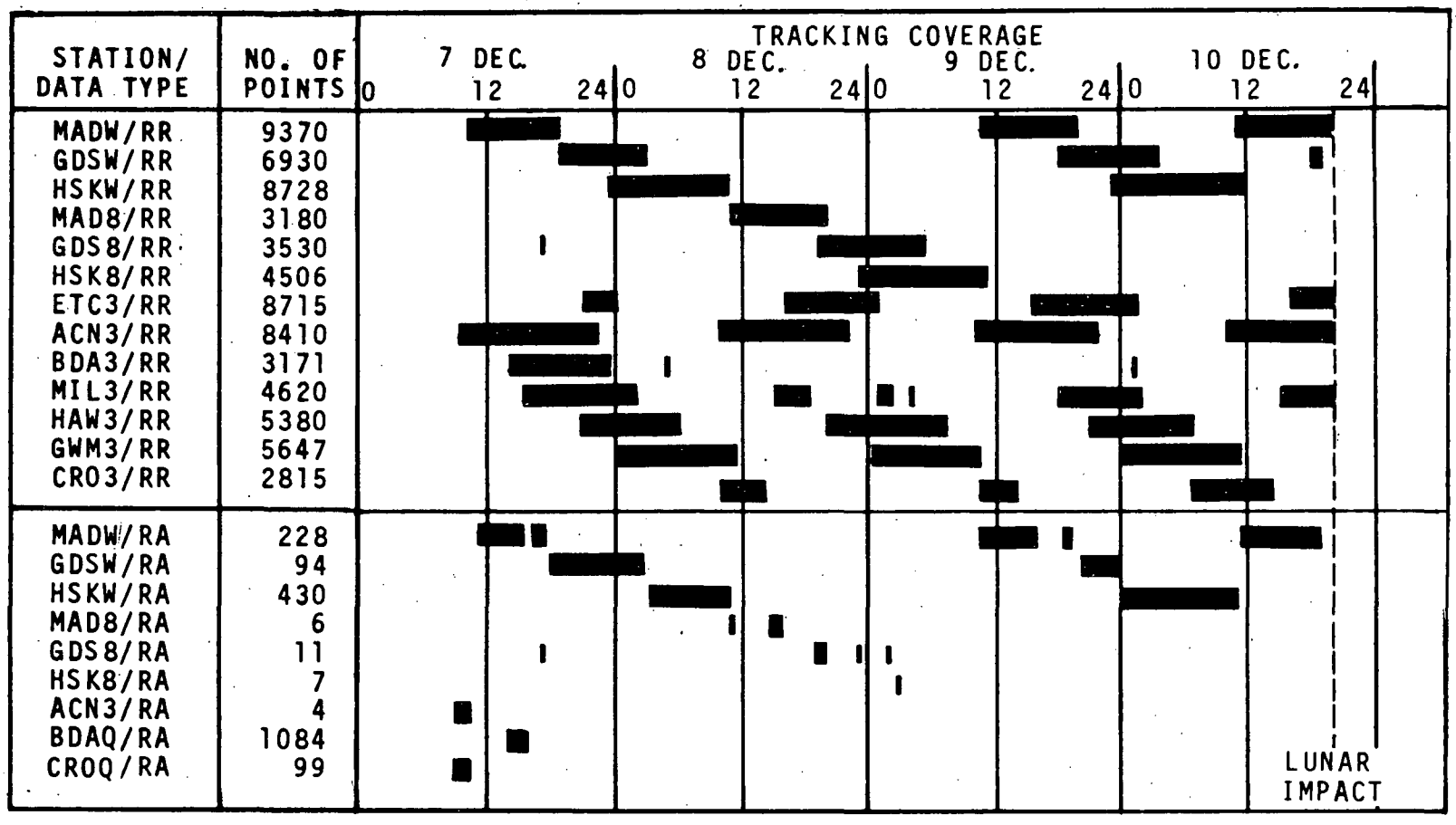

FIGURE 3-1. AS-512 S-IVB/IU TRACKING DATA AVAILABILITY

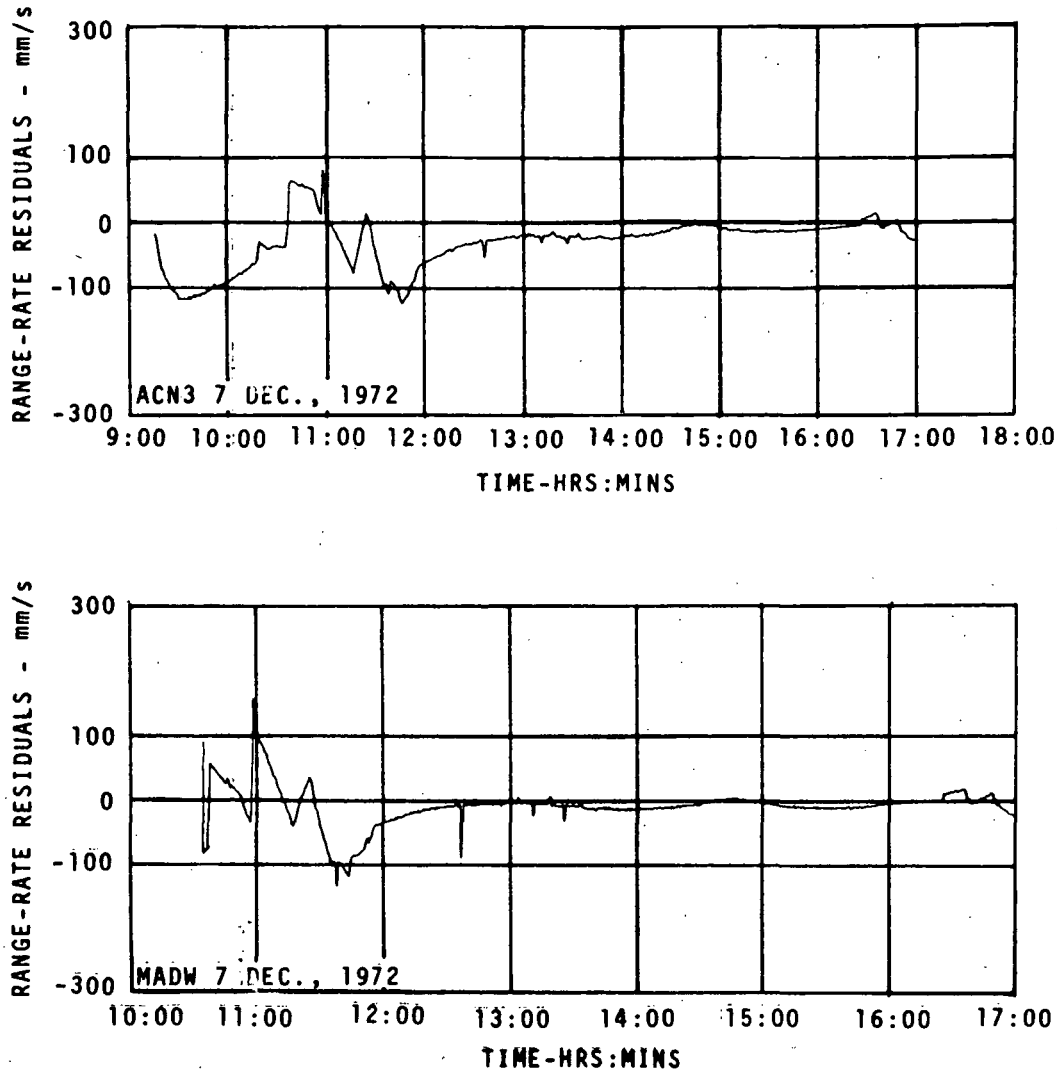

FIGURE 3-2. ASCENSION AND MADRID RANGE-RATE RESIDUALS FOR PRE-PTC DATA FIT

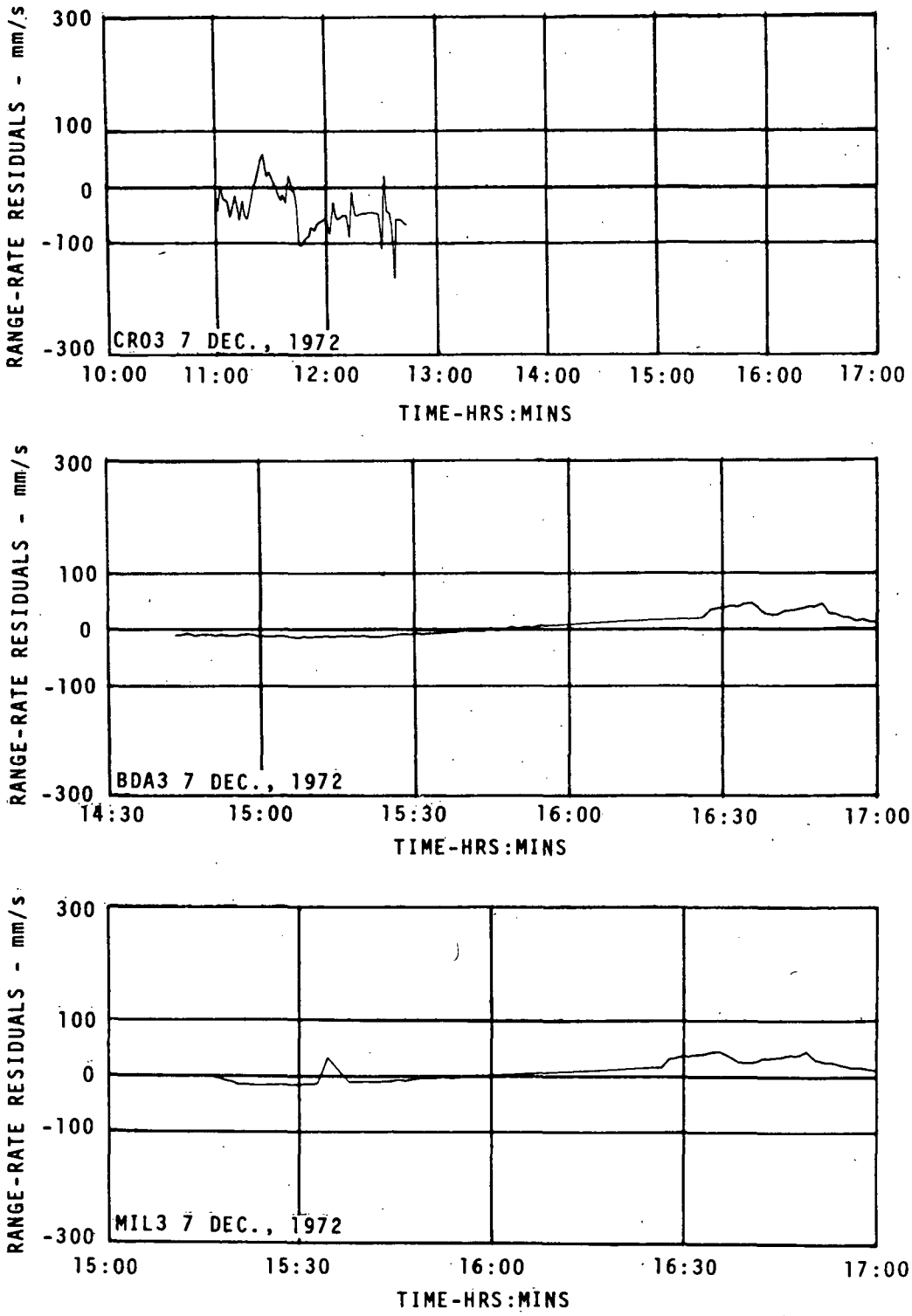

FIGURE 3-3. CARNARVON, BERMUDA AND MERRITT ISLAND RANGE-RATE RESIDUALS FOR PRE-PTC DATA FIT

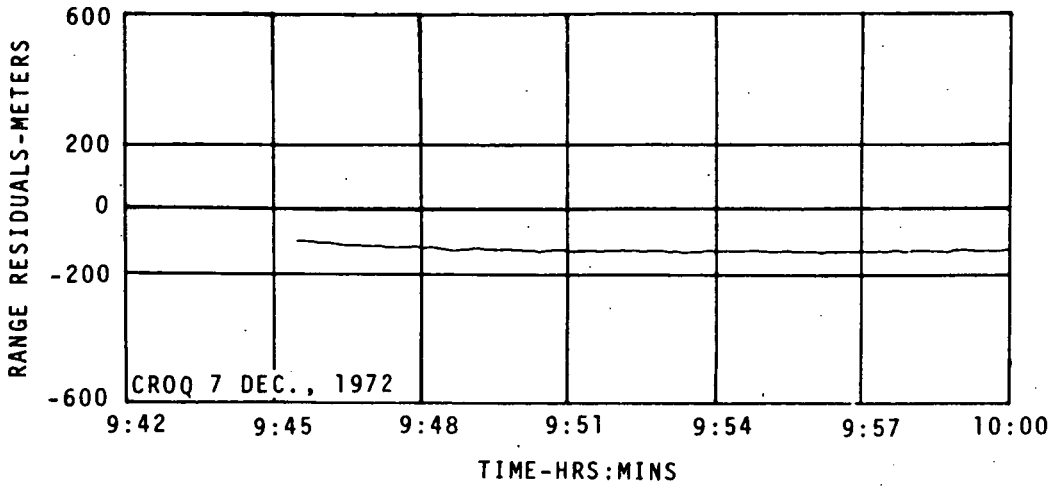

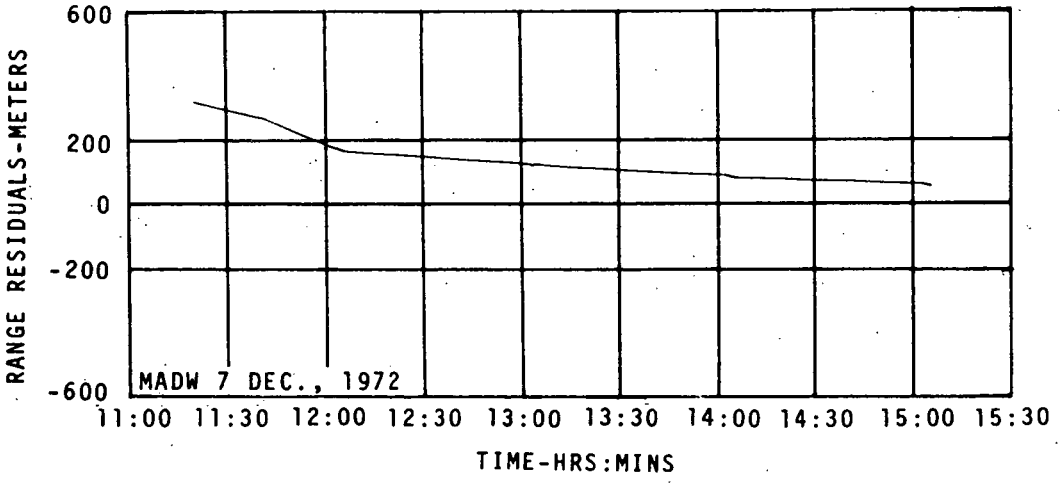

FIGURE 3-4. CARNARVON C-BAND AND MADRID RANGE RESIDUALS FOR PRE-PTC DATA FIT

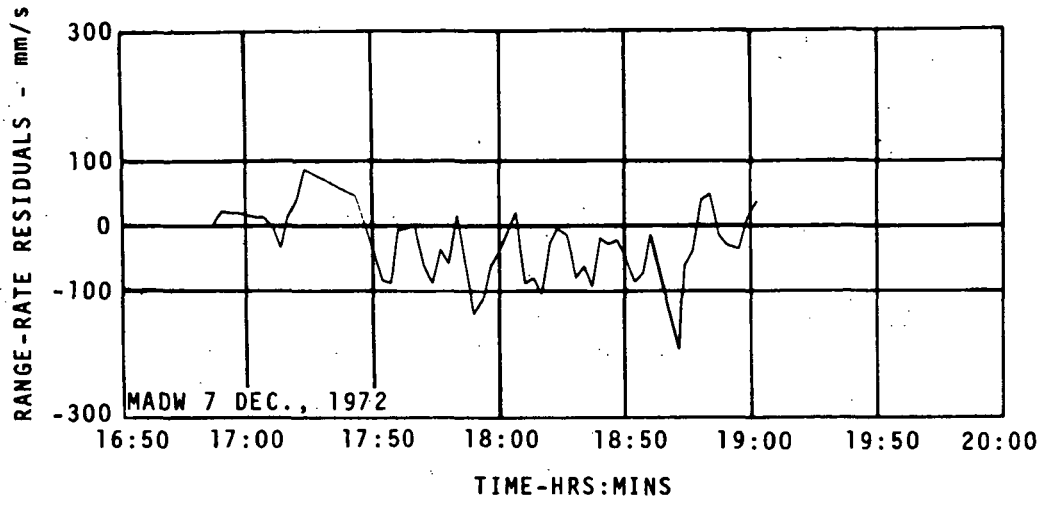

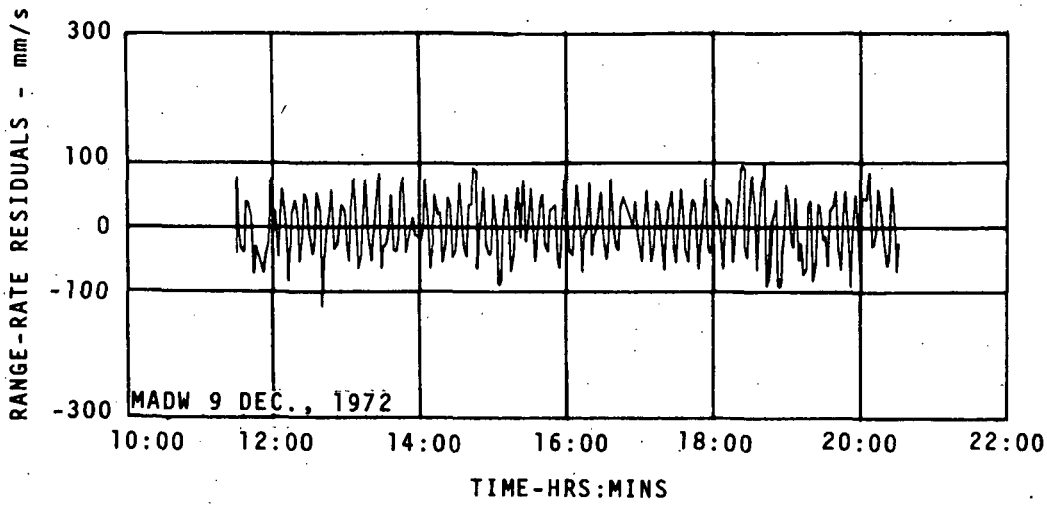

FIGURE 3-5. MADRID RANGE-RATE RESIDUALS FOR PTC DATA FIT - BEST-ESTIMATE TRAJECTORY

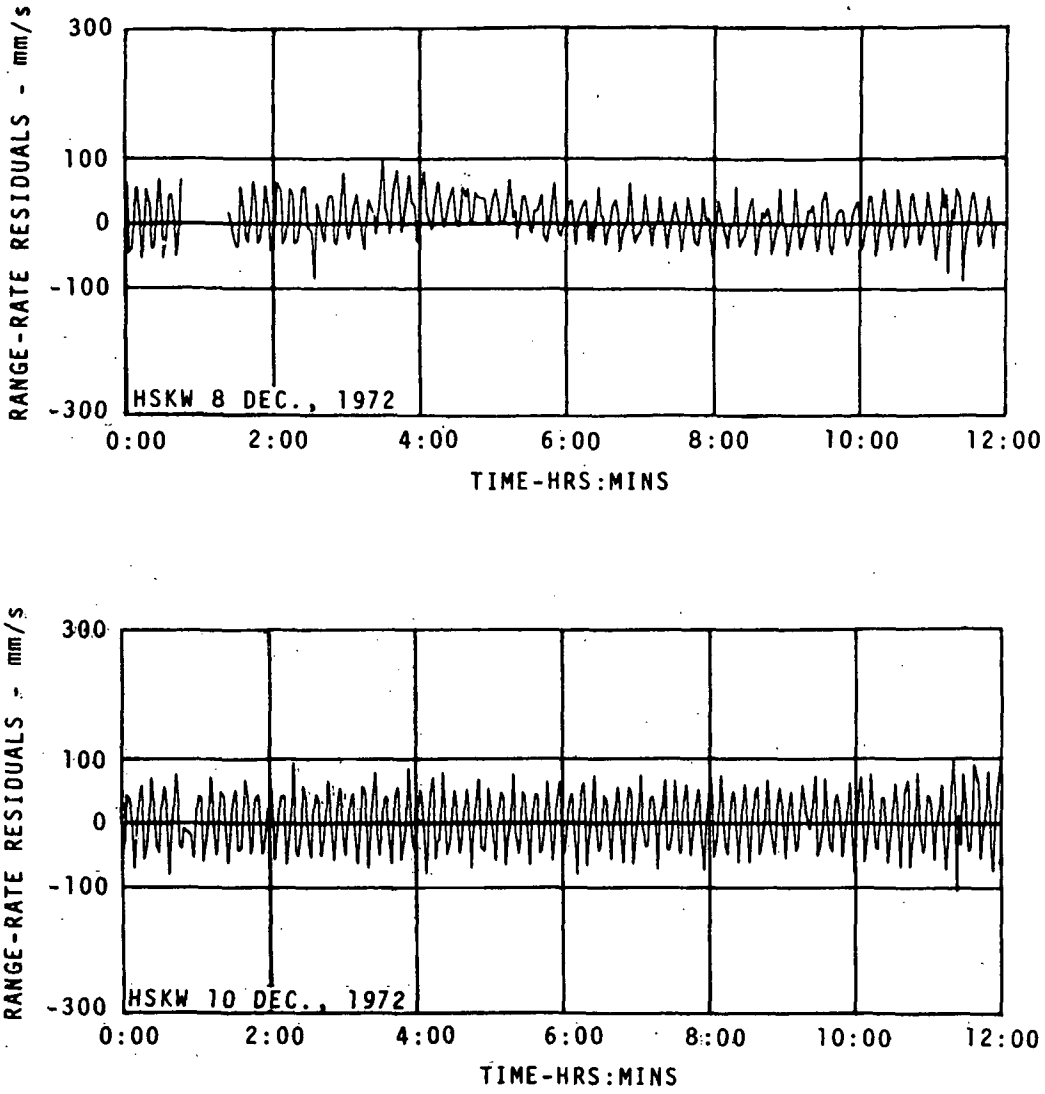

FIGURE 3-6. TIDBINBILLA RANGE-RATE RESIDUALS FOR PTC DATA FIT - BEST-ESTIMATE TRAJECTORY

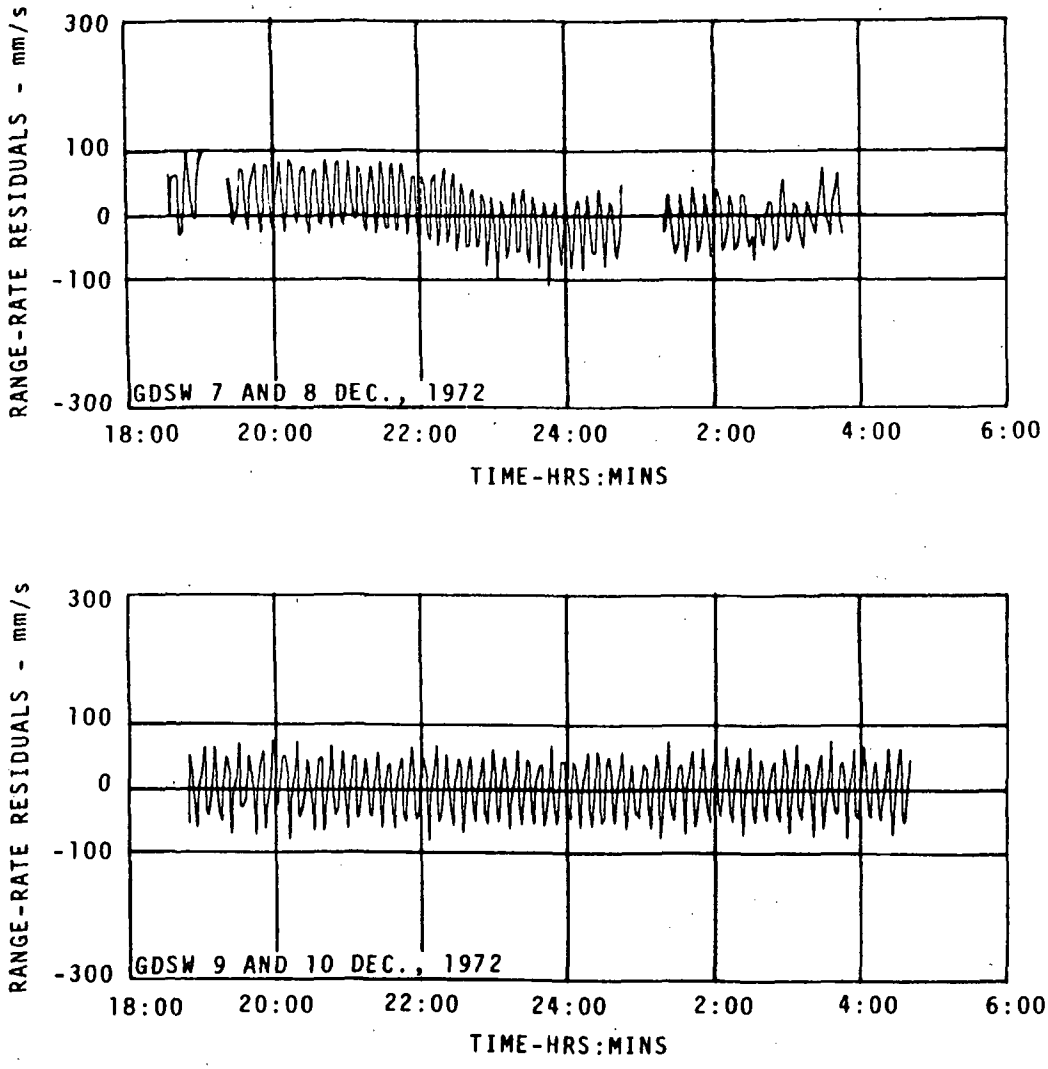

FIGURE 3-7. GOLDSTONE RANGE-RATE RESIDUALS FOR PTC DATA FIT - BEST-ESTIMATE TRAJECTORY

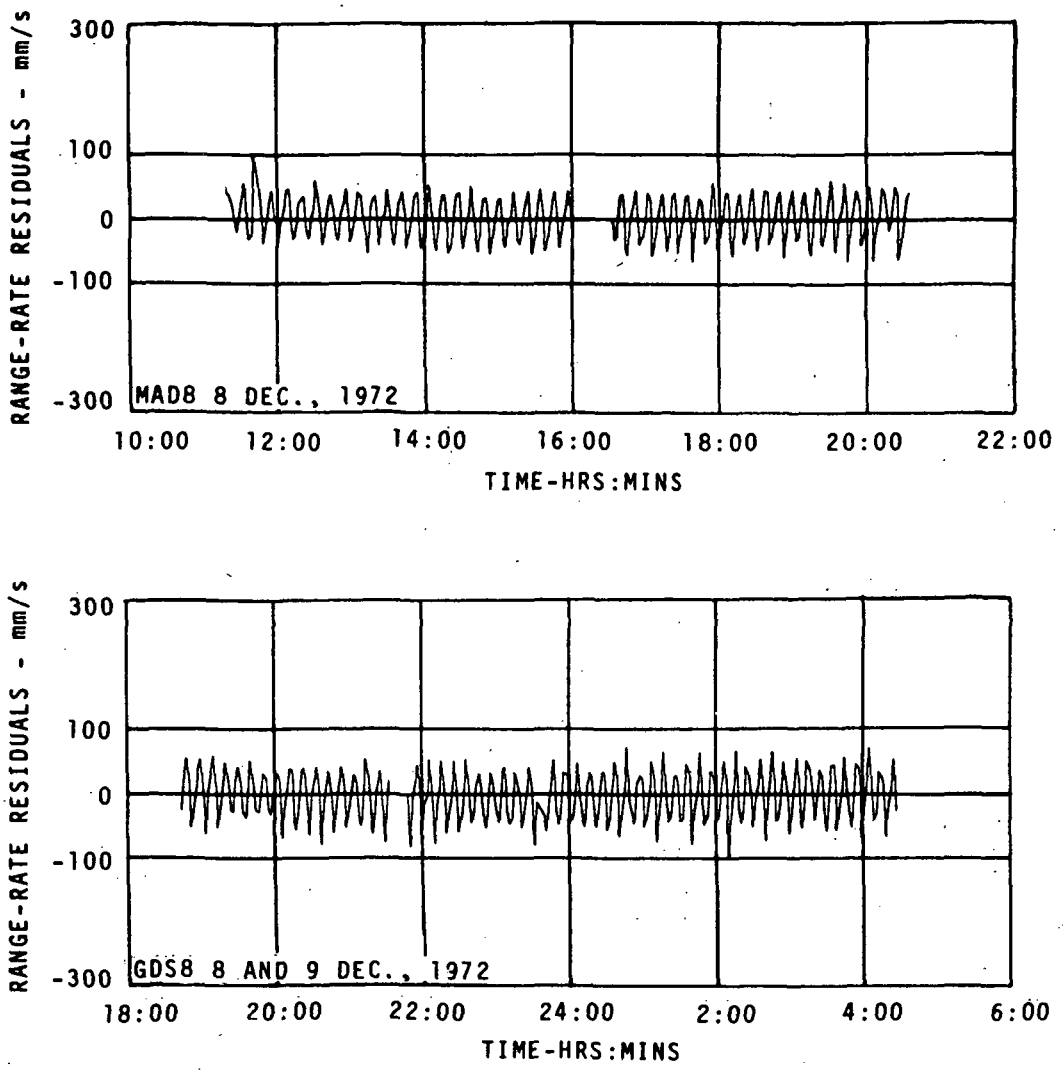

FIGURE 3-8. MADRID AND GOLDSTONE RANGE-RATE RESIDUALS FOR PTC DATA FIT - BEST-ESTIMATE TRAJECTORY

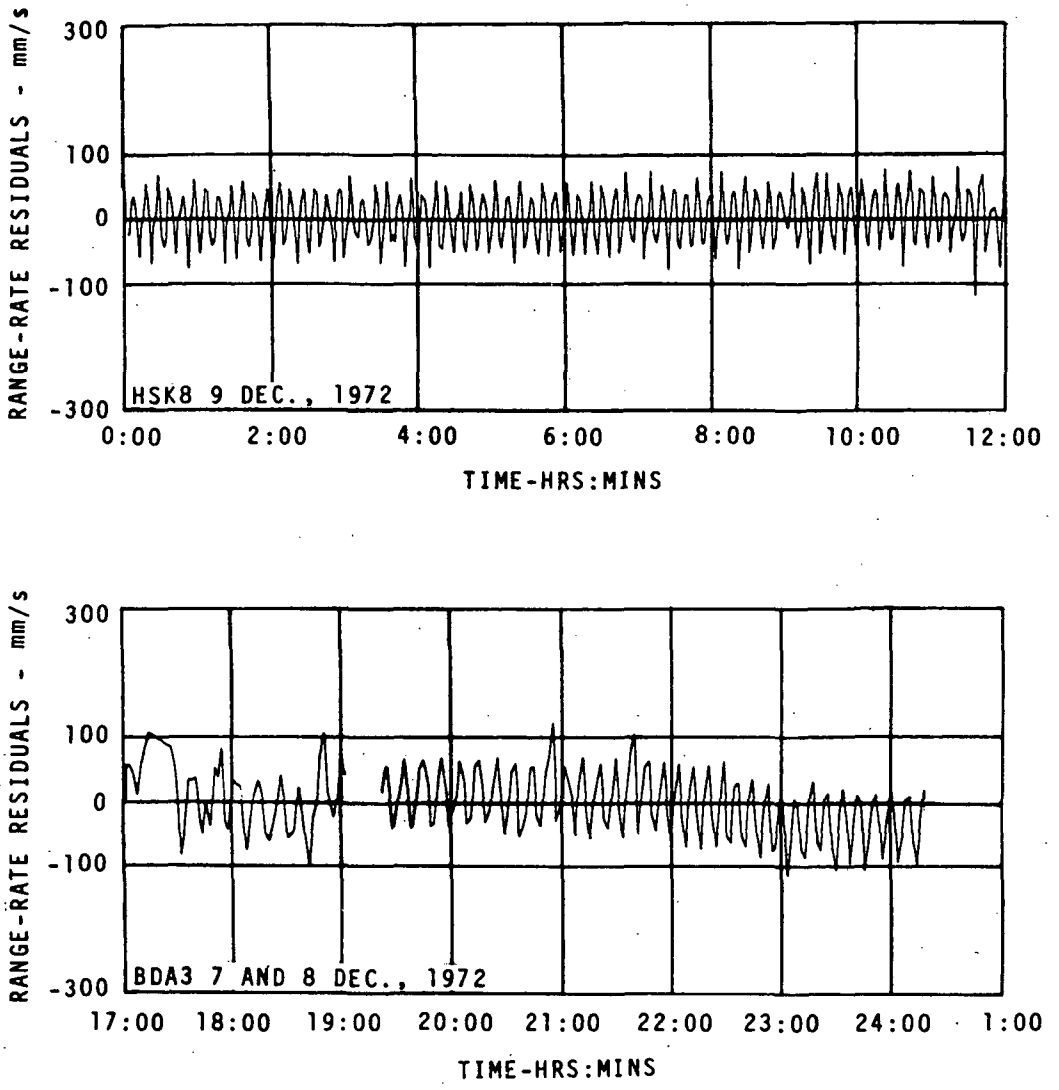

FIGURE 3-9. CANBERRA AND BERMUDA RANGE-RATE RESIDUALS FOR PTC DATA FIT - BEST-ESTIMATE TRAJECTORY

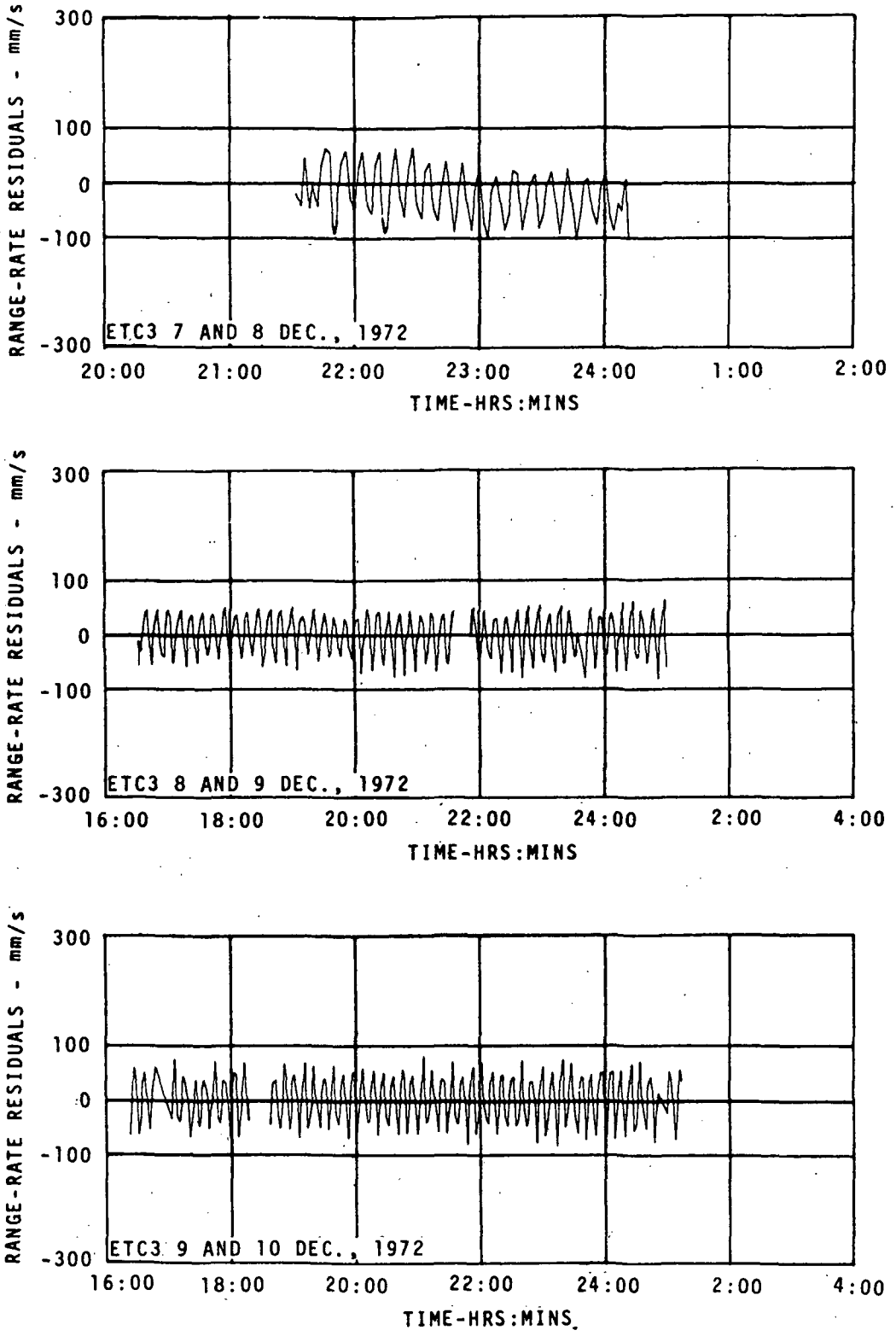

FIGURE 3-10. GREENBELT RANGE-RATE RESIDUALS FOR PTC DATA FIT - BEST-ESTIMATE TRAJECTORY

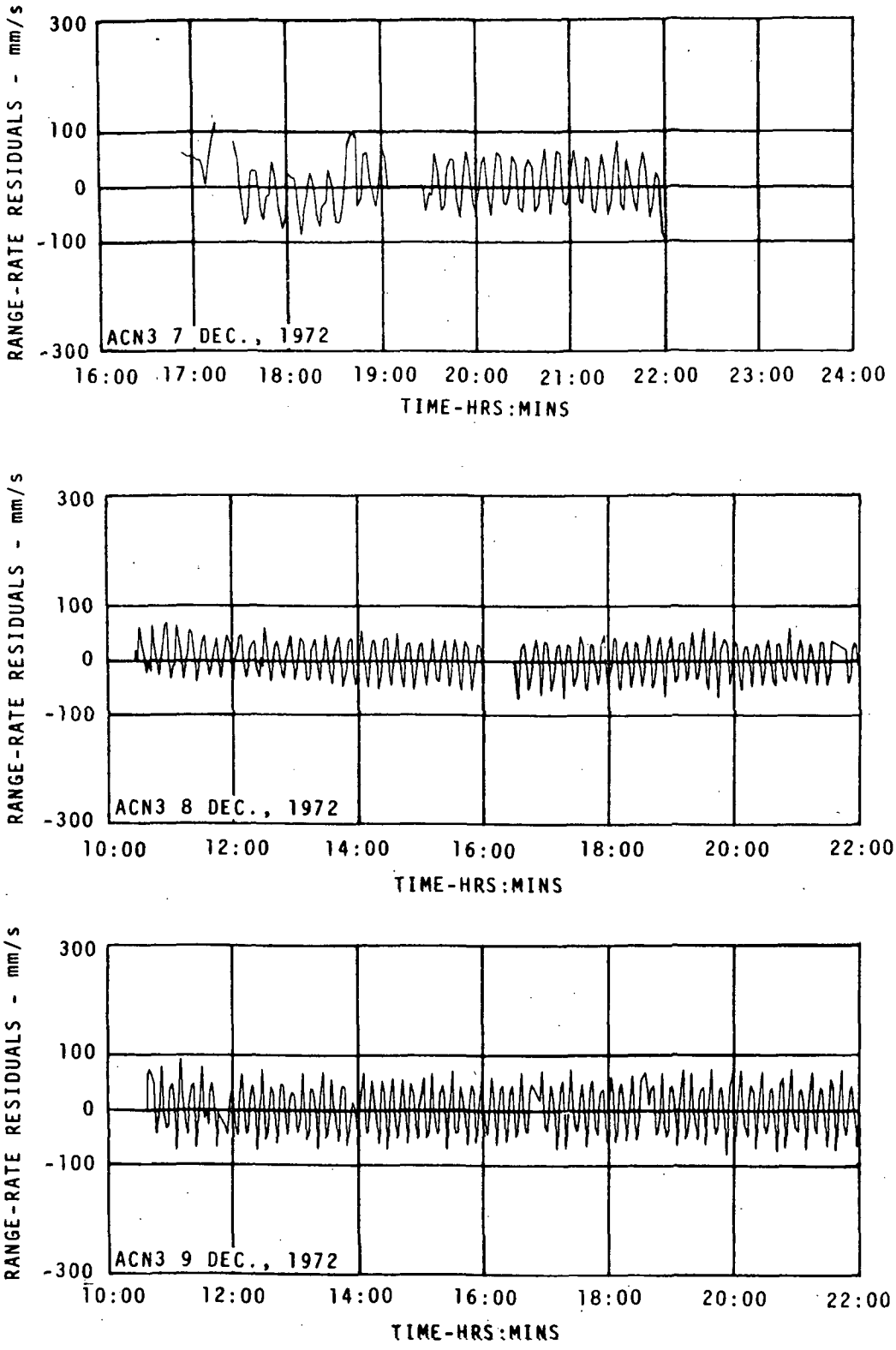

FIGURE 3-11. ASCENSION RANGE-RATE RESIDUALS FOR PTC DATA FIT - BEST-ESTIMATE TRAJECTORY

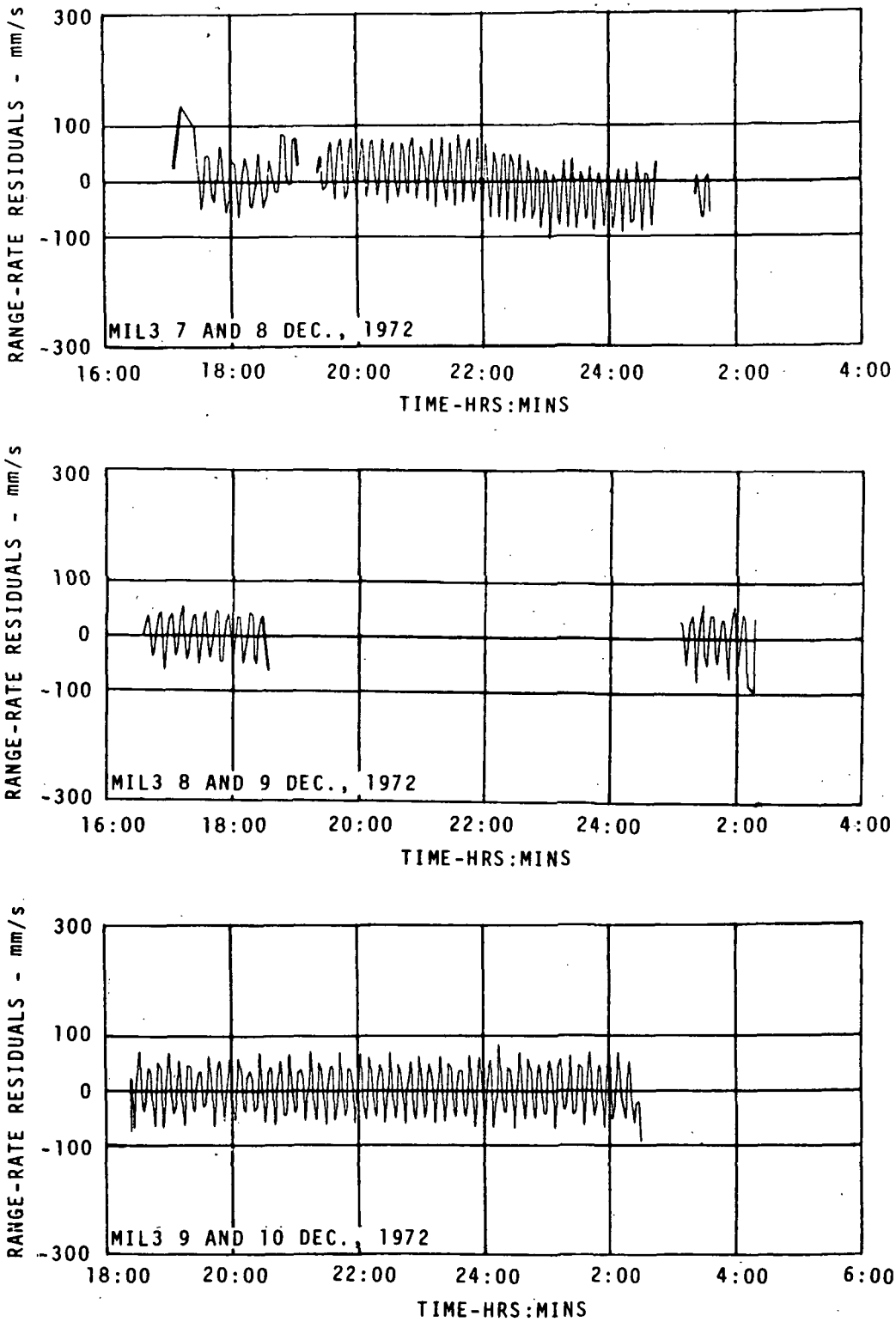

FIGURE 3-12. MERRITT ISLAND RANGE-RATE RESIDUALS FOR PTC DATA FIT - BEST-ESTIMATE TRAJECTORY

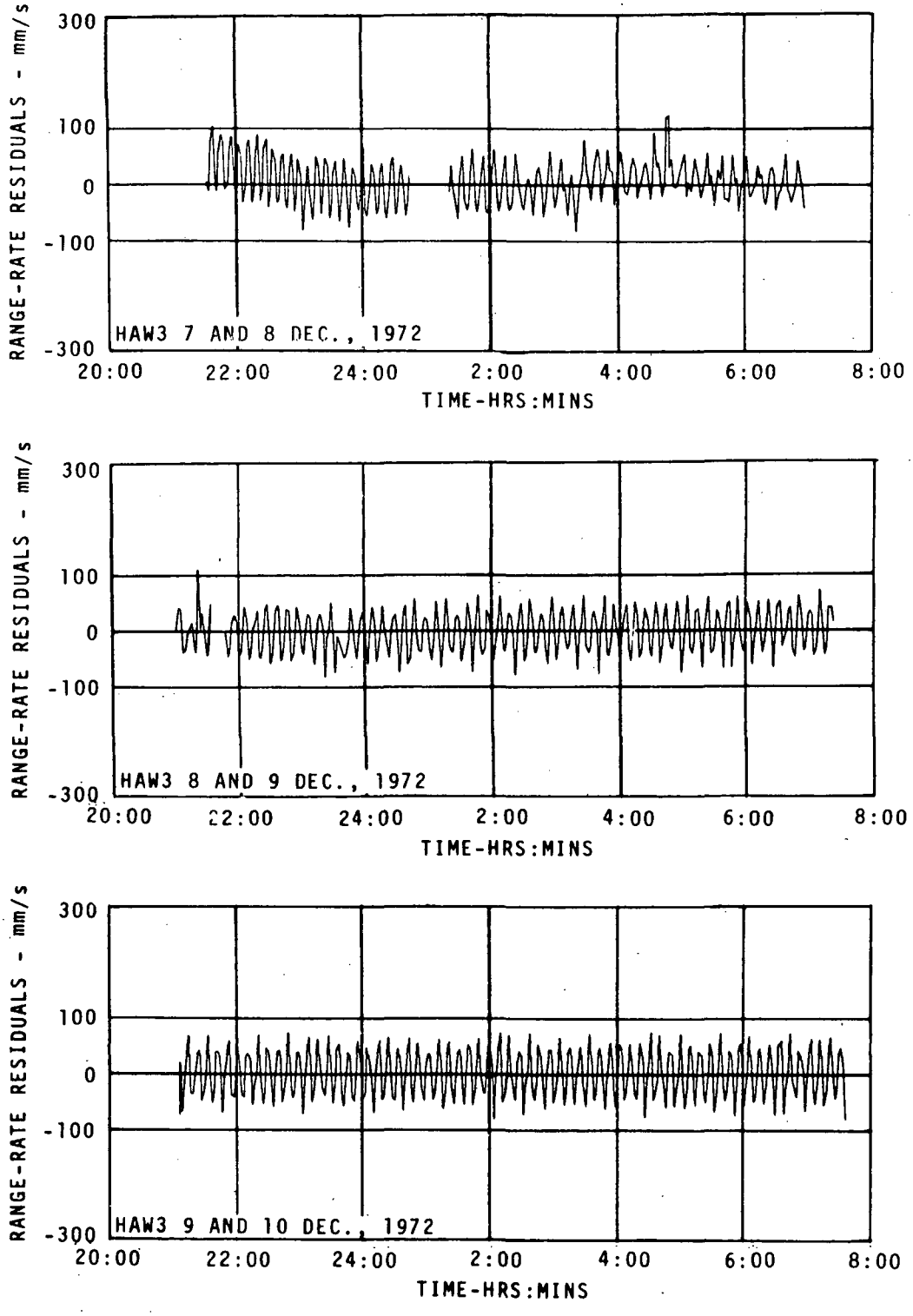

FIGURE 3-13. HAWAII RANGE-RATE RESIDUALS FOR PTC DATA FIT - BEST-ESTIMATE TRAJECTORY

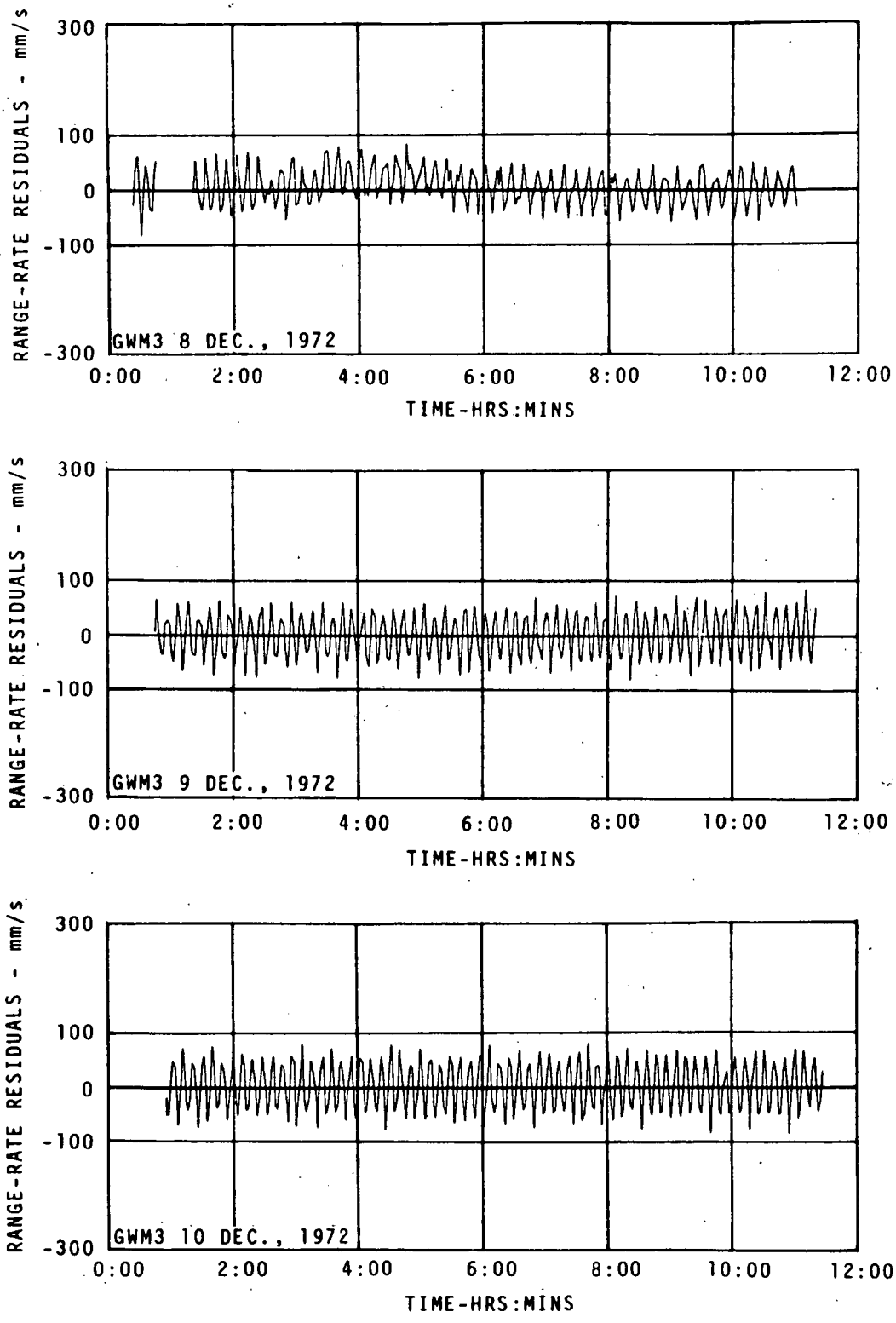

FIGURE 3-14. GUAM RANGE-RATE RESIDUALS FOR PTC DATA FIT - BEST-ESTIMATE TRAJECTORY

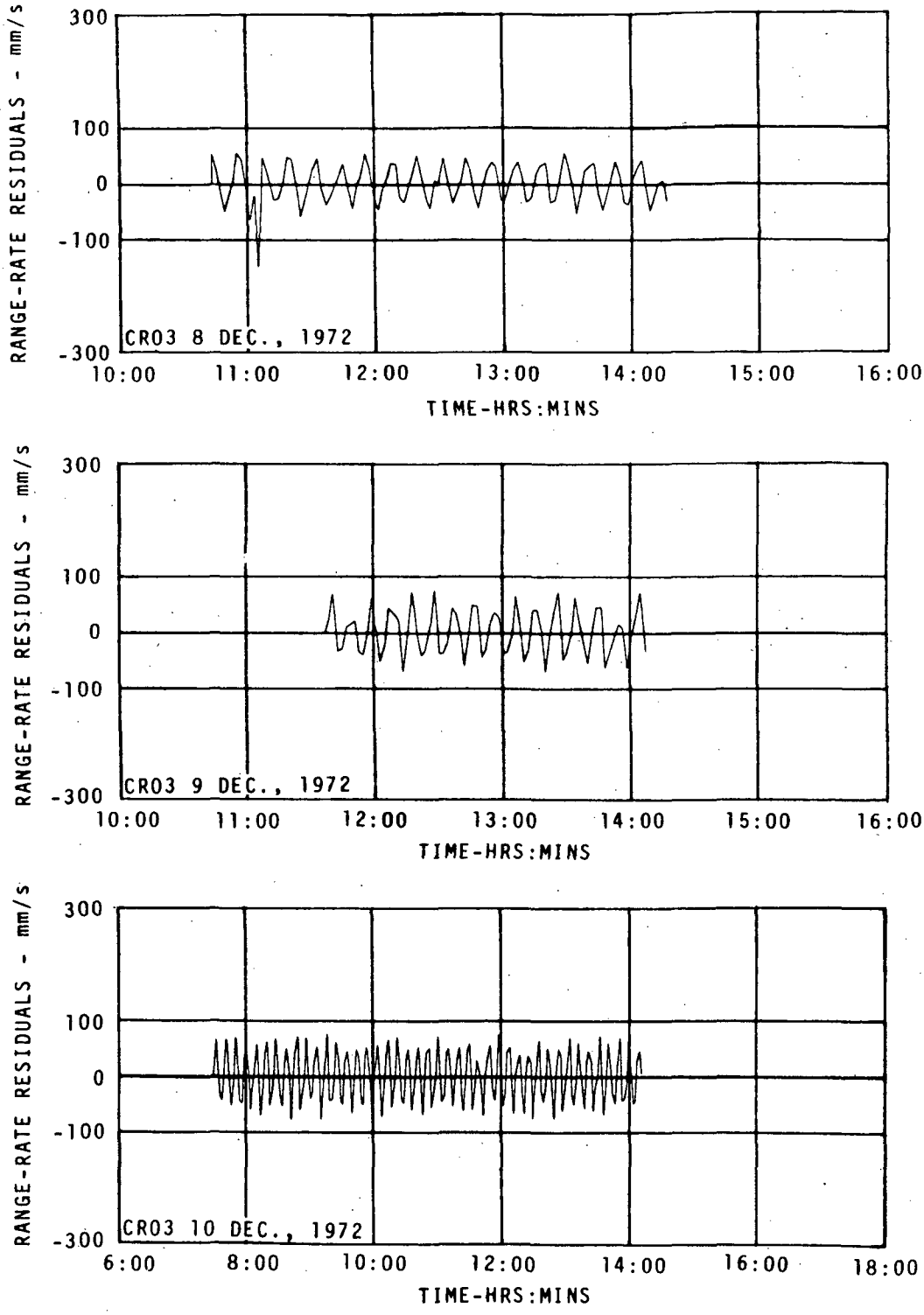

FIGURE 3-15. CARNARVON RANGE-RATE RESIDUALS FOR PTC DATA FIT - BEST-ESTIMATE TRAJECTORY

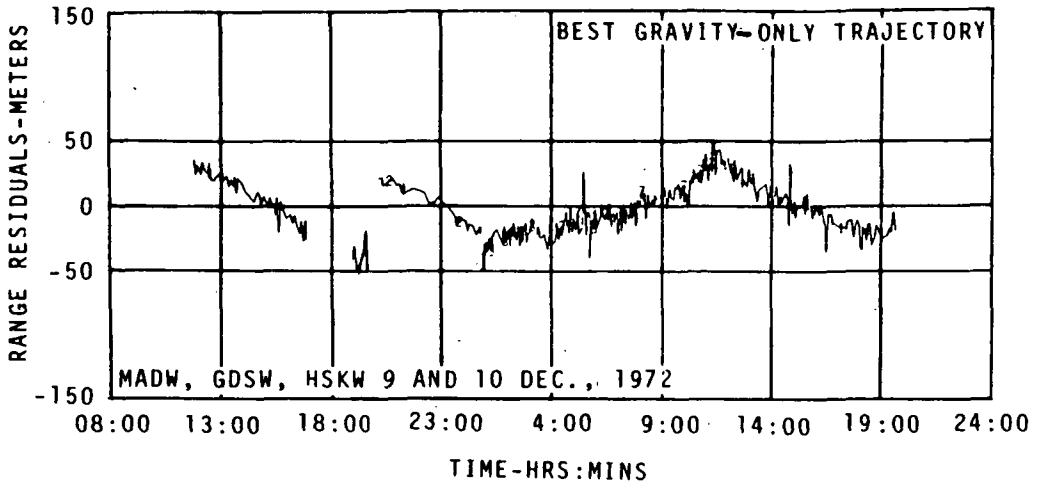

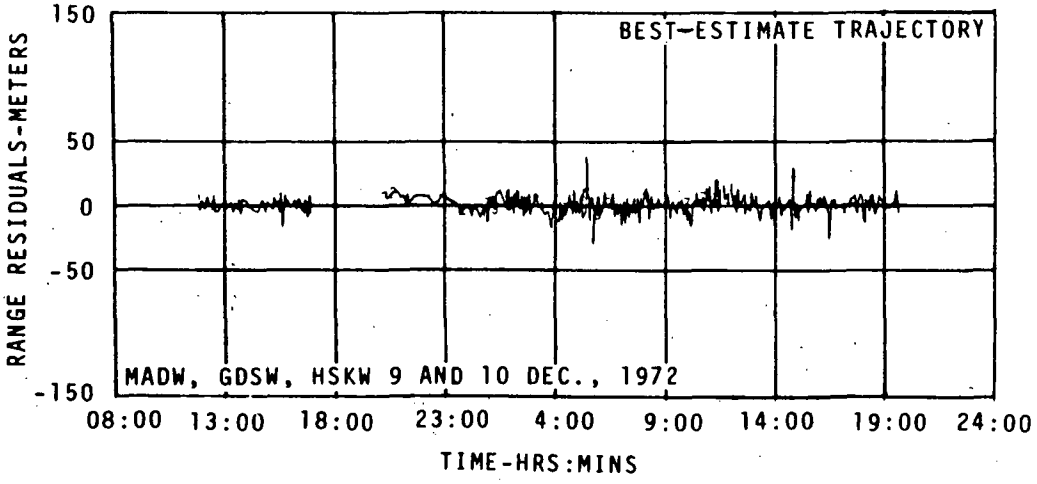

FIGURE 3-16. COMPARISON OF GRAVITY-ONLY TRAJECTORY AND BEST-ESTIMATE TRAJECTORY RANGE RESIDUALS

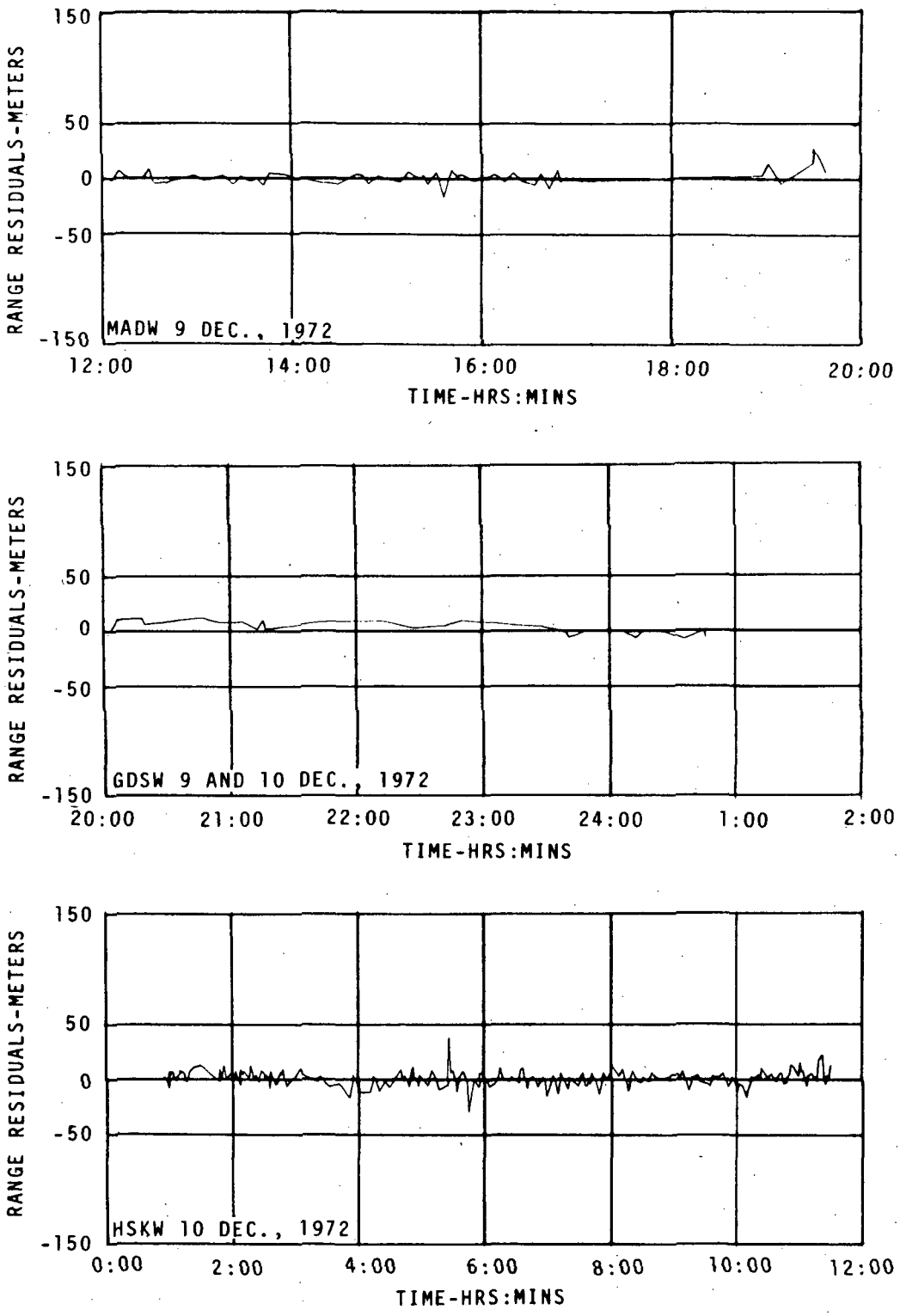

FIGURE 3-17. MADRID, GOLDSTONE AND TIDBINBILLA RANGE RESIDUALS FOR LATE DATA PTC FIT - BEST-ESTIMATE TRAJECTORY

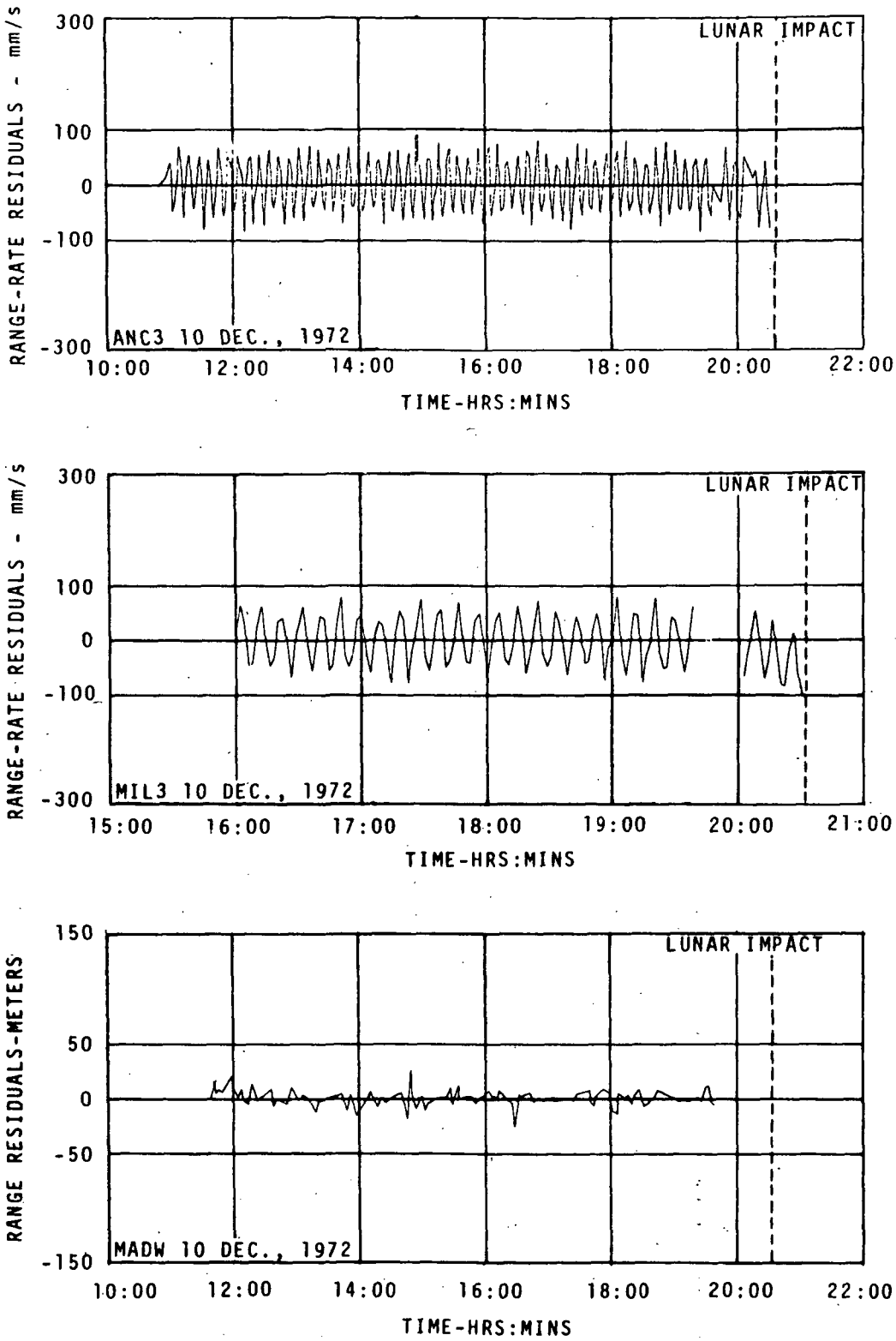

FIGURE 3-18. RANGE-RATE AND RANGE RESIDUAL AT LUNAR IMPACT

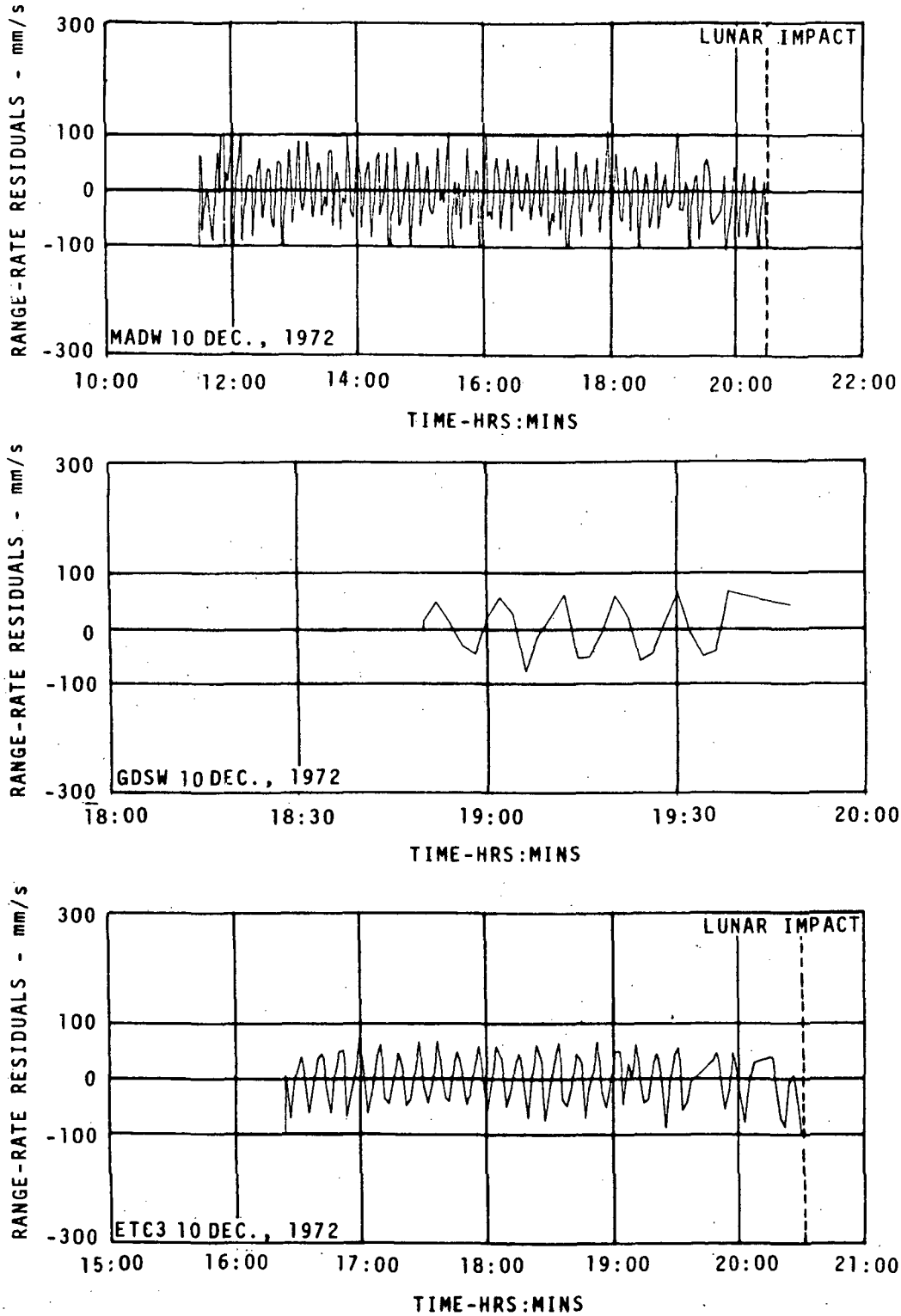

FIGURE 3-19. RANGE-RATE RESIDUALS AT LUNAR IMPACT

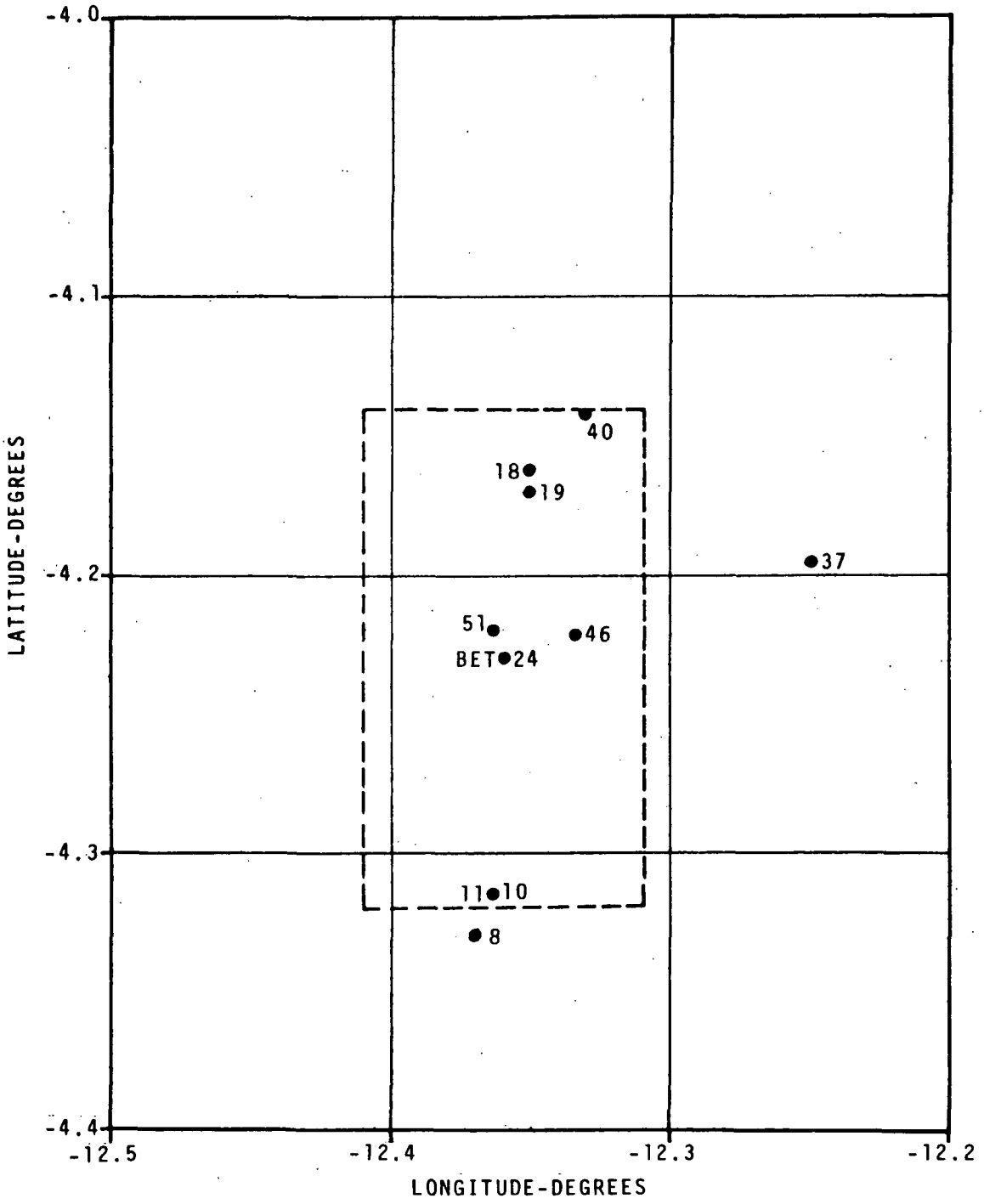

FIGURE 3-20. DISTRIBUTION OF LUNAR IMPACT SOLUTIONS

TABLE 3-I. TRACKING STATION LOCATIONS

ABBREVIATION	STATION	LOCATION			CONFIGURATION
		LATITUDE	LONGITUDE	HEIGHT*	
MADW	Madrid, Spain	40°25'41.85"	355°45'03.62"	767m	DSN 85' S-Band
MAD8	Madrid, Spain	40°27'17.97"	355°49'53.57"	763m	STDN 85' S-Band
GDSW	Goldstone, California	35°23'22.45"	243°09'02.26"	985m	DSN 85' S-Band
GDS8	Goldstone, California	35°20'29.74"	243°07'35.05"	921m	STDN 85' S-Band
HSKW	Tidbinbilla, Australia	-35°24'03.56"	148°58'52.65"	669m	DSN 85' S-Band
HSK8	Canberra, Australia	-35°35'00.58"	148°58'40.12"	1143m	STDN 85' S-Band
ACN3	Ascension	- 7°57'17.26"	345°40'22.59"	527m	STDN 30' S-Band
BDA3	Bermuda	32°21'04.50"	295°20'31.93"	-43m	STDN 30' S-Band
ETC3	Greenbelt, Maryland	38°59'54.53"	283°09'25.51"	-22m	STDN 30' S-Band
MIL3	Merritt Island, Florida	28°30'29.78"	279°18'23.51"	-54m	STDN 30' S-Band
HAW3	Kauai, Hawaii	22°07'34.71"	200°20'05.42"	1143m	STDN 30' S-Band
GWM3	Guam	13°18'38.07"	144°44'12.54"	114m	STDN 30' S-Band
CRO3	Carnarvon, Australia	-24°54'23.68"	113°43'32.06"	5m	STDN 30' S-Band
BDAQ	Bermuda	32°20'52.54"	295°20'47.91"	-45m	STDN FPQ-6 C-Band
CROQ	Carnarvon, Australia	-24°53'47.01"	113°43'02.65"	9m	STDN FPQ-6 C-Band

*Height above Fischer Ellipsoid

TABLE 3-II. PRE-PTC TRAJECTORY SEGMENT - RESIDUAL STATISTICS AND DATA UTILIZATION

RUN 69 RANGE-RATE RESIDUAL STATISTICS				
STATION	NUMBER OF POINTS	MEAN mm/s	SIGMA mm/s	RMS mm/s
MADW	521	-11.0	76.0	76.8
ACN3	354	-38.2	44.3	58.5
BDA3	77	4.0	19.8	20.2
MIL3	51	10.5	21.1	23.6
CRO3	122	-0.8	76.6	76.6

RUN 69 RANGE RESIDUAL STATISTICS				
STATION	NUMBER OF POINTS	MEAN meters	SIGMA meters	RMS meters
MADW	12	152.3	83.0	173.5
CROQ	83	-128.4	7.0	128.6

RUN 69 DATA UTILIZATION

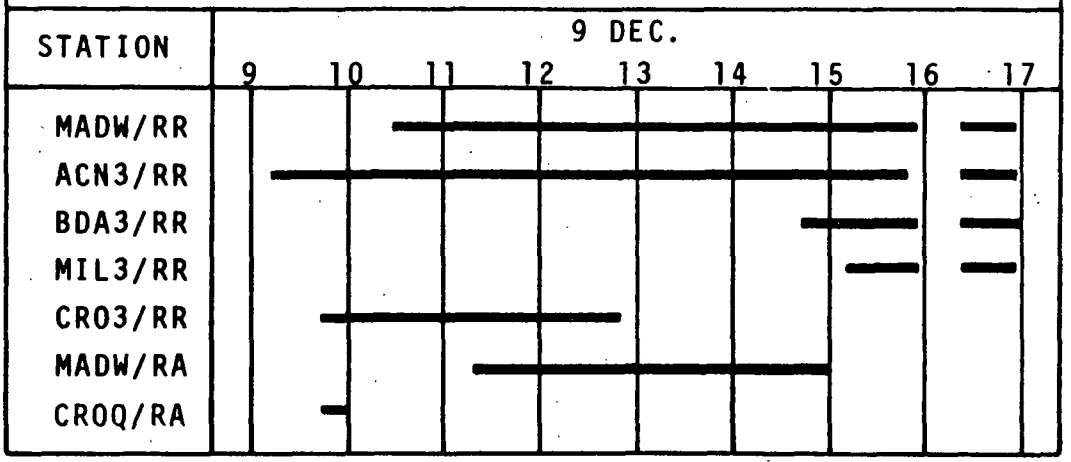

TABLE 3-III. EARLY PTC TRAJECTORY SEGMENT - RESIDUAL STATISTICS AND DATA UTILIZATION

RUN 46 RANGE-RATE RESIDUAL STATISTICS

STATION	NUMBER OF POINTS	MEAN mm/s	SIGMA mm/s	RMS mm/s
MADW	165	-7.7	32.3	33.2
GDSW	163	-11.1	150.3	150.7
HSKW	207	2.4	141.6	141.6
MAD8	74	-2.2	24.8	24.9
GDS8	80	-3.8	16.5	17.0
HSK8	107	0.5	16.3	16.3
ETC3	190	-6.0	23.2	24.0
ACN3	38	7.4	42.4	43.0
BDA3	59	-2.5	30.4	30.5
MIL3	91	0.7	17.8	17.8
HAW3	119	0.6	13.5	13.5
GWM3	134	1.5	10.2	10.3
CRO3	52	-4.6	16.2	16.3

RUN 46 RANGE RESIDUAL STATISTICS

STATION	NUMBER OF POINTS	MEAN meters	SIGMA meters	RMS meters
MADW	165	4.3	18.6	19.1
GDSW	34	14.3	5.9	15.5
HSKW	161	12.6	8.6	15.3

RUN 46 DATA UTILIZATION

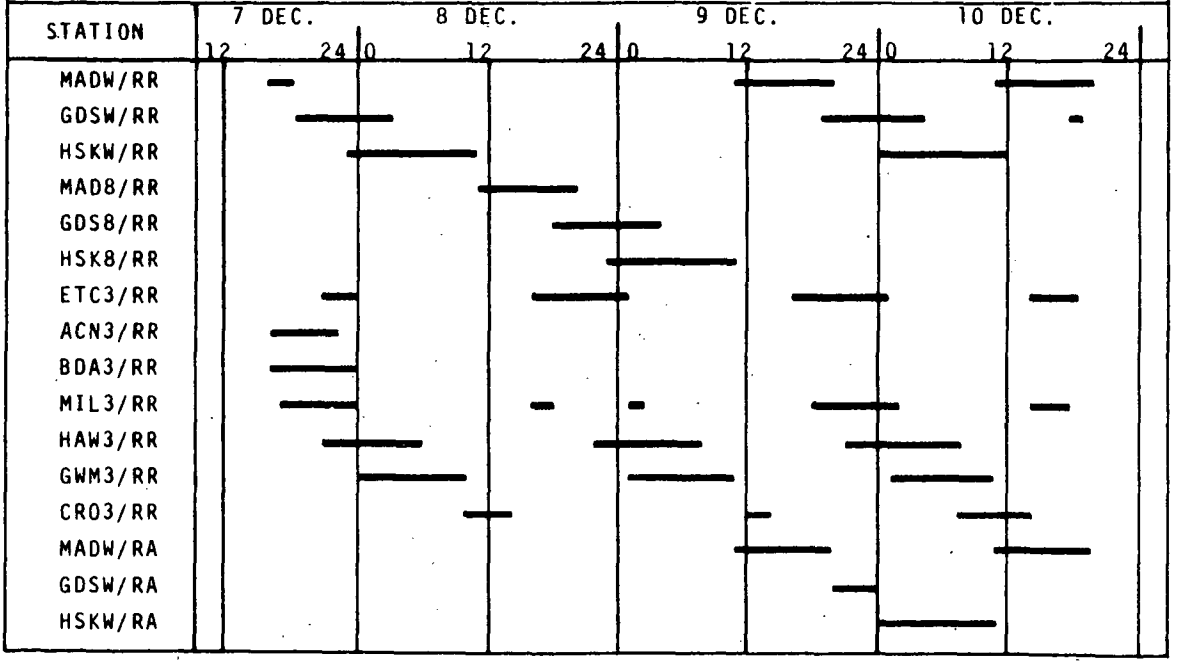

TABLE 3-IV. LATE PTC SEGMENT RESIDUAL STATISTICS AND DATA UTILIZATION FOR BEST-ESTIMATE TRAJECTORY

RUN 24 RANGE-RATE RESIDUAL STATISTICS				
STATION	NUMBER OF POINTS	MEAN mm/s	SIGMA mm/s	RMS mm/s
MADW	152	-2.4	27.8	27.9
GDSW	91	-0.1	15.3	15.3
HSKW	105	1.7	16.3	16.4
GDS8	54	-5.3	16.3	17.1
HSK8	107	-0.6	16.5	16.5
ETC3	125	-0.5	16.5	16.5
ACN3	182	1.7	20.0	20.0
MIL3	115	-0.6	16.6	16.7
HAW3	172	-1.6	16.1	16.2
GWM3	186	-0.1	16.5	16.6
CRO3	79	1.6	16.5	16.6

RUN 24 RANGE RESIDUAL STATISTICS				
STATION	NUMBER OF POINTS	MEAN meters	SIGMA meters	RMS meters
MADW	165	-0.2	7.1	7.1
GDSW	34	0.7	6.3	6.4
HSKW	161	-0.1	7.8	7.8

RUN 24 DATA UTILIZATION

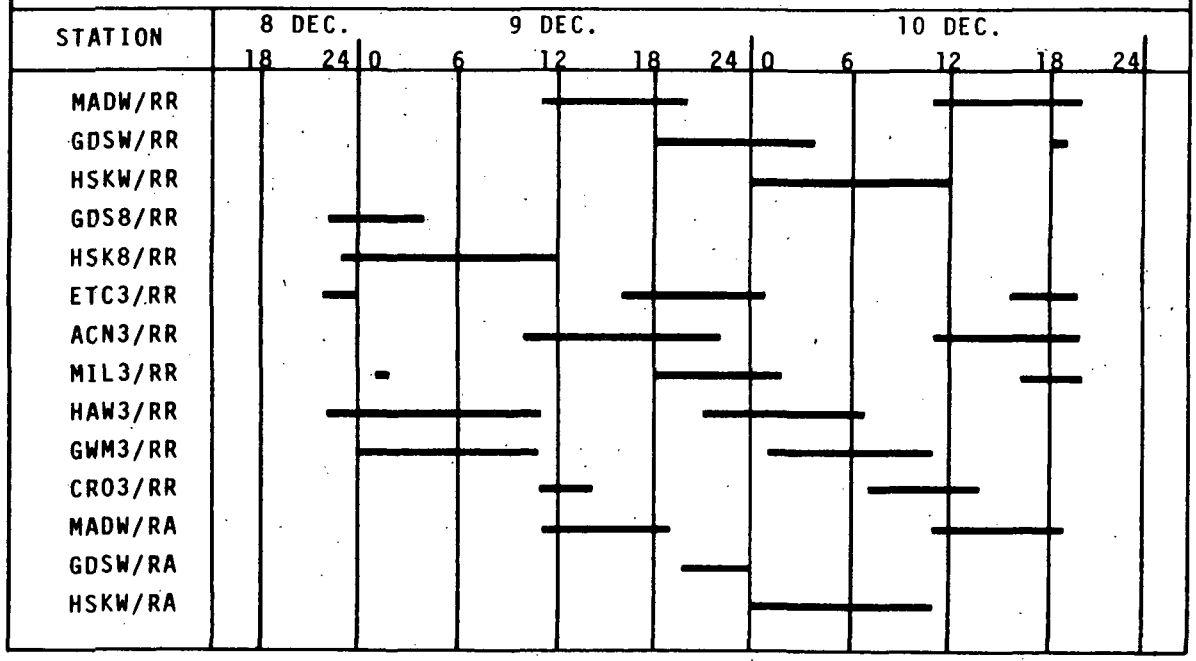

TABLE 3-V. LATE PTC SEGMENT RESIDUAL STATISTICS AND DATA UTILIZATION FOR BEST GRAVITY-ONLY TRAJECTORY

RUN 8 RANGE-RATE RESIDUAL STATISTICS				
STATION	NUMBER OF POINTS	MEAN mm/s	SIGMA mm/s	RMS mm/s
MADW	118	-3.6	13.2	23.5
GDSW	72	-0.8	6.8	6.9
HSKW	82	3.6	6.4	7.4
GDS8	43	-16.2	8.2	18.2
HSK8	85	-5.7	8.0	9.8
ETC3	96	-3.6	13.0	13.5
ACN3	142	-0.1	11.3	11.3
MIL3	90	-1.7	11.5	11.6
HAW3	136	-5.6	10.3	11.7
GWM3	148	-2.9	8.8	9.3
CRO3	63	1.6	6.3	6.4

RUN 8 RANGE RESIDUAL STATISTICS				
STATION	NUMBER OF POINTS	MEAN meters	SIGMA meters	RMS meters
MADW	165	-0.3	19.1	19.2
GDSW	34	0.7	15.1	15.1
HSKW	161	-3.0	20.2	20.4

RUN 8 DATA UTILIZATION

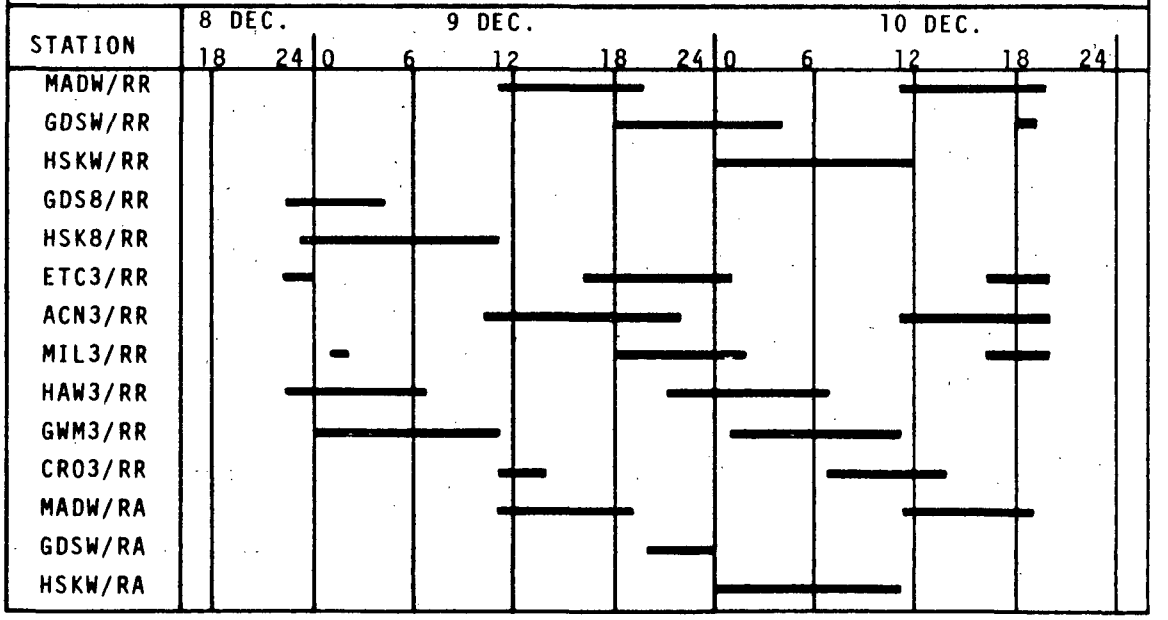

TABLE 3-VI. TRAJECTORY SOLUTIONS AND LUNAR IMPACT POINTS

RUN	LATITUDE LONGITUDE TIME*	DESCRIPTION
8	-4.329 -12.367 40.340	Gravity only solution using available data after 22:00:00, 8 December 1972 (∿47 hours of data). Range rate averaged over 8 minutes. See Table 3-V.
10	-4.315 -12.364 40.207	Gravity only solution using available data after 22:00:00, 8 December 1972 (∿47 hours of data). Range rate averaged over 2 minutes.
11	-4.318 -12.364 40.217	Gravity only solution using available data after 22:00:00, 8 December 1972 except GDS8 RR and GDSW RA (∿47 hours of data). Range rate averaged over 4 minutes.
18	-4.163 -12.351 40.151	Non-gravity solution using available data after 00:00:00, 8 December 1972 (∿69 hours of data). Range rate averaged over 7 minutes.
19	-4.170 -12.351 40.116	Non-gravity solution using available data after 10:00:00, 8 December 1972 (∿59 hours of data). Range rate averaged over 7 minutes.
24 (BET)	-4.232 -12.352 40.173	Non-gravity solution using available data after 22:00:00, 8 December 1972 (∿47 hours of data). Range rate averaged over 7 minutes. See Table 3-IV.
37	-4.195 -12.250 43.216	Non-gravity solution using available data after CSM/LV separation (∿83 hours of data). Range rate averaged over 7 minutes.
40	-4.142 -12.332 39.554	Non-gravity solution using available data after APS-2 burn (∿76 hours of data). Range rate averaged over 7 minutes.
46	-4.214 -12.345 39.988	Non-gravity solution using available range rate after APS-2 burn (∿76 hours of data) and range after 22:00:00, 8 December 1972. Range rate averaged over 7 minutes. See Table 3-III.
51	-4.221 -12.364 40.083	Non-gravity solution using available data after Timebase 8 (∿82 hours of data). Range rate averaged over 7 minutes.
MEAN	-4.230 -12.344 40.404	Latitude Sigma 0.065 Longitude Sigma 0.033 Time Sigma 0.958

* Impact Time on 10 December 1972, at 20:32:XX at a lunar radius of 1738.09 km and a DE19 ephemeris.

TABLE 3-VII. APOLLO 17 LUNAR IMPACT TIMES

STATION	RECORDED LOSS OF SIGNAL 10 DEC 1972	RANGE, METERS	TRANSMISSION DELAY, SECONDS	CORRECTED IMPACT TIME 10 DEC 1972
MADW	20:32:42.30	391,704.7	1.306	20:32:40.99
ACN3	20:32:42.30	388,959.1	1.297	20:32:41.00
BDA3	20:32:42.25	388,116.2	1.294	20:32:40.96
MIL3	20:32:42.28	386,126.7	1.288	20:32:40.99
GDSW	20:32:42.30	389,818.5	1.300	20:32:41.00

THIS PAGE LEFT BLANK INTENTIONALLY

APPENDIX A

ANALYSIS METHODS

The trajectories reconstructed for this analysis are based on tracking data and onboard measurements by the S-IVB/IU. Goddard Space Flight Center is the central collection agency for all tracking data recorded by the Manned Space Flight Network tracking stations. This data is transmitted to The Boeing Company via Marshall Space Flight Center in the form of two angles and range measurements and, in the case of S-band data, in the form of doppler counts. Onboard measurements in the form of platform attitudes and velocity accumulations are collected by the Marshall Space Flight Center and transmitted to The Boeing Company. Trajectory determination is accomplished by:

a. Propagating an a priori initial state forward by means of an a priori acceleration model.

b. Transformation of the propagated initial state (the trajectory) into tracking observations.

c. Converting the difference in the observed tracking data and the calculated tracking data into an estimate of the correction to the initial state.

This appendix briefly summarizes the three steps outlined above as implemented in the Lunar Impact Determination (LID) program (see Reference 6). The LID program, originally received from MSFC, was modified by The Boeing Company in several ways. First, the program was converted to run on an IBM 360/370 and was made double-precision. Second, computer graphics capability was added to provide a quick-response man/machine interface for on-line decision making. Finally, numerous improvements were made in the model which transforms the trajectory into tracking data, and the capability to solve for non-gravitational acceleration was added.

A.1 INITIAL STATE PROPAGATION

Initial state propagation is accomplished by numerical integration of an acceleration model which consists of the gravitational attractions of the earth, moon, and sun, plus non-gravitational accelerations.

The earth's gravitational potential is the Fischer ellipsoid of 1960 with sectorial term; the moon's includes the second zonal and second sectorial harmonics. The ephemeris used is

A.1 (Continued)

the JPL ephemeris DE19, transformed to PACSS4 coordinates (Reference 7) by the Johnson Space Center. The ephemeris time to universal time correction used is 43.18 seconds. The non-gravitational acceleration is a square wave time history input via cards. The acceleration history is derived from platform data or other sources. The total acceleration is the sum of gravitational and non-gravitational acceleration:

$$\vec{A} = \vec{G} + \vec{T}.$$

The non-gravitational acceleration is calculated as follows:

$$\vec{T} = [B]\vec{T}_o \qquad \text{if } t < t_s \text{ or } t_e < t,$$

or

$$\vec{T} = [B](\vec{C}'_o + [C''_o]\vec{T}_o + \vec{T}_o) \qquad \text{if } t_s \leq t \leq t_e;$$

where $\vec{T}_o$ is the initial a priori time history of the thrust accelerations,

$\vec{C}'_o$ is the a priori thrust bias vector,

$[C''_o]$ is a diagonal matrix where the diagonal terms are the a priori thrust scale factors,

$[B]$ is a transformation matrix relating PACSS13 to PACSS4,

t_s is the start of the window over which corrections are made to the thrust history,

t_e is the end of the window over which corrections are made to the thrust history,

and t is the current time.

A.2 CALCULATION OF OBSERVABLES

Tracking observations are calculated by determining the instantaneous tracker position and velocity in the reference system and examining the relationship of the vehicle to the tracker. This examination includes consideration of signal travel time and atmospheric refraction. A summary of the calculation of observables is presented below. Figure A-1 will help in understanding the equations.

A.2 (Continued)

Define: t_4 = time of signal reception at tracker, also time tag of observation;

t_3 = time of signal transmission from vehicle;

t_2 = time of signal reception at vehicle;

t_1 = time of signal transmission from tracker.

From the vehicle trajectory:

$\vec{P}_V^4$ = position of vehicle at t_4; and

$\vec{V}_V^4$ = velocity of vehicle at t_4.

The tracker position(s)

$\vec{P}_T^4$ (the position of transmitting tracker at t_4) and

$\vec{P}_R^4$ (the position of receiving tracker at t_4)

are determined as follows:

$$\vec{P}_T^4 = [P][N][R]\vec{R}_T, \text{ and}$$

$$\vec{P}_R^4 = [P][N][R]\vec{R}_R;$$

where

$\vec{R}_T$ and $\vec{R}_R$ are the earth fixed position(s) of the tracker(s),

[R] is the matrix modeling the earth's rotation,

[N] is the matrix modeling the earth's nutation,

[P] is the matrix modeling the earth's precession.

Note that [R], [N], and [P] are time dependent.

A.2 (Continued)

The following nomenclature is introduced:

c is the speed of light;

δ is the vehicle transponder delay distance, (apparent distance from receiving antenna to transmitting antenna);

ω is earth spin rate; and

n is atmospheric refraction coefficient ($n = (\eta-1)(10^6)$ where η is the index of refraction).

Calculation of downlink distance, d":

$$\left.\begin{aligned} d &= |\vec{P}_V^4 - \vec{P}_R^4| \\ \vec{P}_V^3 &= \vec{P}_V^4 - \frac{d}{c}\,\vec{V}_V^4 \\ \vec{P}^{34} &= \vec{P}_R^4 - \vec{P}_V^3 \\ d &= |\vec{P}^{34}|. \end{aligned}\right\} \text{ iterated twice}$$

Calculation of elevation:

$$e = \sin^{-1}\left(\frac{\vec{P}^{34} \cdot \vec{P}_T^4}{d\ |\vec{P}_T^4|}\right).$$

Calculation of downlink distance refraction correction:

$$\Delta d" = \left(\frac{0.00118958}{(0.06483 + \sin e)^{1.4}}\right)\left(\frac{n}{340}\right), \quad e \leq 15°$$

$$\Delta d" = \left(\frac{0.0026}{0.015 + \sin e}\right)\left(\frac{n}{340}\right), \quad e > 15°$$

$$d" = d + \Delta d".$$

Calculation of uplink distance, d':

$$\vec{P}_V^2 = \vec{P}_V^3 - \frac{\delta}{c}\,\vec{V}_V^4$$

A.2 (Continued)

$$\vec{V}_T^4 = \left[[P][N] \begin{bmatrix} 0 \\ 0 \\ \omega \end{bmatrix} \right] \times \vec{P}_T^4$$

$$d = d''$$

$$\vec{P}_T^1 = \vec{P}_T^4 - \frac{d + d'' + \delta}{c} \vec{V}_T^4$$

$$\vec{P}^{12} = \vec{P}_V^2 - \vec{P}_T^1$$

$$d = |\vec{P}^{12}|.$$

2 way tracking-iterated once

3 way tracking-iterated twice

Calculation of uplink distance refraction correction:

$$d' = d + \Delta d'', \qquad \text{if 2 way, or if 3 way}$$

$$e' = \sin^{-1}\left(\frac{\vec{P}^{12} \cdot \vec{P}_T^1}{d \ |\vec{P}_T^1|} \right)$$

$$\Delta d' = \left(\frac{0.00118958}{(0.06483 + \sin e')^{1/4}} \right) \left(\frac{n}{340} \right), \quad e' \leq 15°$$

$$\Delta d' = \left(\frac{0.0026}{0.015 + \sin e'} \right) \left(\frac{n}{340} \right), \qquad e' > 15°$$

$$d' = d + \Delta d'.$$

Calculation of range:

$$\rho = \frac{1}{2}(d'' + d' + \delta).$$

Calculation of average range rate:

$$\dot{\rho} = \frac{\rho - \rho^*}{t_4 - t_4^*}, \quad \text{*indicates previous value.}$$

A.3 CORRECTION OF INITIAL STATE

The LID program uses Kalman estimation techiques (described in Reference 8) to correct an initial state consisting of the initial position, initial velocity, thrust acceleration biases, and thrust acceleration scale factors. For simplicity of notation let

$\vec{C}_o = (\vec{C}'_o, \vec{C}''_o)^T$, a six element vector with $\vec{C}''_o$ representing the diagonal terms of $[C''_o]$,

$\vec{S}_o = (\vec{P}_o, \vec{V}_o)^T$, a six element vector,

and $\vec{S}^*_o = (\vec{S}_o, \vec{C}_o)^T$, a twelve element vector.

The Kalman Optimal Estimation technique adapted to solve for corrections to the extended initial state is given below.

Assume that there exists a first guess to the initial state and an estimate of its uncertainty, then the correction to the initial state, $\hat{S}^*_o$, which results in the best fit of a set of measurements is given by:

$$\hat{S}^*_{o,j} = \hat{S}^*_{o,j-1} + K_j(Y_j - H_j\phi_j\hat{S}^*_{o,j-1}), \text{ with}$$

$$K_j = P_{j-1}\phi_j{}^T H_j{}^T (H_j\phi_j P_{j-1}\phi_j{}^T H_j{}^T + Q_j)^{-1}, \text{ and}$$

$$P_j = P_{j-1} - K_j H_j \phi_j P_{j-1};$$

where $\hat{S}^*_{o,j}$ is the correction matrix (12 × 1) to the initial state at time j,

K_j is the Kalman gain matrix (12 × 1) at time j,

Y_j is the measurement matrix (1 × 1) at time j perturbed by noise,

H_j is the matrix (1 × 6) relating, at time j, the measurement matrix to the propagated initial state,

ϕ_j is the transition matrix (6 × 12) relating, at time j, changes in the propagated initial state to changes in the initial state,

A.3 (Continued)

P_j is the covariance matrix (12 × 12), at time j, of the perturbations to the initial state,

and Q_j is the covariance matrix (1 × 1) of the error in the measurements at time j.

DEFINITIONS:

t_4 = TIME OF SIGNAL RECEPTION AT TRACKER. ALSO, TIME TAG OF OBSERVATION.

t_3 = TIME OF SIGNAL TRANSMISSION FROM VEHICLE.

t_2 = TIME OF SIGNAL RECEPTION AT VEHICLE.

t_1 = TIME OF SIGNAL TRANSMISSION FROM TRACKER.

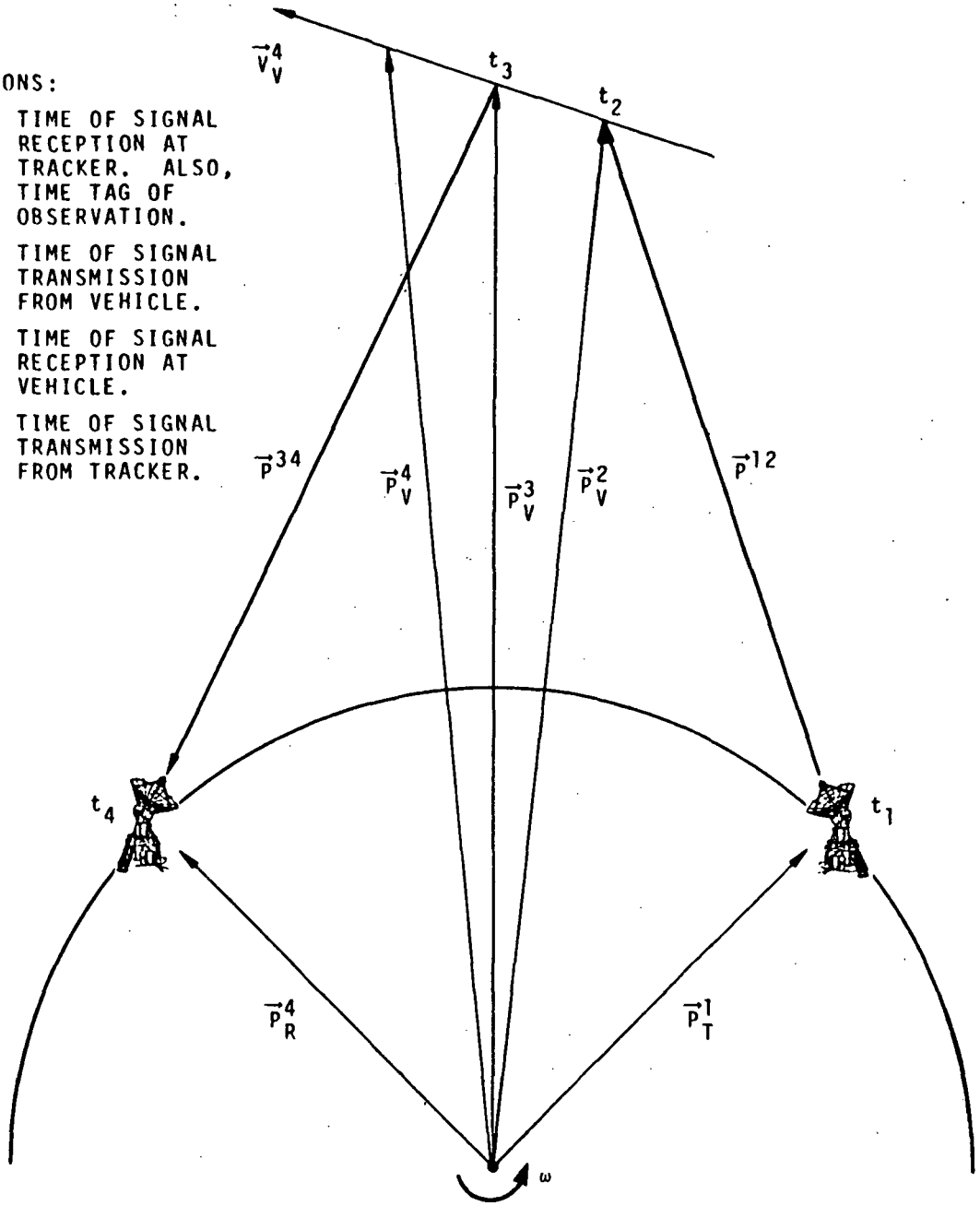

FIGURE A-1. DIAGRAM FOR USB RANGE CALCULATION

APPENDIX B

MATHEMATICAL MODEL OF TUMBLING S-IVB/IU

Modulations of actual range-rate tracking data occur because of transponder motion about the center of mass. Since the LID program models the center of mass trajectory, these range-rate modulations are visible in the actual range-rate residuals following PTC initiation (see typical effects in Figure 2-4).

This appendix develops the rotational equations of motion for a non-symmetrical body with no external moments acting (Reference 9). These equations are applied to the case of the spent S-IVB stage after PTC so that the motion of the tumbling stage is developed. Range-rate modulations are simulated by determining the velocities of the transponders about the C.G. and transforming them to a reference coordinate system. The rotational equation of motion is initialized by using inertial platform attitude data.

The simulated range-rate modulations can be compared with actual range-rate modulations. Hence, significant differences in amplitude and period between simulated and actual modulations can be assessed. This assessment aids in determining if external moments are acting on the actual vehicle.

The velocity accumulation of a perturbing force acting at the C.G. is also developed. Hence, the effectiveness of the PTC maneuver in minimizing translational effects of perturbing forces can be assessed.

The following nomenclature will be used in the development.

$\vec{A}_B$	The perturbing acceleration vector in the body-fixed coordinate system.
$\vec{h}_j$	The angular momentum vector in the j coordinate system.
H	The magnitude of the angular momentum vector.
I_{XP}, I_{YP}, I_{ZP}	The moments of inertia about the X,Y, and Z principal axes.
$\vec{R}_4$	The vector pointing from the ground station to the vehicle center of mass in the PACSS4 coordinate system (see Reference 7) available from the LID program.

APPENDIX B (Continued)

$\hat{R}_4$	The unit vector in the same direction as $\vec{R}_4$.
S1	The projection of the position of antenna 1 onto $\hat{R}_4$.
S2	The projection of the position of antenna 2 onto $\hat{R}_4$.
$\vec{T1}_j, \dot{\vec{T1}}_j$	The position and velocity vectors of antenna 1 in the j system.
$\vec{T2}_j, \dot{\vec{T2}}_j$	The position and velocity vectors of antenna 2 in the j system.
$\Delta\vec{V}_4$	The accumulated change in velocity vector in the PACSS4 system due to $\vec{A}_B$ being applied to the center of mass.
$\delta 1$	The modulation in range rate of antenna 1, projection of $\dot{\vec{T1}}_4$ onto $\hat{R}_4$.
$\delta 2$	The modulation in range rate of antenna 2, projection of $\dot{\vec{T2}}_4$ onto $\hat{R}_4$.
η	The angle between the X-axis in the PACSS4 coordinate system and the X-axis in the angular momentum coordinate system.
$\theta, \dot{\theta}$	The angle of nutation of the body longitudinal axis and its rate relative to the angular momentum coordinate system
$\theta_p, \theta_y, \theta_r$	The vehicle attitudes (pitch, yaw, and roll) as measured by the inertial platform.
$\dot{\theta}_p, \dot{\theta}_y, \dot{\theta}_r$	The vehicle attitude rates.
ξ	The angle between the Z-axis in the PACSS4 coordinate system and the Z-axis in the angular momentum coordinate system.

APPENDIX B (Continued)

$\phi, \dot{\phi}$	The angle of spin of the body and its rate relative to the angular momentum coordinate system.
$\psi, \dot{\psi}$	The angle of precession of the body longitudinal axis and its rate relative to the angular momentum coordinate system.
$\vec{\omega}_j$	The angular velocity vector in the j system.

Definition of subscript j

A	Angular momentum coordinate system.
B	Body-fixed geometric coordinate system.
P	Body-fixed principal axis coordinate system.
4	Geocentric inertial coordinate system (PACSS4).
13	Geocentric plumbline coordinate system (PACSS13).

The motion of the body will be defined relative to an inertial coordinate system. Under the assumption of no external moments, the angular momentum vector is constant in magnitude and direction. For convenience, the inertial frame will be oriented so that the Z-axis is along the angular momentum vector. Figure B-1 shows the relation between the angular momentum coordinate system and the principal axis coordinate system with the transformation defined as follows:

$$\vec{h}_A = [D]\vec{h}_P,$$

where

$$[D] = \begin{bmatrix} \cos\psi & -\sin\psi & 0 \\ \sin\psi & \cos\psi & 0 \\ 0 & 0 & 1 \end{bmatrix} \begin{bmatrix} 1 & 0 & 0 \\ 0 & \cos\theta & -\sin\theta \\ 0 & \sin\theta & \cos\theta \end{bmatrix} \begin{bmatrix} 0 & \cos\phi & -\sin\phi \\ 0 & \sin\phi & \cos\phi \\ 1 & 0 & 0 \end{bmatrix}.$$

APPENDIX B (Continued)

Equations B-1 through B-6 define the Euler angles ψ,θ,ϕ. Using Figure B-1, the angular velocity in the principal axis coordinate system is given in terms of the inertial angular rates by:

$$\vec{\omega}_P = \begin{bmatrix} \dot{\phi} + \dot{\psi}\cos\theta \\ \dot{\psi}\sin\theta\sin\phi + \dot{\theta}\cos\phi \\ \dot{\psi}\sin\theta\cos\phi - \dot{\theta}\sin\phi \end{bmatrix}. \qquad \text{B-1}$$

In a similar manner, the angular momentum vector in the principal axis coordinate system is

$$\vec{h}_P = \begin{bmatrix} H\cos\theta \\ H\sin\theta\sin\phi \\ H\sin\theta\cos\phi \end{bmatrix}. \qquad \text{B-2}$$

Because products of inertia are zero in the principal axis system, the following relation is true:

$$\vec{h}_P = \begin{bmatrix} I_{XP} & 0 & 0 \\ 0 & I_{YP} & 0 \\ 0 & 0 & I_{ZP} \end{bmatrix} \vec{\omega}_P. \qquad \text{B-3}$$

Equating equations B-2 and B-3, solving for $\vec{\omega}_P$, and substituting into equation B-1 gives

$$\begin{aligned} H\cos\theta &= (\dot{\phi} + \dot{\psi}\cos\theta)I_{XP}, \\ H\sin\theta\sin\phi &= (\dot{\psi}\sin\theta\sin\phi + \dot{\theta}\cos\phi)I_{YP}, \text{ and} \\ H\sin\theta\cos\phi &= (\dot{\psi}\sin\theta\cos\phi - \dot{\theta}\sin\phi)I_{ZP}. \end{aligned} \qquad \text{B-4}$$

Solving equations B-4 for the inertial rates gives

$$\begin{aligned} \dot{\psi} &= H\left(\frac{\sin^2\phi}{I_{YP}} + \frac{\cos^2\phi}{I_{ZP}}\right), \\ \dot{\theta} &= H\sin\theta\sin\phi\cos\phi\left(\frac{1}{I_{YP}} - \frac{1}{I_{ZP}}\right), \text{ and} \\ \dot{\phi} &= H\cos\theta\left(\frac{1}{I_{XP}} - \frac{\sin^2\phi}{I_{YP}} - \frac{\cos^2\phi}{I_{ZP}}\right). \end{aligned} \qquad \text{B-5}$$

APPENDIX B (Continued)

Equations B-5 give the inertial angular rates of the body-fixed principal axes as functions of the inertial angles and the principal moments of inertia. The inertial angles can be determined by

$$\psi = \psi_0 + \int_{t_0}^{t} \dot{\psi} dt,$$

$$\theta = \theta_0 + \int_{t_0}^{t} \dot{\theta} dt, \text{ and} \qquad \text{B-6}$$

$$\phi = \phi_0 + \int_{t_0}^{t} \dot{\phi} dt;$$

where ψ_0, θ_0, and ϕ_0 are constants of integration.

The constants of integration in Equations B-6 are determined by use of the attitude angles measured by the inertial platform. Since the platform gives only the attitudes, the initial attitude rates are determined by differentiation of a polynomial fitted to the attitudes. It should be noted that soon after initiation of the PTC maneuver, the inertial platform attitudes become invalid due to platform gimbal lock. Therefore, the initiation of the simulation occurs after PTC but prior to gimbal lock. Using Figure B-2, the angular velocity in the body coordinate system is determined from platform attitude angles and rates by

$$\vec{\omega}_B = \begin{bmatrix} \dot{\theta}_r + \dot{\theta}_p \sin\theta_y \\ \dot{\theta}_y \sin\theta_r + \dot{\theta}_p \cos\theta_y \cos\theta_r \\ \dot{\theta}_y \cos\theta_r - \dot{\theta}_p \cos\theta_y \sin\theta_r \end{bmatrix}, \qquad \text{B-7}$$

and

$$\vec{\omega}_P = [E]\vec{\omega}_B;$$

APPENDIX B (Continued)

where the E matrix is the transformation from the body system to the principal axis system and is determined by knowing vehicle mass distributions. Since

$$\vec{h}_P = \begin{bmatrix} I_{XP} & 0 & 0 \\ 0 & I_{YP} & 0 \\ 0 & 0 & I_{ZP} \end{bmatrix} \vec{\omega}_P ,$$

the angular momentum vector in the principal axis system is now known. In order to be compatible with the LID program, the PACSS4 coordinate system is used as the reference system. The angular momentum vector in the PACSS4 system is given by

$$\vec{h}_4 = [B][A][E]^{-1} \vec{h}_P ,$$

where

$$[A] = \begin{bmatrix} \cos\theta_p & 0 & \sin\theta_p \\ 0 & 1 & 0 \\ -\sin\theta_p & 0 & \cos\theta_p \end{bmatrix} \begin{bmatrix} \cos\theta_y & -\sin\theta_y & 0 \\ \sin\theta_y & \cos\theta_y & 0 \\ 0 & 0 & 1 \end{bmatrix} \begin{bmatrix} 1 & 0 & 0 \\ 0 & \cos\theta_r & -\sin\theta_r \\ 0 & \sin\theta_r & \cos\theta_r \end{bmatrix} .$$

The B matrix is given in Appendix C and relates the inertial platform system and the geocentric plumbline system, PACSS13 to PACSS4. The A matrix relates the body coordinate system to PACSS13 and can be determined by inspection of Figure B-2. The angular momentum coordinate system is related to the PACSS4 system as shown in Figure B-3 by

$$\vec{h}_A = [C] \vec{h}_4 ;$$

where

$$[C] = \begin{bmatrix} 1 & 0 & 0 \\ 0 & \cos\xi & \sin\xi \\ 0 & -\sin\xi & \cos\xi \end{bmatrix} \begin{bmatrix} \cos\eta & \sin\eta & 0 \\ -\sin\eta & \cos\eta & 0 \\ 0 & 0 & 1 \end{bmatrix} ,$$

APPENDIX B (Continued)

$$\eta = \tan^{-1}\left(\frac{h_{X4}}{-h_{Y4}}\right),$$

$$\xi = \cos^{-1}\left(\frac{h_{Z4}}{H}\right), \text{ and}$$

$$\vec{h}_4 = (h_{X4}, h_{Y4}, h_{Z4}).$$

Using Equations B-8 and Figure B-1, ϕ_0 and θ_0 for Equations B-6 are determined by

$$\phi_0 = \tan^{-1}\left(\frac{h_{YP}}{h_{ZP}}\right), \text{ and}$$

$$\theta_0 = \cos^{-1}\left(\frac{h_{XP}}{H}\right), \qquad \text{B-8}$$

where

$$\vec{h}_P = (h_{XP}, h_{YP}, h_{ZP}).$$

Additional information is needed to define ψ_0 and is obtained by transforming a unit vector along the X principal axis to the angular momentum system as follows:

$$\hat{X}_A = [C][B][A][E]^{-1}\,\hat{X}_P$$

where $\hat{X}_P = (1,0,0)$.

Using $\hat{X}_A$, ψ_0 is given by

$$\psi_0 = \tan^{-1}\left(\frac{X_A}{-Y_A}\right) \qquad \text{B-9}$$

where $\hat{X}_A = (X_A, Y_A, Z_A)$.

Using Equations B-8 and B-9 to determine the initial inertial angles, the angles at any time are determined by numerical integration of Equations B-5. At any time, the inertial angles and rates are substituted into Equation B-1 to determine the

APPENDIX B (Continued)

angular velocity in the principal axis system. Knowing the position of the two S-band antennas in the principal axis system, the velocities of the antennas are given by

$$\dot{\vec{T}}1_P = \vec{\omega}_P \times \vec{T}1_P \text{ and}$$

$$\dot{\vec{T}}2_P = \vec{\omega}_P \times \vec{T}2_P.$$

These velocities are transformed to the reference coordinate system by

$$\dot{\vec{T}}1_4 = [C]^{-1}[D]\ \dot{\vec{T}}1_P, \text{ and}$$

$$\dot{\vec{T}}2_4 = [C]^{-1}[D]\ \dot{\vec{T}}2_P.$$

The modulation in a given station's range rate produced by each antenna is given by

$$\delta 1 = \dot{\vec{T}}_4 \cdot \hat{R}_4, \text{ and}$$

$$\delta 2 = \dot{\vec{T}}_4 \cdot \hat{R}_4.$$

It is noted that for the majority of the time only one antenna is seen by the tracking station. The positions of the antennas in the principal axis system are transformed to the reference system and the projections of them on the tracking station vector are determined by

$$\vec{T}1_4 = [C]^{-1}[D]\ \vec{T}1_P,$$

$$\vec{T}2_4 = [C]^{-1}[D]\ \vec{T}2_P,$$

$$S1 = \vec{T}1_4 \cdot \hat{R}_4, \text{ and}$$

$$S2 = \vec{T}2_4 \cdot \hat{R}_4.$$

APPENDIX B (Continued)

When S1 and S2 are compared, the smallest one indicates the antenna that is closest to the tracker. The closest antenna is used as the one that can be seen by the tracker. Figure B-4 shows a set of simulated range-rate modulations for a moment-free S-IVB/IU. Antenna switchings are seen as small, sharp peaks in the figure. Figure B-4 indicates that a moment-free vehicle does not exhibit a significant change in frequency or amplitude of the range-rate modulations.

When a longitudinal body-fixed acceleration is applied to the center of mass, the accumulated velocities in PACSS4 are given by

$$\Delta\vec{V}_4 = \int_{t_0}^{t} [C]^{-1}[D][E]\vec{A}_B dt.$$

Figure B-5 depicts the magnitude of the accumulated change in velocity in the PACSS4 coordinate system for an acceleration of 1 mm/s^2 along the vehicle longitudinal axis. Figure B-5 indicates that the passive thermal control maneuver does not completely disperse body-fixed perturbing accelerations so that the accumulated velocity change is zero.

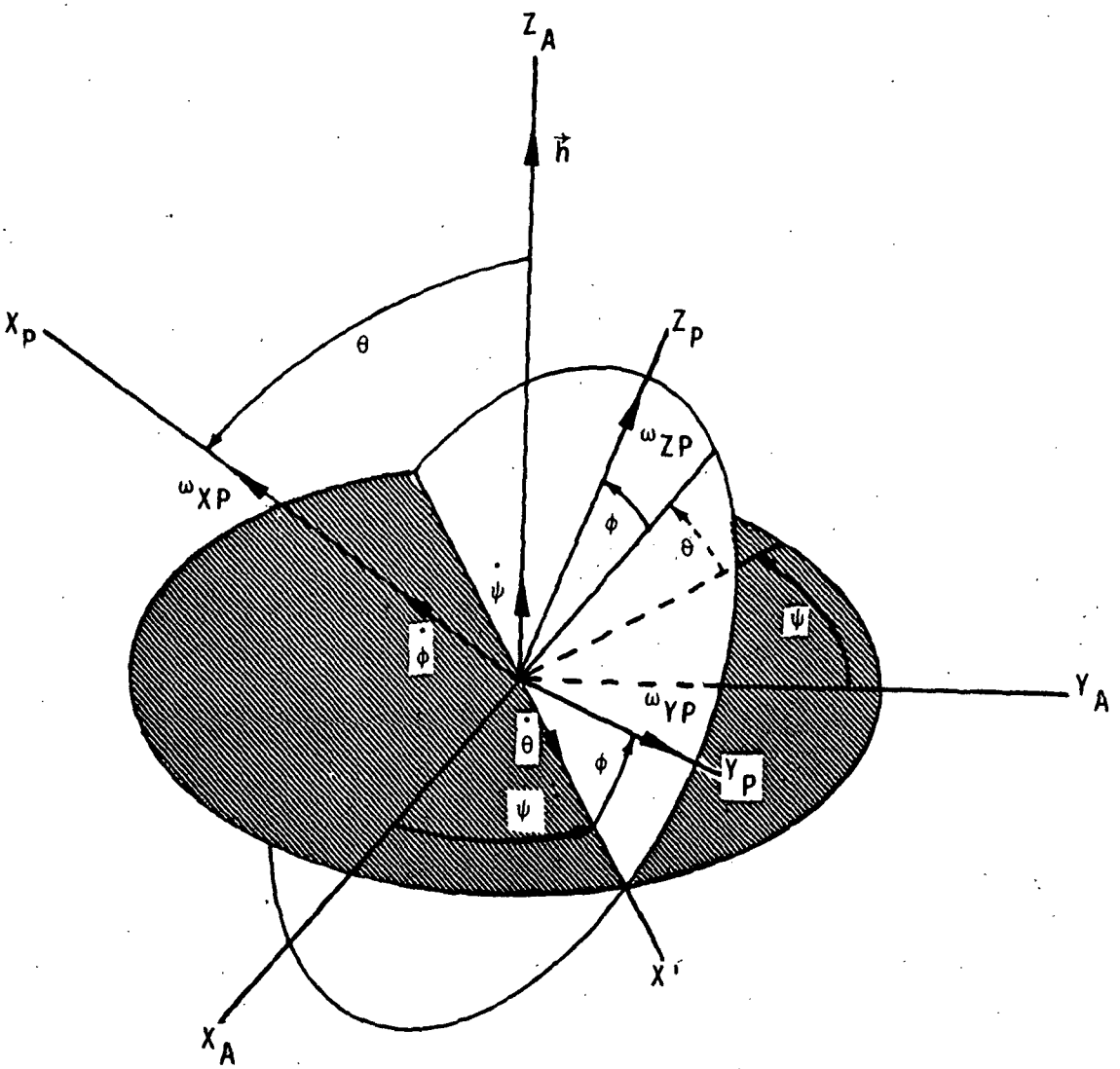

ORDER OF ROTATION:

1 ABOUT Z_A THROUGH ψ

2 ABOUT X' THROUGH θ

3 ABOUT X_P THROUGH ϕ

FIGURE B-1. VEHICLE ROTATIONS AND ROTATION RATES

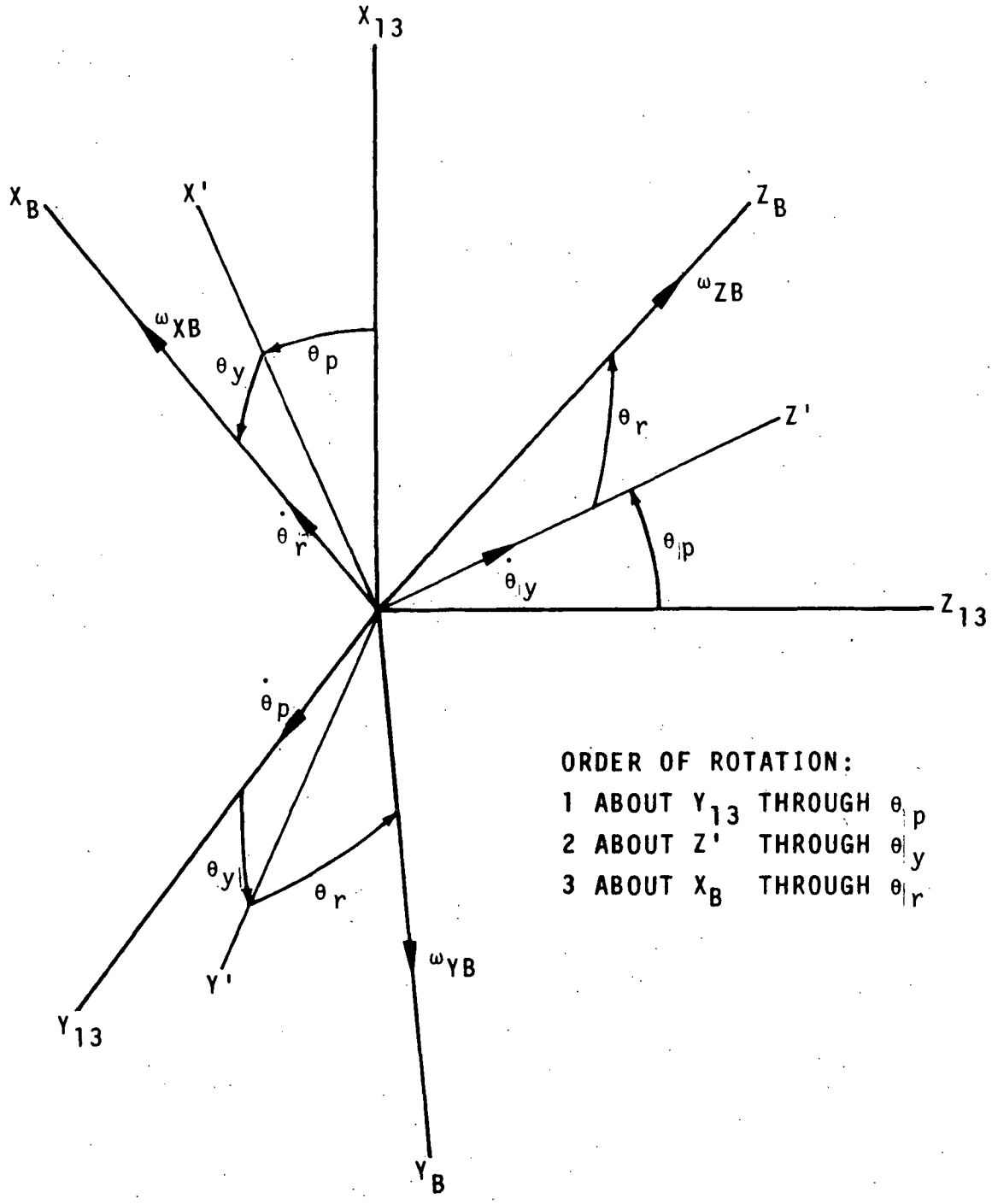

FIGURE B-2. VEHICLE ATTITUDE AND ATTITUDE RATES

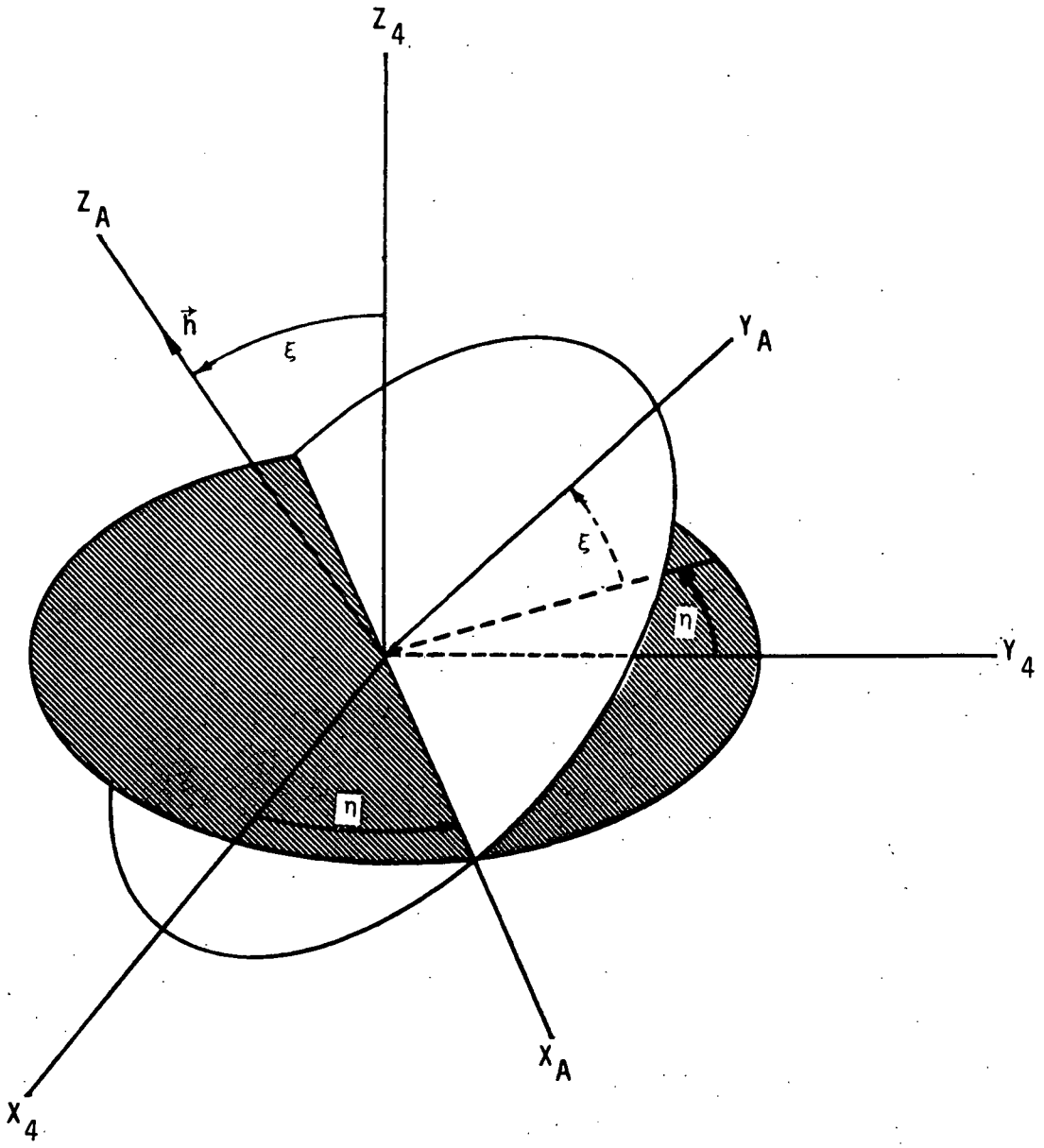

ORDER OF ROTATION:

1 ABOUT Z_4 THROUGH η

2 ABOUT X_A THROUGH ξ

FIGURE B-3. RELATIONSHIP BETWEEN THE ANGULAR MOMENTUM COORDINATE SYSTEM AND PACSS4

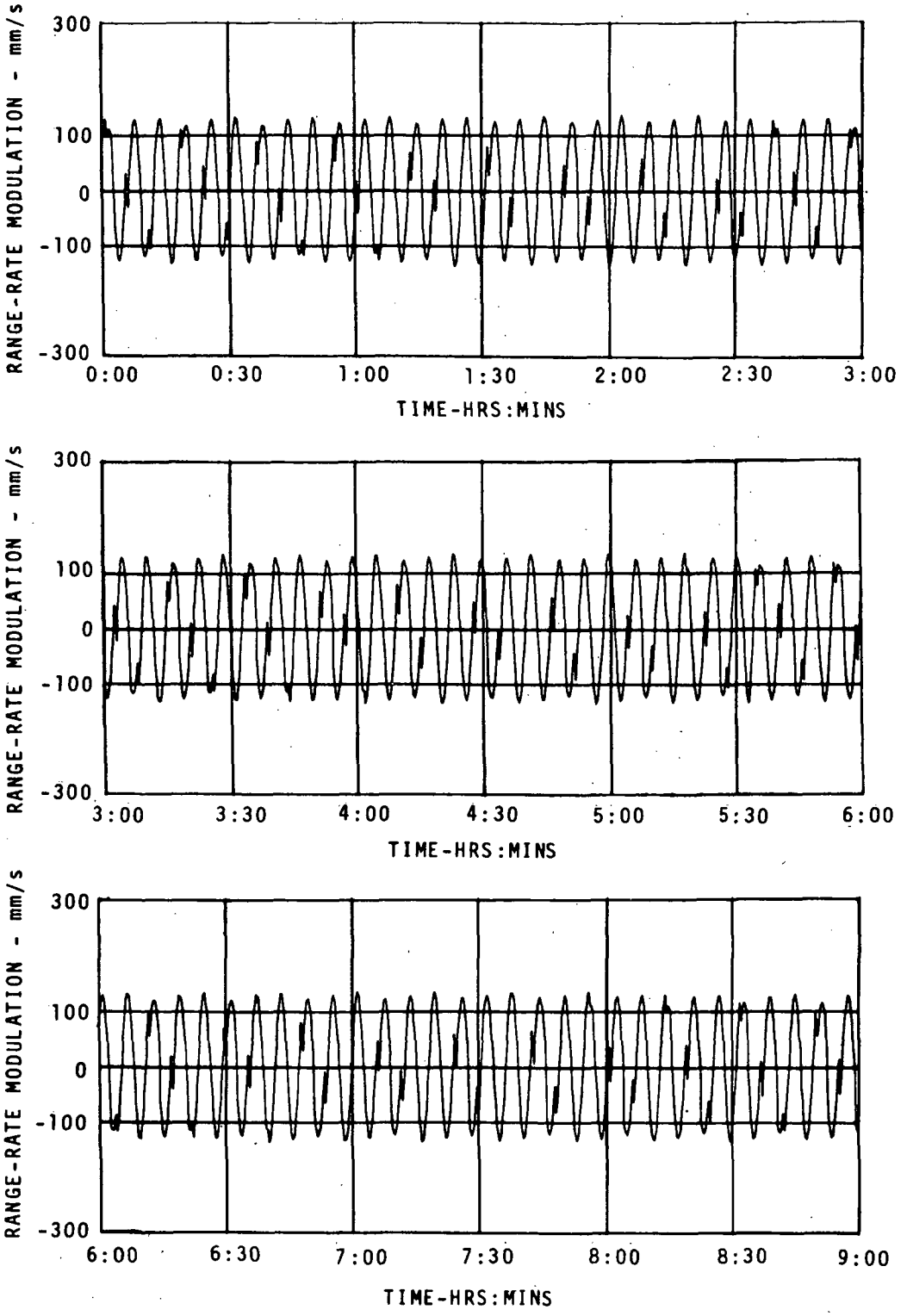

FIGURE B-4. SIMULATED RANGE-RATE MODULATIONS

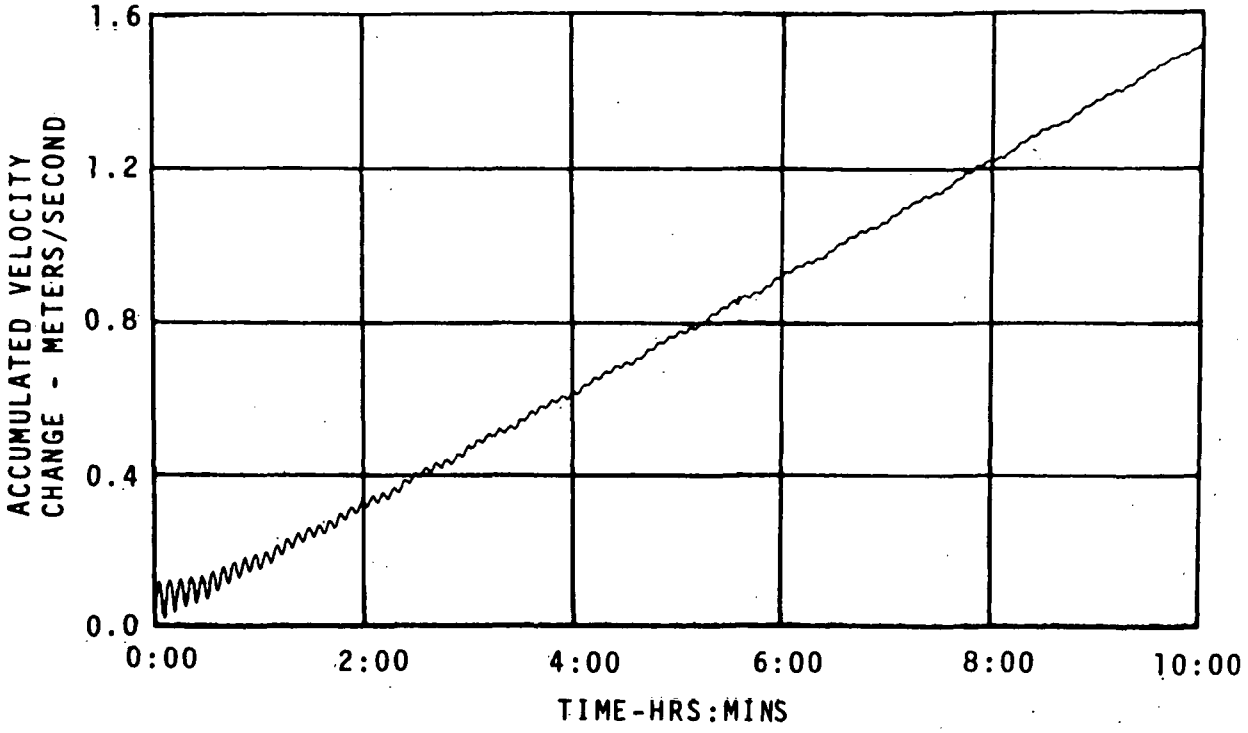

FIGURE B-5. SIMULATED S-IVB/IU VELOCITY CHANGE DURING PTC

APPENDIX C

BEST-ESTIMATE TRAJECTORY HISTORY

This appendix contains a time history of the composite best-estimate AS-512 lunar impact trajectory from CSM/LV separation to lunar impact. The following parameters are included:

1. Greenwich Mean Time in hours, minutes, and seconds.
2. Time, in hours, from beginning of December 6, 1972.
3. PACSS4 (Mean of 1972) position in kilometers and velocity in kilometers per second.
4. Declination and longitude in degrees, both geocentric and selenocentric.
5. The following selected true-of-date osculating orbital elements relative to either the earth or moon.
   a. Semi-major axis in kilometers (orbit is hyperbolic when negative).
   b. Eccentricity.
   c. Inclination in degrees.
   d. Right ascension of ascending node in degrees.
   e. Argument of perifocus in degrees.
   f. True anomaly in degrees.

The integration of the trajectory presented in this appendix included the accelerations given in Tables 2-II and 2-III. The acceleration in these tables are expressed in PACSS13. The transformation of any vector from PACSS13 to PACSS4 (Mean of 1972) is given by

$$\vec{V}_4 = [B]\vec{V}_{13}$$

where

$$[B] = \begin{bmatrix} 0.1725450163 & 0.1197644443 & -0.9776935590 \\ 0.8609078522 & 0.4639545344 & 0.2087674755 \\ 0.4786082797 & -0.8777258505 & -0.0230531069 \end{bmatrix}$$

APPENDIX C (Continued)

The gravitational effects of the earth, moon and sun were also included. Trajectory integration was carried out in double precision and is based on a DE19 ephemeris with a time correction of 43.18 seconds. The lunar impact analysis was conducted on IBM 360 Model 65 and on IBM 370 Model 155 computers.

S-IVB LUNAR-IMPACT TRAJECTORY

7 DEC. 1972 G.M.T. = 9 HR 15 MIN 28.000000 SEC

TIME = 33.25778

CSM/LV SEPARATED

PARAMETER	GEOCENTRIC	SELENOCENTRIC
X -	-7.982018892D 03	-2.239134115D 04
Y -	-8.561384353D 03	3.580126514D 05
Z -	-5.614737982D 03	1.636555177D 05
|R| -	1.298211116D 04	3.942810624D 05
XD -	1.002658356D 00	3.082656853D-02
YD -	-6.846998590D 00	-6.861315863D 00
ZD -	-3.432302690D 00	-3.532501608D 00
|V| -	7.724468605D 00	7.717329412D 00
DECLINATION -	-2.563140686D 01	1.555279763D 00
LONGITUDE -	1.191530083D 01	-1.646717964D 00
SEMI-MAJOR AXIS -	2.289960348D 05	
ECCENTRICITY -	0.971257589D 00	
INCLINATION -	2.844039161D 01	
RIGHT ASC. OF NODE -	-1.533455171D 01	
ARG. OF PERIFOCUS -	1.552395468D 02	
TRUE ANOMALY -	9.003405468D 01	

S-IVB LUNAR-IMPACT TRAJECTORY (CONTINUED)

7 DEC. 1972 G.M.T. = 9 HR 30 MIN 11.000000 SEC

TIME = 33.50306

CSM/LM DOCKED

PARAMETER	GEOCENTRIC	SELENOCENTRIC
X -	-6.697325494D 03	-2.196473514D 04
Y -	-1.407607576D 04	3.524844543D 05
Z -	-8.311003172D 03	1.608703777D 05
|R| -	1.766530077D 04	3.880811975D 05
XD -	1.768878150D 00	7.971378642D-01
YD -	-5.724178023D 00	-5.740451359D 00
ZD -	-2.736615040D 00	-2.837718040D 00
|V| -	6.586668796D 00	6.452972513D 00
DECLINATION -	-2.806842327D 01	1.520943028D 00
LONGITUDE -	2.577643056D 01	-1.793355736D 00
SEMI-MAJOR AXIS -	2.285341017D 05	
ECCENTRICITY -	0.971199253D 00	
INCLINATION -	2.844172170D 01	
RIGHT ASC. OF NODE -	-1.532367213D 01	
ARG. OF PERIFOCUS -	1.552284018D 02	
TRUE ANOMALY -	1.058679578D 02	

S-IVB LUNAR-IMPACT TRAJECTORY (CONTINUED)

7 DEC. 1972 G.M.T. = 10 HR 0 MIN 0.0 SEC

TIME = 34.00000

PARAMETER	GEOCENTRIC	SELENOCENTRIC
X -	-3.089928882D 03	-2.009560607D 04
Y -	-2.304025140D 04	3.434876205D 05
Z -	-1.247810273D 04	1.565207672D 05
|R| -	2.638378087D 04	3.780030782D 05
XD -	2.148106269D 00	1.176565668D 00
YD -	-4.448065638D 00	-4.468302682D 00
ZD -	-2.017369098D 00	-2.120302720D 00
|V| -	5.335674891D 00	5.083868532D 00
DECLINATION -	-2.822728442D 01	1.492725270D 00
LONGITUDE -	3.610881795D 01	-2.264274560D 00
SEMI-MAJOR AXIS -	2.282494534D 05	
ECCENTRICITY -	0.971161523D 00	
INCLINATION -	2.844140456D 01	
RIGHT ASC. OF NODE -	-1.527122703D 01	
ARG. OF PERIFOCUS -	1.551829365D 02	
TRUE ANOMALY -	1.215549276D 02	

S-IVB LUNAR-IMPACT TRAJECTORY (CONTINUED)

7 DEC. 1972 G.M.T. = 10 HR 18 MIN 2.000000 SEC

TIME = 34.30056

CSM/LM EJECTED

PARAMETER	GEOCENTRIC	SELENOCENTRIC
X -	-7.401188365D 02	-1.879693318D 04
Y -	-2.759045456D 04	3.389142238D 05
Z -	-1.452062391D 04	1.543662732D 05
|R| -	3.118700815D 04	3.728875436D 05
XD -	2.185187382D 00	1.213776846D 00
YD -	-3.987318528D 00	-4.009953238D 00
ZD -	-1.772381104D 00	-1.876421181D 00
|V| -	4.880070462D 00	4.590635648D 00
DECLINATION -	-2.774982258D 01	1.487142644D 00
LONGITUDE -	3.768990122D 01	-2.587536740D 00
SEMI-MAJOR AXIS -	2.281586918D 05	
ECCENTRICITY -	0.971147793D 00	
INCLINATION -	2.843799781D 01	
RIGHT ASC. OF NODE -	-1.522872887D 01	
ARG. OF PERIFOCUS -	1.551472850D 02	
TRUE ANOMALY -	1.269618420D 02	

S-IVB LUNAR-IMPACT TRAJECTORY (CONTINUED)

7 DEC. 1972 G.M.T. = 10 HR 25 MIN 4.000000 SEC

TIME = 34.41778

EVASIVE BURN ATTITUDE MANEUVER INITIATED

PARAMETER	GEOCENTRIC	SELENOCENTRIC
X -	1.8259847690 02	-1.8284140030 04
Y -	-2.9241991650 04	3.3725293760 05
Z -	-1.5252171740 04	1.5359072950 05
|R| -	3.2981148560 04	3.7103094760 05
XD -	2.1869149650 00	1.2155570570 00
YD -	-3.8424119350 00	-3.8659818540 00
ZD -	-1.6964823650 00	-1.8009538310 00
|V| -	4.7354808580 00	4.4347299070 00
DECLINATION -	-2.7546024460 01	1.4862388150 00
LONGITUDE -	3.7821109270 01	-2.7167860400 00
SEMI-MAJOR AXIS -	2.2819066470 05	
ECCENTRICITY -	0.9711459150 00	
INCLINATION -	2.8437549110 01	
RIGHT ASC. OF NODE -	-1.5225716040 01	
ARG. OF PERIFOCUS -	1.5515079850 02	
TRUE ANOMALY -	1.2864604150 02	

S-IVB LUNAR-IMPACT TRAJECTORY (CONTINUED)

7 DEC. 1972 G.M.T. = 10 HR 35 MIN 60.000000 SEC

TIME = 34.60000

TIMEBASE 8 INITIATED

PARAMETER	GEOCENTRIC	SELENOCENTRIC
X -	1.615845307D 03	-1.748807658D 04
Y -	-3.169619718D 04	3.347827934D 05
Z -	-1.633077280D 04	1.524433752D 05
|R| -	3.569249237D 04	3.682720904D 05
XD -	2.181418878D 00	1.210144896D 00
YD -	-3.645057902D 00	-3.670081685D 00
ZD -	-1.594807179D 00	-1.699949072D 00
|V| -	4.537449214D 00	4.221821537D 00
DECLINATION -	-2.722885790D 01	1.485834849D 00
LONGITUDE -	3.764084667D 01	-2.919743256D 00
SEMI-MAJOR AXIS -	2.281692022D 05	
ECCENTRICITY -	0.971141059D 00	
INCLINATION -	2.843347345D 01	
RIGHT ASC. OF NODE -	-1.519372037D 01	
ARG. OF PERIFOCUS -	1.551245073D 02	
TRUE ANOMALY -	1.309397261D 02	

S-IVB LUNAR-IMPACT TRAJECTORY (CONTINUED)

7 DEC. 1972 G.M.T. = 10 HR 45 MIN 40.000000 SEC

TIME = 34.76111

LOX DUMP ATTITUDE MANEUVER INITIATED

PARAMETER	GEOCENTRIC	SELENOCENTRIC
X -	2.876877292D 03	-1.679036143D 04
Y -	-3.376636120D 04	3.326977429D 05
Z -	-1.723124252D 04	1.514817514D 05
|R| -	3.801788119D 04	3.659459302D 05
XD -	2.168584447D 00	1.197386814D 00
YD -	-3.495175837D 00	-3.521485127D 00
ZD -	-1.514621088D 00	-1.620355566D 00
|V| -	4.383273854D 00	4.057110406D 00
DECLINATION -	-2.695186603D 01	1.486570765D 00
LONGITUDE -	3.716897285D 01	-3.100296325D 00
SEMI-MAJOR AXIS -	2.269744532D 05	
ECCENTRICITY -	0.971049621D 00	
INCLINATION -	2.845927372D 01	
RIGHT ASC. OF NODE -	-1.538073099D 01	
ARG. OF PERIFOCUS -	1.552238184D 02	
TRUE ANOMALY -	1.327640883D 02	

S-IVB LUNAR-IMPACT TRAJECTORY (CONTINUED)

7 DEC. 1972 G.M.T. = 10 HR 52 MIN 40.000000 SEC

TIME = 34.87778

CVS VENTING INITIATED

PARAMETER	GEOCENTRIC	SELENOCENTRIC
X -	3.785752333D 03	-1.628937754D 04
Y -	-3.521329701D 04	3.312395617D 05
Z -	-1.785675605D 04	1.508117393D 05
|R| -	3.966323163D 04	3.643201482D 05
XD -	2.159160233D 00	1.188019145D 00
YD -	-3.396393510D 00	-3.423633730D 00
ZD -	-1.464779171D 00	-1.570942662D 00
|V| -	4.282877515D 00	3.949749138D 00
DECLINATION -	-2.675704584D 01	1.487501379D 00
LONGITUDE -	3.668059352D 01	-3.231503493D 00
SEMI-MAJOR AXIS -	2.269509054D 05	
ECCENTRICITY -	0.971045601D 00	
INCLINATION -	2.845560987D 01	
RIGHT ASC. OF NODE -	-1.535783500D 01	
ARG. OF PERIFOCUS -	1.552043600D 02	
TRUE ANOMALY -	1.339099234D 02	

S-IVB LUNAR-IMPACT TRAJECTORY (CONTINUED)

7 DEC. 1972 G.M.T. = 10 HR 57 MIN 20.000000 SEC

TIME = 34.95556

LOX DUMP INITIATED

PARAMETER	GEOCENTRIC	SELENOCENTRIC
X -	4.3892848800 03	-1.5957759140 04
Y -	-3.6155623950 04	3.3028952070 05
Z -	-1.8262504770 04	1.5037622470 05
|R| -	4.0743269940 04	3.6326137310 05
XD -	2.1517079840 00	1.1806051790 00
YD -	-3.3350668340 00	-3.3629276940 00
ZD -	-1.4337265630 00	-1.5401760160 00
|V| -	4.2199632570 00	3.8826863670 00
DECLINATION -	-2.6630250260 01	1.4882787390 00
LONGITUDE -	3.6296283520 01	-3.3191022880 00
SEMI-MAJOR AXIS -	2.2667371310 05	
ECCENTRICITY -	0.9710236610 00	
INCLINATION -	2.8456333900 01	
RIGHT ASC. OF NODE -	-1.5362131230 01	
ARG. OF PERIFOCUS -	1.5519424530 02	
TRUE ANOMALY -	1.3463700350 02	

S-IVB LUNAR-IMPACT TRAJECTORY (CONTINUED)

7 DEC. 1972 G.M.T. = 11 HR 0 MIN 0.0 SEC

TIME = 35.00000

PARAMETER	GEOCENTRIC	SELENOCENTRIC
X -	4.7320003470 03	-1.5770418350 04
Y -	-3.6686698680 04	3.2975395990 05
Z -	-1.8489963540 04	1.5013172100 05
|R| -	4.1354376300 04	3.6266501410 05
XD -	2.1385212540 00	1.1674405360 00
YD -	-3.3026583680 00	-3.3308738870 00
ZD -	-1.4126047220 00	-1.5192175640 00
|V| -	4.1804637960 00	3.8426111250 00
DECLINATION -	-2.6558213110 01	1.4888649200 00
LONGITUDE -	3.6055621300 01	-3.3689904520 00
SEMI-MAJOR AXIS -	2.2130362350 05	
ECCENTRICITY -	0.9705907100 00	
INCLINATION -	2.8516272860 01	
RIGHT ASC. OF NODE -	-1.5706691800 01	
ARG. OF PERIFOCUS -	1.5522576560 02	
TRUE ANOMALY -	1.3529761670 02	

S-IVB LUNAR-IMPACT TRAJECTORY (CONTINUED)

7 DEC. 1972 G.M.T. = 11 HR 35 MIN 26.000000 SEC

TIME = 35.59056

APS-1 IMPACT BURN ATTITUDE MANEUVER INITIATED

PARAMETER	GEOCENTRIC	SELENOCENTRIC
X -	9.213655840D 03	-1.335295772D 04
Y -	-4.329263883D 04	3.230830240D 05
Z -	-2.128768053D 04	1.471050382D 05
|R| -	4.911526618D 04	3.552475663D 05
XD -	2.076132792D 00	1.105360106D 00
YD -	-2.933240814D 00	-2.966169334D 00
ZD -	-1.230733120D 00	-1.339515811D 00
|V| -	3.798543544D 00	3.437191308D 00
DECLINATION -	-2.568420290D 01	1.499431669D 00
LONGITUDE -	3.183780950D 01	-4.031359942D 00
SEMI-MAJOR AXIS -	2.211509627D 05	
ECCENTRICITY -	0.970558231D 00	
INCLINATION -	2.848970804D 01	
RIGHT ASC. OF NODE -	-1.557419464D 01	
ARG. OF PERIFOCUS -	1.551169704D 02	
TRUE ANOMALY -	1.395682447D 02	

S-IVB LUNAR-IMPACT TRAJECTORY (CONTINUED)

7 DEC. 1972 G.M.T. = 11 HR 42 MIN 60.000000 SEC

TIME = 35.71667

APS-1 IMPACT BURN INITIATED

PARAMETER	GEOCENTRIC	SELENOCENTRIC
X -	1.015305501D 04	-1.285427365D 04
Y -	-4.460959694D 04	3.217508879D 05
Z -	-2.183929767D 04	1.465039286D 05
|R| -	5.069571567D 04	3.537686626D 05
XD -	2.062184720D 00	1.091481321D 00
YD -	-2.869030664D 00	-2.902965737D 00
ZD -	-1.199661798D 00	-1.308907564D 00
|V| -	3.731371223D 00	3.362710160 00
DECLINATION -	-2.551694253D 01	1.502142550D 00
LONGITUDE -	3.074833182D 01	-4.172394817D 00
SEMI-MAJOR AXIS -	2.211771534D 05	
ECCENTRICITY -	0.970557654D 00	
INCLINATION -	2.848285322D 01	
RIGHT ASC. OF NODE -	-1.554344475D 01	
ARG. OF PERIFOCUS -	1.550931516D 02	
TRUE ANOMALY -	1.403121068D 02	

S-IVB LUNAR-IMPACT TRAJECTORY (CONTINUED)

7 DEC. 1972 G.M.T. = 11 HR 50 MIN 45.000000 SEC

TIME = 35.84583

COMMUNICATION ATTITUDE MANEUVER INITIATED

PARAMETER	GEOCENTRIC	SELENOCENTRIC
X -	1.1107674320 04	-1.2351014650 04
Y -	-4.5928585730 04	3.2041587970 05
Z -	-2.2388556960 04	1.4590375980 05
|R| -	5.2288267310 04	3.5228793630 05
XD -	2.0454990720 00	1.0748679190 00
YD -	-2.8059220190 00	-2.8408880690 00
ZD -	-1.1659988420 00	-1.2757187950 00
|V| -	3.6628975050 00	3.2944566330 00
DECLINATION -	-2.5350861160 01	1.5052257980 00
LONGITUDE -	2.9579244750 01	-4.3164323190 00
SEMI-MAJOR AXIS -	2.1786901200 05	
ECCENTRICITY -	0.9701574060 00	
INCLINATION -	2.8530880760 01	
RIGHT ASC. OF NODE -	-1.5753797630 01	
ARG. OF PERIFOCUS -	1.5520804700 02	
TRUE ANOMALY -	1.4110025670 02	

S-IVB LUNAR-IMPACT TRAJECTORY (CONTINUED)

7 DEC. 1972 G.M.T. = 12 HR 0 MIN 0.0 SEC

TIME = 36.00000

PARAMETER	GEOCENTRIC	SELENOCENTRIC
X -	1.223816295D 04	-1.175920197D 04
Y -	-4.746661626D 04	3.188581015D 05
Z -	-2.302630880D 04	1.452049564D 05
|R| -	5.415776203D 04	3.505613308D 05
XD -	2.028358032D 00	1.057814805D 00
YD -	-2.737357946D 00	-2.773554563D 00
ZD -	-1.132635419D 00	-1.242921196D 00
|V| -	3.590296342D 00	3.218140795D 00
DECLINATION -	-2.516041336D 01	1.509098212D 00
LONGITUDE -	2.812216546D 01	-4.487923194D 00
SEMI-MAJOR AXIS -	2.178339694D 05	
ECCENTRICITY -	0.970152837D 00	
INCLINATION -	2.853127526D 01	
RIGHT ASC. OF NODE -	-1.575543842D 01	
ARG. OF PERIFOCUS -	1.552089191D 02	
TRUE ANOMALY -	1.419031355D 02	

S-IVB LUNAR-IMPACT TRAJECTORY (CONTINUED)

7 DEC. 1972 G.M.T. = 14 HR 0 MIN 0.0 SEC

TIME = 38.00000

PARAMETER	GEOCENTRIC	SELENOCENTRIC
X -	2.6101886570 04	-4.8788675720 03
Y -	-6.4772857080 04	3.0123376380 05
Z -	-3.0032509630 04	1.3737830800 05
|R| -	7.6018307870 04	3.3111686990 05
XD -	1.8314305240 00	8.6219528560-01
YD -	-2.1399155020 00	-2.1920799260 00
ZD -	-8.4885683640-01	-9.6646855270-01
|V| -	2.9417569660 00	2.5461061600 00
DECLINATION -	-2.3268344360 01	1.5687667910 00
LONGITUDE -	5.5303934060 00	-6.6632990730 00
SEMI-MAJOR AXIS -	2.1744788780 05	
ECCENTRICITY -	0.9701026690 00	
INCLINATION -	2.8538225500 01	
RIGHT ASC. OF NODE -	-1.5779434410 01	
ARG. OF PERIFOCUS -	1.5522315490 02	
TRUE ANOMALY -	1.4899723250 02	

S-IVB LUNAR-IMPACT TRAJECTORY (CONTINUED)

7 DEC. 1972 G.M.T. = 16 HR 0 MIN 0.0 SEC

TIME = 40.00000

PARAMETER	GEOCENTRIC	SELENOCENTRIC
X -	3.8725860510 04	7.7225392200 02
Y -	-7.8884787570 04	2.8668875210 05
Z -	-3.5547802940 04	1.3098992120 05
|R| -	9.4795296690 04	3.1519738880 05
XD -	1.6817646230 00	7.1414829420-01
YD -	-1.8060263510 00	-1.8741622920 00
ZD -	-6.9566319760-01	-8.2057249180-01
|V| -	2.5639833680 00	2.1669866860 00
DECLINATION -	-2.2021586140 01	1.6345982620 00
LONGITUDE -	-2.0353015800 01	-8.7451082000 00
SEMI-MAJOR AXIS -	2.1713290930 05	
ECCENTRICITY -	0.9700893780 00	
INCLINATION -	2.8561209950 01	
RIGHT ASC. OF NODE -	-1.5843480170 01	
ARG. OF PERIFOCUS -	1.5525978640 02	
TRUE ANOMALY -	1.5308729460 02	

S-IVB LUNAR-IMPACT TRAJECTORY (CONTINUED)

7 DEC. 1972 G.M.T. = 16 HR 35 MIN 40.000000 SEC

TIME = 40.59444

APS-2 IMPACT BURN ATTITUDE MANEUVER INITIATED

PARAMETER	GEOCENTRIC	SELENOCENTRIC
X -	4.228407128D 04	2.260339848D 03
Y -	-8.266838194D 04	2.827542672D 05
Z -	-3.699975045D 04	1.292683527D 05
|R| -	9.995491778D 04	3.109105806D 05
XD -	1.644109175D 00	6.770339998D-01
YD -	-1.731439118D 00	-1.804322192D 00
ZD -	-6.619621211D-01	-7.890346330D-01
|V| -	2.477734903D 00	2.082433495D 00
DECLINATION -	-2.172320431D 01	1.654370442D 00
LONGITUDE -	-2.835204094D 01	-9.347373472D 00
SEMI-MAJOR AXIS -	2.170462895D 05	
ECCENTRICITY -	0.970092662D 00	
INCLINATION -	2.857173154D 01	
RIGHT ASC. OF NODE -	-1.587081360D 01	
ARG. OF PERIFOCUS -	1.552753478D 02	
TRUE ANOMALY -	1.540194948D 02	

S-IVB LUNAR-IMPACT TRAJECTORY (CONTINUED)

7 DEC. 1972 G.M.T. = 16 HR 47 MIN 60.000000 SEC

TIME = 40.80000

APS-2 IMPACT BURN INITIATED

PARAMETER	GEOCENTRIC	SELENOCENTRIC
X -	4.349609732D 04	2.756801652D 03
Y -	-8.394073295D 04	2.814273753D 05
Z -	-3.748558976D 04	1.286882032D 05
|R| -	1.017011631D 05	3.094666679D 05
XD -	1.631685596D 00	6.648039449D-01
YD -	-1.707494035D 00	-1.782018603D 00
ZD -	-6.511866307D-01	-7.790065336D-01
|V| -	2.449893424D 00	2.055335925D 00
DECLINATION -	-2.162583181D 01	1.661202003D 00
LONGITUDE -	-3.114101495D 01	-9.553998992D 00
SEMI-MAJOR AXIS -	2.170170383D 05	
ECCENTRICITY -	0.970094105D 00	
INCLINATION -	2.857555339D 01	
RIGHT ASC. OF NODE -	-1.588052425D 01	
ARG. OF PERIFOCUS -	1.552809184D 02	
TRUE ANOMALY -	1.543202153D 02	

S-IVB LUNAR-IMPACT TRAJECTORY (CONTINUED)

7 DEC. 1972 G.M.T. = 17 HR 4 MIN 50.000000 SEC

TIME = 41.08056

PTC INITIATED

PARAMETER	GEOCENTRIC	SELENOCENTRIC
X -	4.513342238D 04	3.417711785D 03
Y -	-8.565489327D 04	2.796368137D 05
Z -	-3.813586234D 04	1.279083176D 05
|R| -	1.040583036D 05	3.075206715D 05
XD -	1.614219288D 00	6.476070781D-01
YD -	-1.679402152D 00	-1.756167090D 00
ZD -	-6.405725833D-01	-7.694120389D-01
|V| -	2.415870181D 00	2.023737300D 00
DECLINATION -	-2.149640331D 01	1.670978942D 00
LONGITUDE -	-3.496729357D 01	-9.834266089D 00
SEMI-MAJOR AXIS -	2.184459289D 05	
ECCENTRICITY -	0.970553707D 00	
INCLINATION -	2.849971880D 01	
RIGHT ASC. OF NODE -	-1.569635825D 01	
ARG. OF PERIFOCUS -	1.550267705D 02	
TRUE ANOMALY -	1.548008123D 02	

S-IVB LUNAR-IMPACT TRAJECTORY (CONTINUED)

7 DEC. 1972 G.M.T. = 18 HR 0 MIN 0.0 SEC

TIME = 42.00000

PARAMETER	GEOCENTRIC	SELENOCENTRIC
X -	5.0391866110 04	5.4781834080 03
Y -	-9.1055998980 04	2.7396946500 05
Z -	-4.0186009410 04	1.2542618750 05
|R| -	1.1155917920 05	3.0136523380 05
XD -	1.5639140340 00	5.9822777600-01
YD -	-1.5863981840 00	-1.6705048040 00
ZD -	-5.9926359570-01	-7.3143995770-01
|V| -	2.3068600220 00	1.9192360940 00
DECLINATION -	-2.1111034660 01	1.7001798920 00
LONGITUDE -	-4.7621654940 01	-1.0743469800 01
SEMI-MAJOR AXIS -	2.1848008540 05	
ECCENTRICITY -	0.9705619440 00	
INCLINATION -	2.8504281230 01	
RIGHT ASC. OF NODE -	-1.5707577720 01	
ARG. OF PERIFOCUS -	1.5503570890 02	
TRUE ANOMALY -	1.5596234500 02	

S-IVB LUNAR-IMPACT TRAJECTORY (CONTINUED)

8 DEC. 1972 G.M.T. = 0 HR 0 MIN 0.0 SEC

TIME = 48.00000

PARAMETER	GEOCENTRIC	SELENOCENTRIC
X -	8.133918898D 04	1.564435034D 04
Y -	-1.205704155D 05	2.421212437D 05
Z -	-5.105630902D 04	1.114670542D 05
|R| -	1.541429060D 05	2.670062658D 05
XD -	1.321352596D 00	3.633248453D-01
YD -	-1.191695128D 00	-1.323663092D 00
ZD -	-4.280018319D-01	-5.817748404D-01
|V| -	1.830108065D 00	1.490822219D 00
DECLINATION -	-1.933995641D 01	1.877737853D 00
LONGITUDE -	-1.328248755D 02	-1.635282973D 01
SEMI-MAJOR AXIS -	2.187039040D 05	
ECCENTRICITY -	0.970643635D 00	
INCLINATION -	2.854515107D 01	
RIGHT ASC. OF NODE -	-1.579622653D 01	
ARG. OF PERIFOCUS -	1.550998073D 02	
TRUE ANOMALY -	1.610285363D 02	

S-IVB LUNAR-IMPACT TRAJECTORY (CONTINUED)

8 DEC. 1972 G.M.T. = 6 HR 0 MIN 0.0 SEC

TIME = 54.00000

PARAMETER	GEOCENTRIC	SELENOCENTRIC
X -	1.0804056840 05	2.1760265120 04
Y -	-1.4370102400 05	2.1562466580 05
Z -	-5.9200635060 04	9.9771102670 04
|R| -	1.8928144090 05	2.3858285140 05
XD -	1.1598841250 00	2.1231715940-01
YD -	-9.6666358080-01	-1.1463202550 00
ZD -	-3.3348833410-01	-5.0850600310-01
|V| -	1.5462807420 00	1.2718911350 00
DECLINATION -	-1.8222320110 01	2.0302667730 00
LONGITUDE -	1.3986156880 02	-2.1519388810 01
SEMI-MAJOR AXIS -	2.1892043910 05	
ECCENTRICITY -	0.9707795680 00	
INCLINATION -	2.8604674580 01	
RIGHT ASC. OF NODE -	-1.5908892100 01	
ARG. OF PERIFOCUS -	1.5517269890 02	
TRUE ANOMALY -	1.6404768580 02	

S-IVB LUNAR-IMPACT TRAJECTORY (CONTINUED)

8 DEC. 1972 G.M.T. = 12 HR 0 MIN 0.0 SEC

TIME = 60.00000

PARAMETER	GEOCENTRIC	SELENOCENTRIC
X -	1.3173060350 05	2.5121014100 04
Y -	-1.6283212650 05	1.9210050900 05
Z -	-6.5687953300 04	8.9277598490 04
|R| -	2.1950435190 05	2.1331704200 05
XD -	1.0385738480 00	1.0426489220-01
YD -	-8.1302031840-01	-1.0400679630 00
ZD -	-2.7087474950-01	-4.6672708340-01
|V| -	1.3464808970 00	1.1447474420 00
DECLINATION -	-1.7409068660 01	2.1586255730 00
LONGITUDE -	5.1650367660 01	-2.6342476420 01
SEMI-MAJOR AXIS -	2.1915278770 05	
ECCENTRICITY -	0.9710128390 00	
INCLINATION -	2.8624589440 01	
RIGHT ASC. OF NODE -	-1.5943889370 01	
ARG. OF PERIFOCUS -	1.5515897080 02	
TRUE ANOMALY -	1.6619346770 02	

S-IVB LUNAR-IMPACT TRAJECTORY (CONTINUED)

8 DEC. 1972 G.M.T. = 18 HR 0 MIN 0.0 SEC

TIME = 66.00000

PARAMETER	GEOCENTRIC	SELENOCENTRIC
X -	1.5307480280 05	2.6452416140 04
Y -	-1.7909788980 05	1.7042239330 05
Z -	-7.1021069570 04	7.9493215360 04
|R| -	2.4607304140 05	1.8990179790 05
XD -	9.4082671030-01	2.2562062270-02
YD -	-6.9798090010-01	-9.7199564270-01
ZD -	-2.2503817450-01	-4.4125726640-01
|V| -	1.1928849130 00	1.0677043370 00
DECLINATION -	-1.6771224130 01	2.2632968940 00
LONGITUDE -	-3.7048379590 01	-3.0879953690 01
SEMI-MAJOR AXIS -	2.1940573870 05	
ECCENTRICITY -	0.9713742240 00	
INCLINATION -	2.8641910730 01	
RIGHT ASC. OF NODE -	-1.5971845480 01	
ARG. OF PERIFOCUS -	1.5511882840 02	
TRUE ANOMALY -	1.6786910940 02	

S-IVB LUNAR-IMPACT TRAJECTORY (CONTINUED)

9 DEC. 1972 G.M.T. = 0 HR 0 MIN 0.0 SEC

TIME = 72.00000

PARAMETER	GEOCENTRIC	SELENOCENTRIC
X -	1.724839613D 05	2.622528082D 04
Y -	-1.931562449D 05	1.499429182D 05
Z -	-7.548201440D 04	7.014665600D 04
|R| -	2.697361421D 05	1.676042877D 05
XD -	8.582922557D-01	-4.115865805D-02
YD -	-6.070310127D-01	-9.274619866D-01
ZD -	-1.894661593D-01	-4.255263691D-01
|V| -	1.068199266D 00	1.021250441D 00
DECLINATION -	-1.624631701D 01	2.346103969D 00
LONGITUDE -	-1.260512746D 02	-3.516883120D 01
SEMI-MAJOR AXIS -	2.196820659D 05	
ECCENTRICITY -	0.971931009D 00	
INCLINATION -	2.867604258D 01	
RIGHT ASC. OF NODE -	-1.602418670D 01	
ARG. OF PERIFOCUS -	1.550717087D 02	
TRUE ANOMALY -	1.692648721D 02	

S-IVB LUNAR-IMPACT TRAJECTORY (CONTINUED)

9 DEC. 1972 G.M.T. = 6 HR 0 MIN 0.0 SEC

TIME = 78.00000

PARAMETER	GEOCENTRIC	SELENOCENTRIC
X -	1.902236108D 05	2.476972019D 04
Y -	-2.054399837D 05	1.302425671D 05
Z -	-7.925526958D 04	6.106541290D 04
|R| -	2.909878159D 05	1.459645482D 05
XD -	7.862093666D-01	-9.168131427D-02
YD -	-5.326848185D-01	-8.988533993D-01
ZD -	-1.608957250D-01	-4.162139174D-01
|V| -	9.632059584D-01	9.947748096D-01
DECLINATION -	-1.580088948D 01	2.407862669D 00
LONGITUDE -	1.447365281D 02	-3.923093528D 01
SEMI-MAJOR AXIS -	2.199930601D 05	
ECCENTRICITY -	0.972763978D 00	
INCLINATION -	2.873965288D 01	
RIGHT ASC. OF NODE -	-1.611700700D 01	
ARG. OF PERIFOCUS -	1.550230596D 02	
TRUE ANOMALY -	1.704841942D 02	

S-IVB LUNAR-IMPACT TRAJECTORY (CONTINUED)

9 DEC. 1972 G.M.T. = 12 HR 0 MIN 0.0 SEC

TIME = 84.00000

PARAMETER	GEOCENTRIC	SELENOCENTRIC
X -	2.065027644D 05	2.233877278D 04
Y -	-2.162569126D 05	1.110295794D 05
Z -	-8.247022727D 04	5.213330872D 04
|R| -	3.101802417D 05	1.246774638D 05
XD -	7.217330831D-01	-1.318798833D-01
YD -	-4.707199358D-01	-8.818191197D-01
ZD -	-1.375643941D-01	-4.115002458D-01
|V| -	8.725822962D-01	9.820029103D-01
DECLINATION -	-1.541483223D 01	2.448718583D 00
LONGITUDE -	5.536998878D 01	-4.307656241D 01
SEMI-MAJOR AXIS -	2.203762536D 05	
ECCENTRICITY -	0.973952226D 00	
INCLINATION -	2.883452080D 01	
RIGHT ASC. OF NODE -	-1.624950983D 01	
ARG. OF PERIFOCUS -	1.549685532D 02	
TRUE ANOMALY -	1.715860440D 02	

S-IVB LUNAR-IMPACT TRAJECTORY (CONTINUED)

9 DEC. 1972 G.M.T. = 18 HR 0 MIN 0.0 SEC

TIME = 90.00000

PARAMETER	GEOCENTRIC	SELENOCENTRIC
X -	2.214472804D 05	1.913162202D 04
Y -	-2.258488166D 05	9.208098837D 04
Z -	-8.522945839D 04	4.326221513D 04
|R| -	3.275830376D 05	1.035207528D 05
XD -	6.627987001D-01	-1.638543580D-01
YD -	-4.190509965D-01	-8.741448847D-01
ZD -	-1.186199623D-01	-4.104763377D-01
|V| -	7.930804183D-01	9.795245550D-01
DECLINATION -	-1.507614682D 01	2.466691276D 00
LONGITUDE -	-3.411851806D 01	-4.669946368D 01
SEMI-MAJOR AXIS -	2.208787569D 05	
ECCENTRICITY -	0.975681841D 00	
INCLINATION -	2.898344775D 01	
RIGHT ASC. OF NODE -	-1.644890723D 01	
ARG. OF PERIFOCUS -	1.549124961D 02	
TRUE ANOMALY -	1.726225057D 02	

S-IVB LUNAR-IMPACT TRAJECTORY (CONTINUED)

10 DEC. 1972 G.M.T. = 0 HR 0 MIN 0.0 SEC

TIME = 96.00000

PARAMETER	GEOCENTRIC	SELENOCENTRIC
X -	2.351637728D 05	1.530738284D 04
Y -	-2.344313242D 05	7.320278048D 04
Z -	-8.762556797D 04	3.437519733D 04
|R| -	3.434214407D 05	8.230806245D 04
XD -	6.077678521D-01	-1.892847042D-01
YD -	-3.773847178D-01	-8.754081193D-01
ZD -	-1.040140855D-01	-4.130374727D-01
|V| -	7.229245585D-01	9.862900326D-01
DECLINATION -	-1.477828503D 01	2.455814211D 00
LONGITUDE -	-1.237118363D 02	-5.006217559D 01
SEMI-MAJOR AXIS -	2.216007574D 05	
ECCENTRICITY -	0.978300923D 00	
INCLINATION -	2.924049645D 01	
RIGHT ASC. OF NODE -	-1.677813538D 01	
ARG. OF PERIFOCUS -	1.548698114D 02	
TRUE ANOMALY -	1.736506786D 02	

S-IVB LUNAR-IMPACT TRAJECTORY (CONTINUED)

10 DEC. 1972 G.M.T. = 6 HR 0 MIN 0.0 SEC

TIME = 102.00000

PARAMETER	GEOCENTRIC	SELENOCENTRIC
X -	2.4771904170 05	1.0989379320 04
Y -	-2.4224127120 05	5.4182524150 04
Z -	-8.9762691570 04	2.5384998440 04
|R| -	3.5791465170 05	6.0835108390 04
XD -	5.5495666700-01	-2.0990294040-01
YD -	-3.4837937720-01	-8.8813754030-01
ZD -	-9.5049893580-02	-4.2043092240-01
|V| -	6.6210239010-01	1.0047933600 00
DECLINATION -	-1.4519959280 01	2.3993091220 00
LONGITUDE -	1.4659290970 02	-5.3046313030 01
SEMI-MAJOR AXIS -	2.2280969930 05	
ECCENTRICITY -	0.9825366050 00	
INCLINATION -	2.9772775150 01	
RIGHT ASC. OF NODE -	-1.7423689260 01	
ARG. OF PERIFOCUS -	1.5490417510 02	
TRUE ANOMALY -	1.7477066820 02	

S-IVB LUNAR-IMPACT TRAJECTORY (CONTINUED)

10 DEC. 1972 G.M.T. = 12 HR 0 MIN 0.0 SEC

TIME = 108.00000

PARAMETER	GEOCENTRIC	SELENOCENTRIC
X -	2.591343872D 05	6.254335132D 03
Y -	-2.496529946D 05	3.467309392D 04
Z -	-9.181001018D 04	1.614052023D 04
|R| -	3.713574104D 05	3.875379383D 04
XD -	5.014997134D-01	-2.286292363D-01
YD -	-3.444770488D-01	-9.246454738D-01
ZD -	-9.753649187D-02	-4.384104977D-01
|V| -	6.161816022D-01	1.048543916D 00
DECLINATION -	-1.430899012D 01	2.238091846D 00
LONGITUDE -	5.677354548D 01	-5.522279092D 01
SEMI-MAJOR AXIS -		-5.792352915D 03
ECCENTRICITY -		1.093736766D 00
INCLINATION -		8.234708492D 00
RIGHT ASC. OF NODE -		1.404445129D 02
ARG. OF PERIFOCUS -		-4.326452562D 01
TRUE ANOMALY -		-1.525578629D 02

S-IVB LUNAR-IMPACT TRAJECTORY (CONTINUED)

10 DEC. 1972 G.M.T. = 18 HR 0 MIN 0.0 SEC

TIME = 114.00000

PARAMETER	GEOCENTRIC	SELENOCENTRIC
X -	2.693143104D 05	1.060907607D 03
Y -	-2.578535483D 05	1.351744258D 04
Z -	-9.431014860D 04	6.118403342D 03
|R| -	3.845946623D 05	1.487553803D 04
XD -	4.375375028D-01	-2.553847222D-01
YD -	-4.657707525D-01	-1.084895194D 00
ZD -	-1.569908015D-01	-5.124385053D-01
|V| -	6.580483052D-01	1.226707854D 00
DECLINATION -	-1.419023339D 01	1.520220516D 00
LONGITUDE -	-3.329503226D 01	-5.333093251D 01
SEMI-MAJOR AXIS -		-5.797720198D 03
ECCENTRICITY -		1.107138581D 00
INCLINATION -		8.056286681D 00
RIGHT ASC. OF NODE -		1.374759133D 02
ARG. OF PERIFOCUS -		-4.544942524D 01
TRUE ANOMALY -		-1.454625642D 02

S-IVB LUNAR-IMPACT TRAJECTORY (CONTINUED)

10 DEC. 1972 G.M.T. = 20 HR 32 MIN 40.000711 SEC

TIME = 116.54444

LUNAR SURFACE IMPACTED

PARAMETER	GEOCENTRIC	SELENOCENTRIC
X -	2.7344753700 05	-1.0777473770 03
Y -	-2.6433392150 05	1.2921617990 03
Z -	-9.6708562020 04	4.3697959270 02
|R| -	3.9242645620 05	1.7384396990 03
XD -	8.3423514150-01	1.5782250160-01
YD -	-1.6964212080 00	-2.3315951180 00
ZD -	-6.5121740700-01	-1.0125546780 00
|V| -	1.9994692540 00	2.5468629160 00
DECLINATION -	-1.4262242910 01	-4.2306428630 00
LONGITUDE -	-7.1840725210 01	-1.2359821380 01
SEMI-MAJOR AXIS -		-5.7947270900 03
ECCENTRICITY -		1.1078753170 00
INCLINATION -		8.0450195700 00
RIGHT ASC. OF NODE -		1.3608213640 02
ARG. OF PERIFOCUS -		-4.5568815490 01
TRUE ANOMALY -		-1.0261986410 02
HEADING -		8.3129325040 01
IMPACT ANGLE -		3.4949220330 01